RADIO EMISSION
FROM
EXTENSIVE AIR SHOWERS

A thesis submitted

by

PHILIP FRANZ SHUTIE

for the degree of

DOCTOR OF PHILOSOPHY

in the University of London

JULY 1973

Abstract

This thesis describes theoretical and experimental investigations into the lateral distribution of radio emission from extensive air showers. It will be shown that measurements on radio emission help to determine the mass of the primary cosmic ray particle initiating an extensive air shower.

The theoretical work consists firstly of the calculation of the radio emission from electron-photon cascades using Monte Carlo techniques. The results for electron-photon cascades are then used to calculate the emission from composite cascades having arbitary electron development curves. In this way the theoretical lateral distributions of the radio field strength for true extensive air showers are obtained. These distributions provide the basis for interpreting the experimental results.

The experimental investigation was carried out at the British extensive air shower facility at Haverah Park, where a radio receiving system at a frequency of 60 MHz was constructed and brought into operation. Details are given of the experimental procedures and the significance of the results is discussed. A final chapter deals with the future of the radio technique.

List of contents.

Chapter One

Introduction.

Cosmic Ray Astronomy.

Radiation from the universe which continually reaches the earth covers the entire electromagnetic spectrum. Most of the radiation is absorbed by the atmosphere but visible light and radio frequencies are able to penetrate and be studied with ground based detectors. The absorbed radiation is observed by using detectors launched in rockets or balloons. Another form of radiation also reaches the earth. This radiation is not electromagnetic in nature but consists of very energetic particles (10^{10} - 10^{20} eV), and like electromagnetic radiation yields information about its sources and the intervening space it passes through. It is therefore of great value because it provides an independent source of data for investigation of the universe. Cosmic rays of energy $\geq 10^{14}$ eV are of high enough energy to produce extensive air showers in the atmosphere which are then observed by ground level detectors. This indirect observation poses many problems in nuclear physics.

The energies involved in the production of extensive air showers are several orders of magnitude above present accelerator energies. Extensive air showers are produced in the atmosphere by high energy particles entering and interacting with it producing a vast amount of secondary particles that extend over several square kilometres when they reach sea level. By studying these secondary particles at sea level the properties of the primary may be assessed. Some

properties such as primary energy can (it is thought) be measured with reasonable accuracy but others such as primary mass remain a problem.

Lower energy cosmic rays $\leq 10^{13}$ eV have been studied by flying balloons and are generally rather well understood. The masses of the primaries are firmly established: most are protons and alpha particles. The arrival directions of these particles are isotropic. It is difficult to study higher energy particles directly with emulsions because the arrival rate per unit area per unit time falls off rapidly with increasing energy (see fig. 1). To overcome this problem of slow arrival rate the high energy cosmic rays have to be studied indirectly by using large arrays of ground based detectors.

Astrophysical problems.

Experimental evidence from air shower studies has shown there is no detectable anisotropy at 10^{17} eV and that the energy spectrum shows no sign of cutting off at 10^{20} eV. These two points are conflicting. Isotropy at 10^{17} eV suggests that the primaries are of extra-galactic origin because particles of such energy cannot be contained by the magnetic fields in the galaxy: without galactic storage one cannot obtain isotropy from an anisotropic source distribution. If the particles are extra-galactic then the presence of the 3°K black body radiation would cause a high energy cut off for distant sources.

To overcome this difficulty some theorists have proposed that high energy particles have a greater mass. For a given energy the heavier particle has a smaller radius of gyration and could be contained within the galaxy and hence made isotropic.

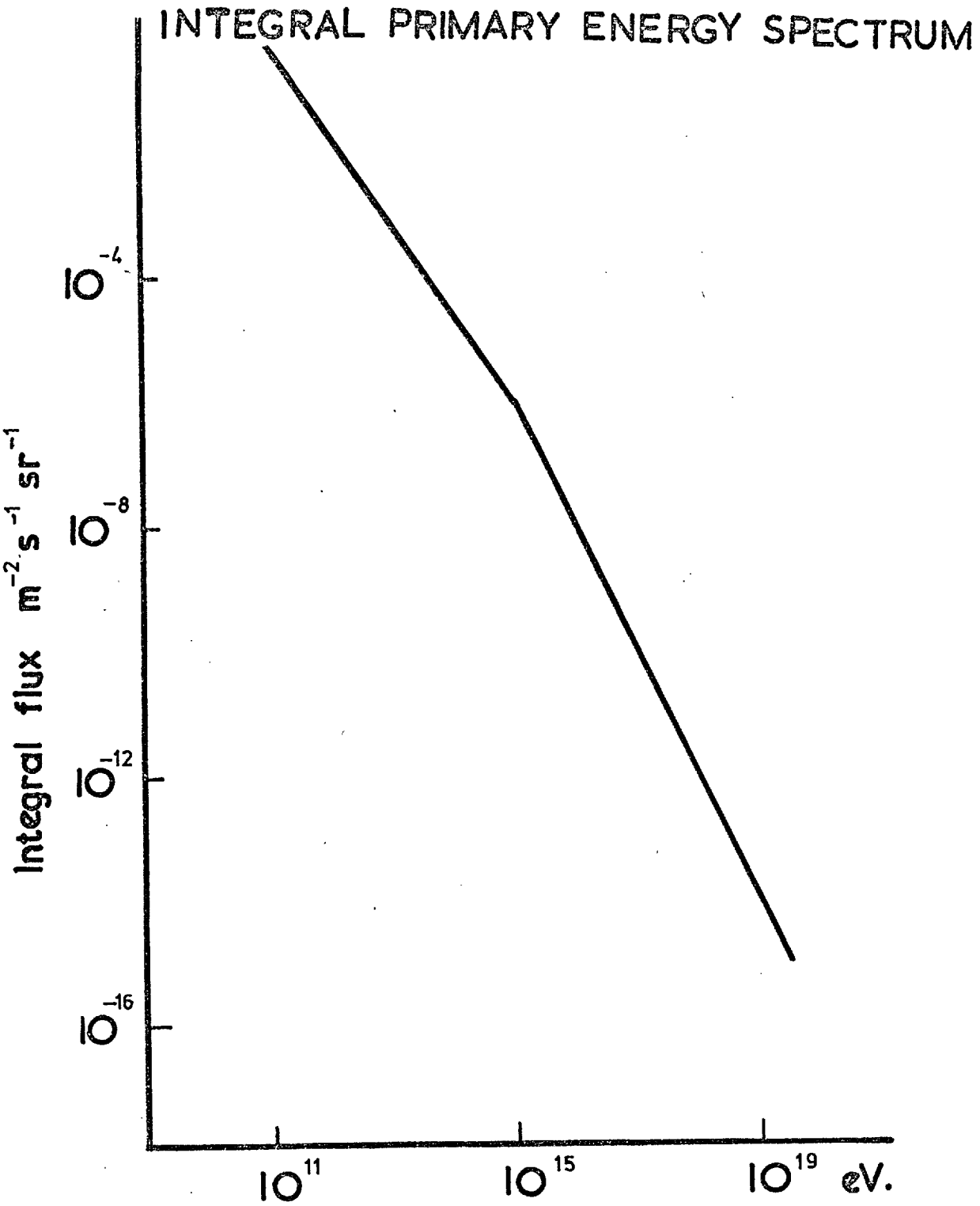
INTEGRAL PRIMARY ENERGY SPECTRUM
Integral flux $m^{-2} s^{-1} sr^{-1}$
10^{-4}
10^{-8}
10^{-12}
10^{-16}
10^{11}
10^{15}
10^{19} eV.

Fig. 1

Various mechanisms have been proposed for the acceleration of such particles to high energies. Fermi (49) suggested that particles colliding with galactic magnetic fields on average gain energy. The mechanism however is unsatisfactory for heavy particles. Another process proposed by Colgate (68,69) involves a supernova explosion where the acceleration process is a shockwave which is produced by a gravitational collapse of the centre of a star. A likely source of heavy nuclei might be pulsars which are thought to have surfaces rich in iron nuclei. They rotate at high speeds, periods of less than one second, and have intense magnetic fields associated with them. This makes possible an acceleration process similar to that of the betatron (Gold 68, Ostriker & Gunn 69).

It is thus left to the experimentalist to resolve this problem by determining the mass of the primary particle initiating an extensive air shower.

Experimental Methods.

Extensive air showers are studied using three techniques.

1) With particle detectors such as scintillators and geiger counters.
2) With atmospheric Cerenkov light detectors which are photomultipliers observing the atmosphere directly (Jelley 67, Greisen 65).
3) Radio receivers to pick up emission caused by particles suffering accelerations in the atmosphere.

The first method studies the distribution of the particles about the shower axis and their relative arrival times. The particles are divided into three classes; nuclear active particles, muons and electrons. The nuclear active particles

together with muons form the hard component. The electrons and associated photons make up the soft component. The hard component can be separated out by using lead shielding. All ground based detectors suffer from a severe drawback in that they only see the shower at one stage of development and give little direct information on the longitudinal development of the shower, though some muons have indeed travelled without change from high in the atmosphere.

Cerenkov light detectors pick up light emitted from the whole shower and hence information about the longitudinal development is obtained. However there is the obvious drawback of extraneous light and clouds which interrupt recording time.

Radio receivers also pick up radiation from the whole shower. The problem with radio is that there is background noise present from natural as well as man made sources. This limits the bandwidth over which the emission can be observed.

Shower Development.

What is seen at sea level in all these experimental methods depends on shower development. To calculate this development requires an extrapolation of results in nuclear physics obtained from present accelerator measurements and on emulsion data from balloon flights. Mathematical models are developed, both analytical and computational. In this country, work has been done by Hillas and more recently by a team at Durham. In the model calculations carried out at Leeds (Hillas 69) a whole range of models were developed with different features acceptable in high energy nuclear physics. Such parameters as the multiplicity are varied from model to model. Only the production of pions in nucleon-nucleon and pion-nucleon

collisions is considered, and an interaction mean free path between 80 - 100 gm is used. Most groups engaged in this work make similar assumptions, the main differences being in the form of multiplicity and details about the interaction products. Not only pions, but also kaons can be produced and at higher energies isobars and anti-baryon pairs occur (Fowler & Perkins 64, Miesowicz 71).

Shower detection at Haverah Park.

The cosmic ray group at Leeds operate an air shower array at Haverah Park. We deal with the radio aspect of air showers and integrate with the facilities at Haverah Park as shown in fig. 2. The particle detectors are of the water cerenkov type of thickness 120 gm-cm^{-2}. There are fifteen tanks at each of four sites, one in the middle and three at 500m from the centre. The detecting area for vertical showers is ~34 m^2 per site. A shower is recorded if the central site, Hut 1, and two other 500m sites have particle densities > 0.3 per square metre. The 500m array is the primary detector. Additional information is provided by a 150m array and a 2 km array. The 500m array has a shower collecting area of 0.6 km^2. A detailed description of the system is given by Tennant (67)

The 500m array has a threshold detection energy of 10^{17} eV and has a suitable collection rate to enable radio studies to be carried out. The 500m array provides the radio array with two trigger pulses when a shower is detected. The first is termed a Local Trigger and comes directly from the detectors at Hut 1. This acts as a timing datum point as the shower plane passes through Hut 1. The second is the 500m array coincidence trigger confirming the presence of an extensive air shower. The time difference is typically 4 μS between the two pulses.

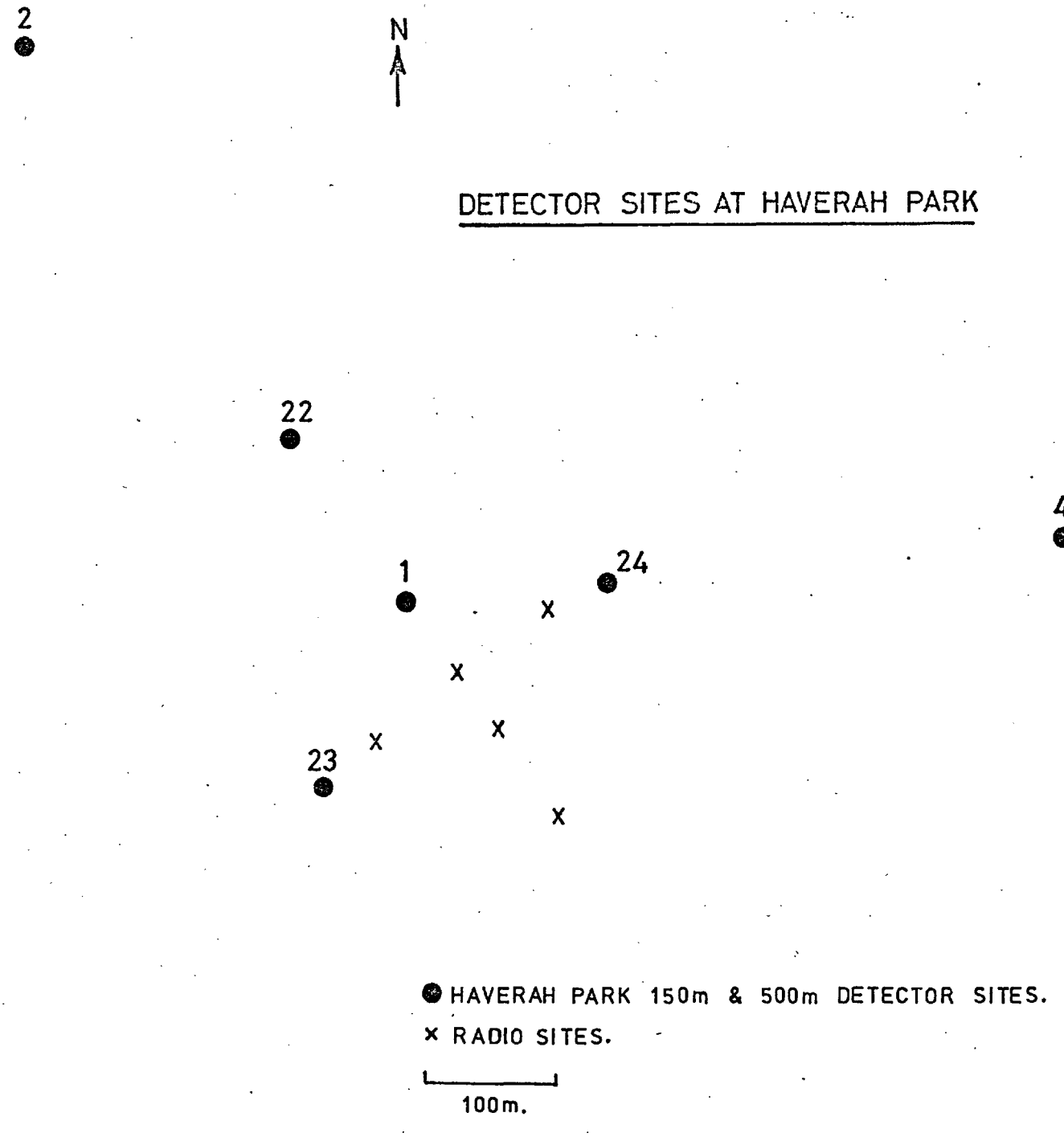
2
N
DETECTOR SITES AT HAVERAH PARK
22
4
1
24
23
3
HAVERAH PARK 150m & 500m DETECTOR SITES.
RADIO SITES.
100m.

Fig.2.

Haverah Park shower analysis.

The raw data output from the particle array consists of a density and a timing measurement. A plane is fitted by the method of least squares to the timing measurements of the detectors at sites 2,3, and 4 to give the shower arrival directions: zenith angle θ and azimuth ϕ (Hollows 68). The uncertainties of θ and ϕ are estimated by Hollows to be:

$$\theta = 2.5 \sec\theta \qquad 0^\circ < \theta < 75^\circ$$

$$\phi = 2.5 \operatorname{cosec}\theta \qquad 15^\circ < \theta < 90^\circ$$

To locate the shower axis a power law lateral distribution of particles is assumed, and an initial core position is found by the method of intersecting loci (Allan 60). A final core position is found by a grid search method (Evans 71) in steps of 25m until the best statistical fit is found for the observed densities. The process is then repeated for smaller steps.

The uncertainties in the coordinates of the shower axis are extremely difficult to determine experimentally and have to be estimated by simulation. At a distance within 300m from Hut 1 there is a 15% chance that the core position will be displaced by $\geq$20m. Beyond 300m there is a 37% chance that the core will be displaced by $\geq$40m.

The primary energy, E_p, can be estimated from the particle data only by assuming some model for shower development. Recent model calculations by Hillas (71), using the best available parameters (model E), gives, for the conversion of the particle density at 500m, ρ_{500}, from the axis to the primary energy

$$E_p = 3.85 \rho_{500}^{1.018} \, e^{0.75(\sec\theta - 1)}$$

It is thought that the value of E_p is within a factor of two of the true energy. The exponential term in the expression is an atmospheric correction factor allowing for the additional attenuation with inclined showers.

Chapter Two

Theoretical Work.

Theories of radio emission.

The successful observation of atmospheric Cerenkov light from muons and small air showers prompted a search in the radio frequency region of the spectrum. The frequency spectrum of the energy given out as Cerenkov radiation takes the form $\nu d\nu$, and at radio frequencies the emission is therefore greatly reduced. The electric field radiated by charged particles has a sign that can be positive or negative depending on the sign of the charge. When equal numbers of positively and negatively charged particles are separated by distances $\ll \lambda$ the total emission reduces to near zero. At higher frequencies the particles radiate incoherently. However a negative charge excess is expected in air showers as a result of negative electrons being produced in Compton scattering, and positron annihilation also contributes to a negative excess. This increases the possibility of emission as was first pointed out by Askaryan (62,65). This led Jelley (65,66) to look for and detect radio pulses from air showers.

It was realised that Cerenkov emission due to the charge excess was not the only possible mechanism causing radio pulses, and a paper by Kahn and Lerch (66) indicated that the separation of charges in the earth's magnetic field could produce a greater electric field than that due to the charge excess. They assumed three possible mechanisms: by charge excess, by a geomagnetically induced electric dipole moment, and by a geomagnetically induced transverse current. Using a highly

simplified shower model they found that the last mechanism was dominant. The work of Kahn and Lerch was extended by many workers: Lerch (67), Castagnoli (69), Fujii and Nishimura (69, 71), and Spencer (71), who used more realistic shower models and also came to the same conclusion that the transverse current mechanism was still dominant though to a lesser extent.

A different approach to radio emission was taken by Colgate (67). He argued that the geomagnetic field absorbs momentum from the particles, the transfer being attained via the Lorentz force. The resulting disturbance of the magnetic field causes radiation. The transverse motion associated with the Lorentz force is comparable to the transverse current of Kahn and Lerch. The differences between the two calculations are:

1) Kahn and Lerch include refractive index.
2) They assume all secondary particles to lie on a plane disc of infinitesimal thickness whereas Colgate gives a finite thickness to the disc.
3) Colgate allows for diffraction effects which determine the lateral spread of the radiation.

In 1963 Feynman formulated a version of electromagnetic theory in which the field, E, due to a moving charged particle, q, is given by:

$$E = \frac{-q}{4\pi\varepsilon_o}\left[\frac{e_r}{r^2} + \frac{r}{c}\frac{d}{dt}\left(\frac{e_r}{r^2}\right) + \frac{1}{c^2}\frac{d^2 e_r}{dt^2}\right]$$

where e_r is a unit vector giving the direction of the charge q with respect to the observer at time t, when the charge is seen by the observer and r is the distance of the charge from the observer at t. The expression is also valid for relativistic particles.

The expression is exact, and completely equivalent to the Maxwell formulation. For radiation purposes, only the third term in the expression is important. It can be written in terms of apparent angular elevation, Θ, as:

$$E = \frac{-q}{4\pi\varepsilon_0 c^2} \frac{d^2\Theta}{dt^2}$$

Using this formulation Allan (71) has calculated the radio emission caused by geomagnetic charge separation.

It is this method adopted by Allan which is used in the present thesis to calculate the radio emission from electron-photon cascades by Monte Carlo techniques and to fold the cascades into a development curve for an extensive air shower.

A Monte Carlo program was developed from a program written by Baxter (67). Emission due to the mechanisms of geomagnetic deflection and charge excess have been calculated separately. Geomagnetic emission from single cascades is studied for different inclinations and heights of injection. Also for this mechanism cascades are folded with development curves, obtained from model calculations, for vertical showers.

Brief program description.

The following physical processes are considered: pair production, Compton scattering, multiple coulomb scattering, single scattering, bremsstrahlung, ionisation loss and magnetic deflection. Positrons are produced and labelled in the program but are treated as electrons for all interactions except deflection in the magnetic field. In the program a particle is defined by the following coordinates:

1) Type: γ, e^+, e^-.

2) Space: x,y,z (fig. 3).

3) Time: given as lag behind an imaginary particle moving at velocity c down the shower axis (fig. 3).

4) Direction: zenith θ and azimuth ϕ.

5) Energy.

The tracking of photons is a relatively simple process. They move in straight lines unless scattered by an interaction, and are unaffected by the presence of the magnetic field. Tracking of electrons is more complicated. Only electrons that move in a forward direction are followed in the program because those that move backwards have a considerable delay compared with those moving forward. The tracking of electrons down to very low energies (1 MeV) is a particularly difficult process. The magnetic field superposes an energy-dependent radius of curvature on the track and the electron continually suffers an energy loss through ionisation. As the energy falls the random coulomb scattering increases. Approximations are made in the program to include random scatter: single scatter is put in half way down the track and multiple scatter is put in at the end of the track. The single scatter is that derived by Bethe (53) and the multiple scatter is that derived by Rossi (65). Single scatter is assumed to have occurred when the scatter angle exceeds a reduced angle which is a function of energy and distance travelled. The inclusion of scattering is described by Crawford and Messel (70).

The approximations become poorer as the energy falls. In order to reduce the inaccuracy the electron track is split into as many as eight segments with equal energy losses apportioned to each segment. The number of segments is calculated from the overall increase in the delay of the

COORDINATE SYSTEM

Fig. 3(a)

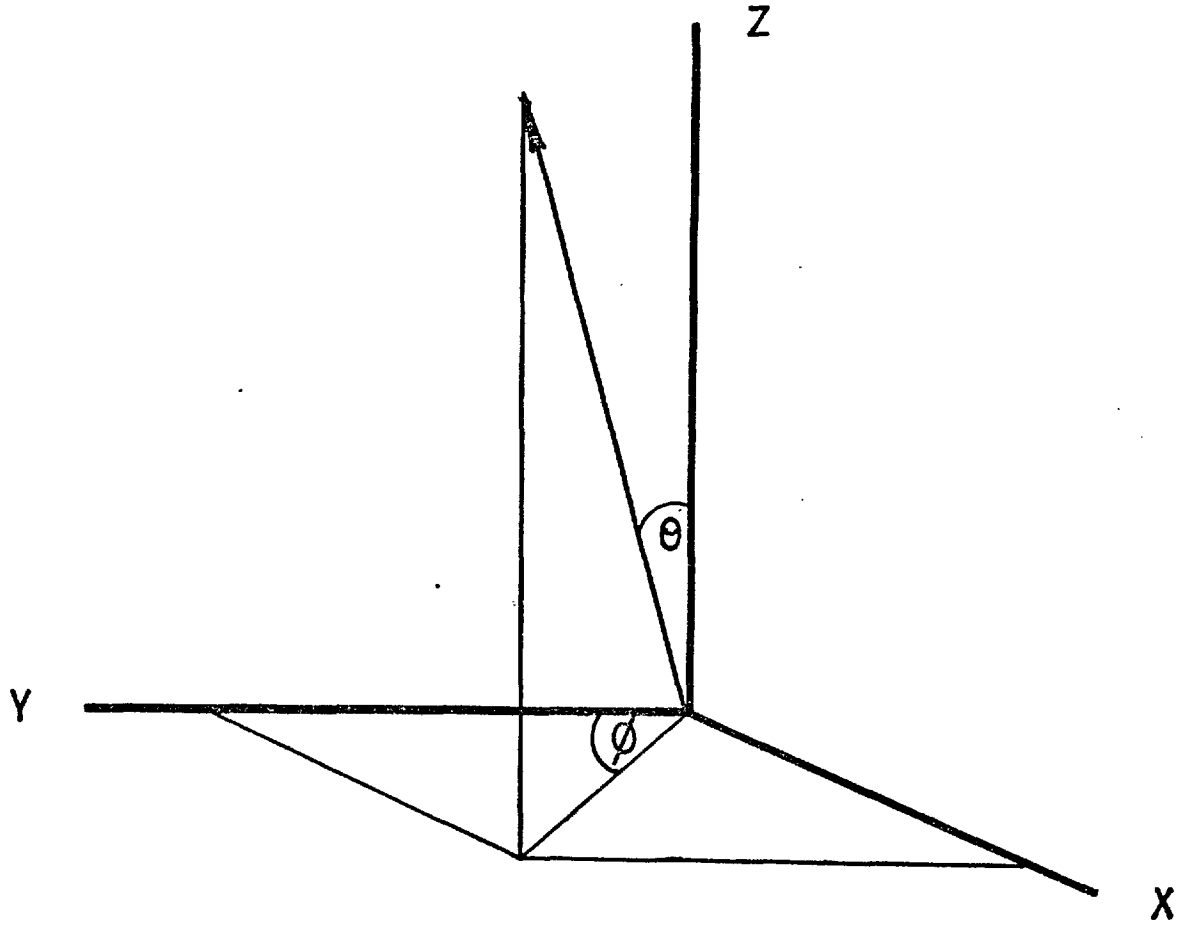

CALCULATION OF DELAY

Fig. 3(b)

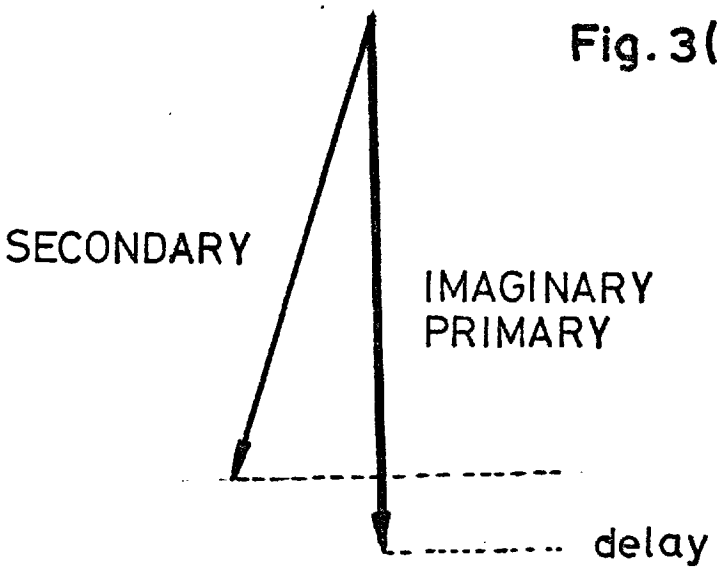

particle. The delay is used as the criterion because it is used directly in the calculation of the radio emission. As it is a measure of how much a particle is slowing up, it is a measure of the degree of inaccuracy involved. The track was split into eight segments if the overall increase in delay was greater than 7 nS, into four segments for an increase greater than 3 nS, and two segments for an increase greater than 1 nS. Fig. 4 shows a histogram of the incremental delays for electron tracks before they are split into segments. It must be noted here that particles with large delays do not contribute to the radiated field at high frequencies. These particles have short ranges and thus do not move large distances. Consequently they have small deflections, and these deflections are seen at a later time. After the division of the tracks in this manner the calculation of the magnetic deflection is simple as it is possible to assign each section a helical trajectory appropiate to an electron of constant energy moving in a uniform magnetic field.

Calculation of the magnetic deflection.

Positrons and electrons are deflected in opposite directions in the earth's magnetic field which is taken as 0.3 gauss. The radius of curvature, r, in metres is given by:

$$r = 100 \sin A \, E \qquad (1)$$

where E is the energy of the particle in MeV and A is the angle made by the trajectory of the particle with the magnetic field. A dip angle of 68° was used in the program. The magnetic deflection is added to the single and multiple scattering angles. It is calculated most easily by using a new coordinate

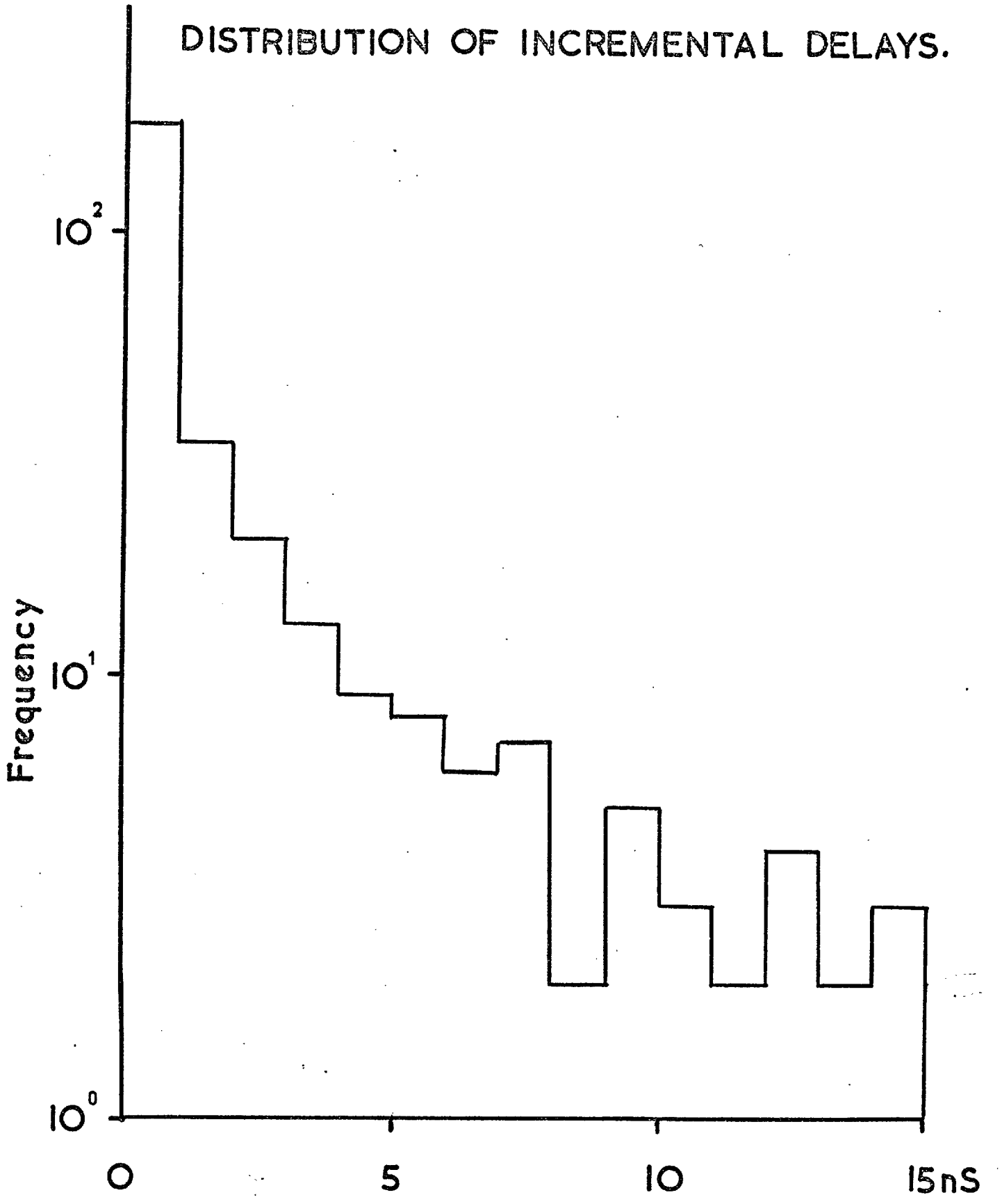
DISTRIBUTION OF INCREMENTAL DELAYS.
Frequency
10^2
10^1
10^0
0
5
10
15nS

Fig. 4.

system x, y, z, Θ, $\emptyset$, similar to that shown in fig. 3 except with the field pointing in the x-direction. If l is the distance travelled by the particle in metres then the distance travelled along the x-axis, along the field lines is:

$$x = l\cos A \qquad (2)$$

The projection of the trajectory on the y-z plane is a circle of radius r given by (1). Suppose the particle makes an angle P with the z-axis as shown in fig. 5. The initial value of P is obtained from the initial direction cosines and is given by:

$$\tan P = \tan\Theta\cos\emptyset \qquad (3)$$

This angle P is increased or decreased depending on the sign of the charge of the particle (fig. 5). The angle D is given by:

$$D = \frac{l\sin A}{r} \qquad (4)$$

The displacements along the y and z-axes are given, from the geometry of a circle, by:

$$y = r(\cos P - \cos(D+P))$$
$$z = r(\sin(D+P) - \sin P)$$

Since the difference between initial and final points are known without magnetic deflection, the additional deflection due to the geomagnetic field can now be calculated. This is required for the calculation of radio emission. Having found the new endpoint for the particle one next finds the new direction. It is assumed that the angle that the particle makes with the magnetic field remains constant, i.e. $\cos A = \text{const}$. If Θ' and $\emptyset'$ are the final directions then from (3):

$$\tan(D+P) = \tan\Theta'\cos\emptyset' \qquad (5)$$

CALCULATION OF MAGNETIC DEFLECTION

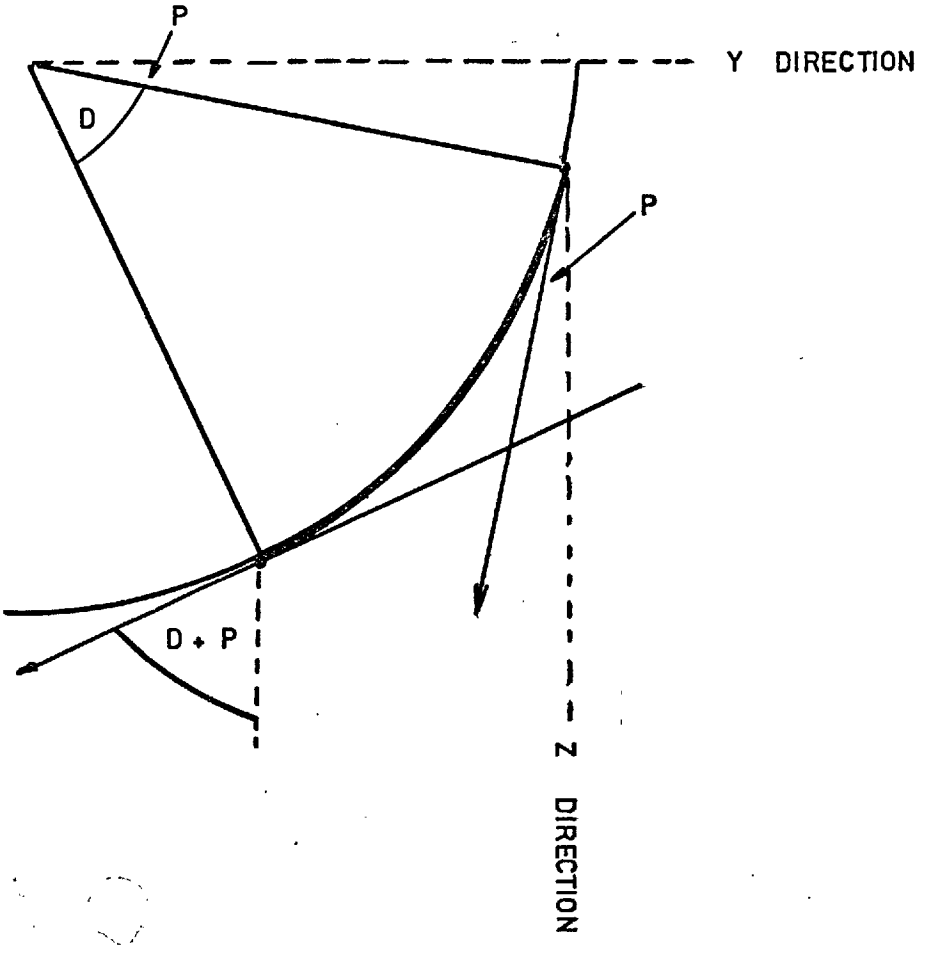

Fig. 5.

also: $\cos A = \sin\theta' \sin\phi'$ (6)

Solving (5) & (6) yields:

$$\sin^2\theta' = \frac{\tan^2(D+P) + \cos^2 A}{1 + \tan^2(D+P)} \quad , \qquad 0 \leqslant \theta < \pi$$

From (6) $\sin\phi' = \frac{\cos A}{\sin\theta'}$,

Accuracy of the magnetic deflection.

An electron track is split up into several segments. The average energy of the electron while it traverses each segment is calculated and the radius of curvature of the trajectory due to the geomagnetic field is obtained. It is assumed that while the electron is in the segment that the initial pitch angle is retained. At the end of the segment the pitch angle is altered due to the inclusion of random scatter. The deflection due to the geomagnetic field is calculated using circular arcs as described in the previous section. The inclusion of the geomagnetic deflection in steps is an approximation to the truth: the electron continually loses energy in the atmosphere leading to a varying radius of gyration. The accuracy of the approximation was determined by studying the distribution of energies in segments and lengths of segments. The energy distribution is shown in fig. 6. The mean value is 70 MeV and the mode 20 MeV per segment. The distribution of the lengths of segments is shown in fig. 7. The mean length is ~18m, which is equivalent to 1 gm for the height in the atmosphere for which the calculations were done, and the mode ~8m, which is equivalent to $\frac{1}{2}$ gm. This corresponds to a loss of 2 and 1 MeV due to ionisation in a segment. For a 20 MeV particle there is a $2\frac{1}{2}\%$ overestimate in the geomagnetic deflection at the beginning of

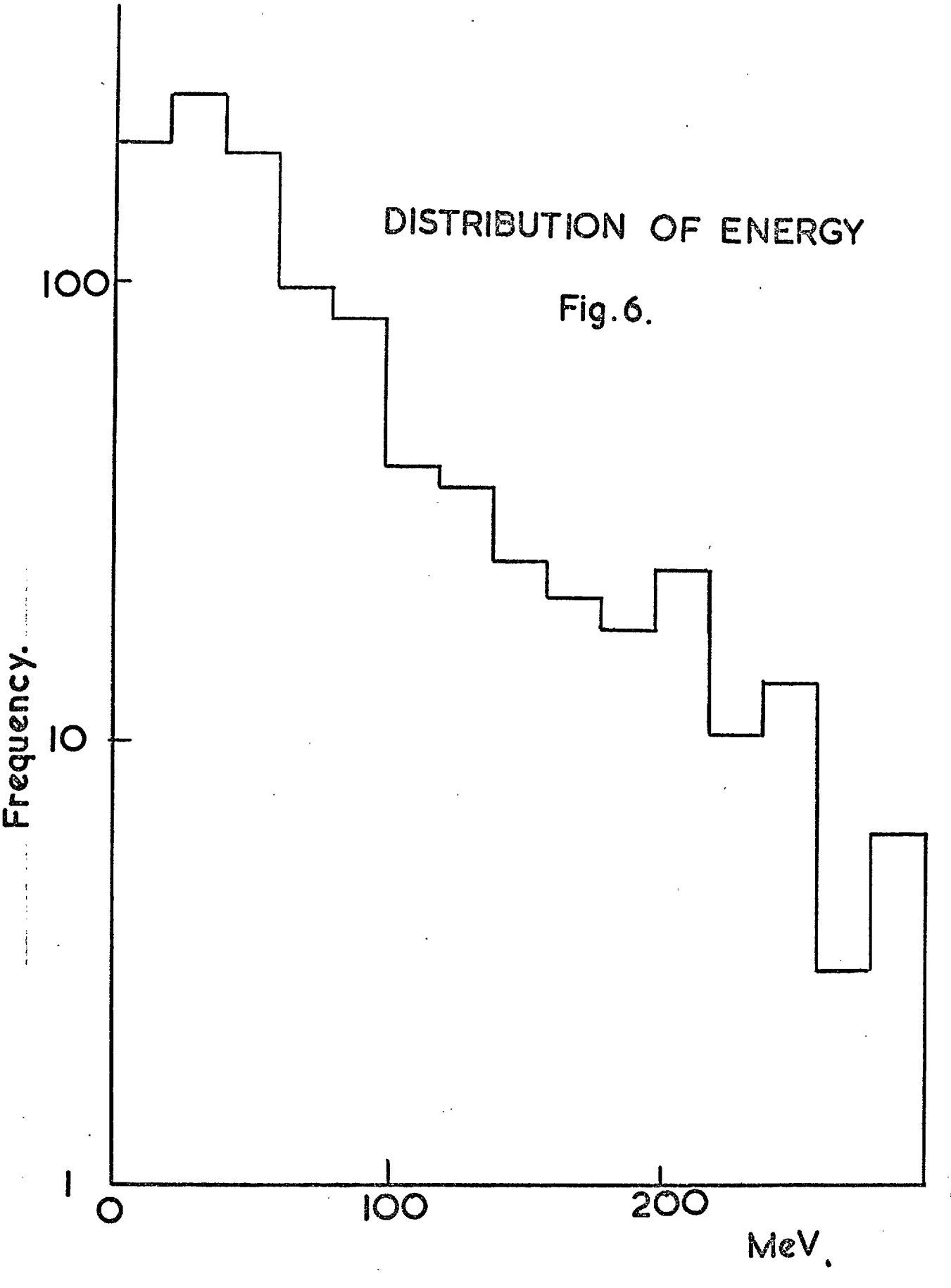
DISTRIBUTION OF ENERGY
Fig. 6.
100
10
1
Frequency.
0
100
200
MeV.

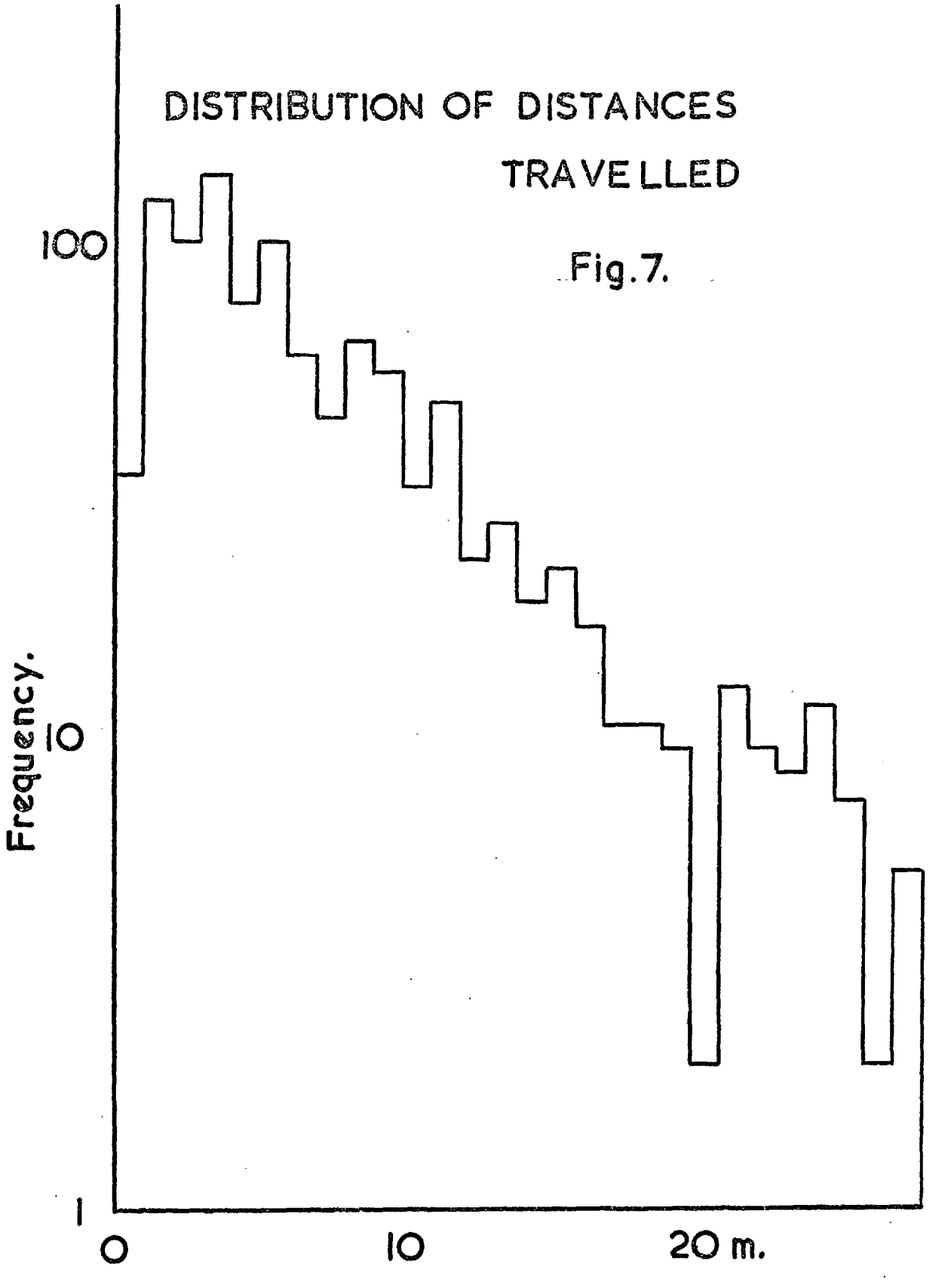
DISTRIBUTION OF DISTANCES
TRAVELLED
100
10
1
Frequency.
0
10
20 m.

Fig. 7.

a segment leading to a 2½% underestimate towards the end of the segment. The overall error is less than 1%. For lower energy particles the error is greater but is less than the accuracy claimed for the rest of the program of 10%. (Marsden, 71)

Calculation of radio emission.

As stated earlier the radiation field is computed from an approximation to Feynman's formulation of the electric field by:

$$E = \frac{e}{4\pi\varepsilon_0 c^2} \frac{d^2\Theta}{dt^2}$$

where $\Theta(t)$ is the angle of elevation of the particle subtended at the observer at time t, the time when it is seen by the observer. In order to calculate the radiation due to the geomagnetic deflection the additional deflection due to the magnetic field is used in the calculation of $\Theta(t)$. These additional deflections subtend angles in the x, y, and z directions at the point of observation and are seen at the retarded time t. These Θ's are summed for the whole cascade and are binned in the appropiate time bin to form $\Theta(t)$. The integrated Θ values are binned in intervals of 1 nS from the beginning of the growth of the pulse up to a maximum time of 200 nS. $\Theta(t)$ is differentiated twice to yield the electric field. Slight smoothing is performed after each differentiation to remove any sharp changes which might be caused by the discrete nature of the computation and the lack of particle numbers as compared to a real shower. The fourier transform of the second differential is then formed. This is done for various radial distances. The radio emission for the geomagnetic mechanism is calculated for particles with energy $\leq$500 MeV as particles with higher energy are hardly deflected by the magnetic field. The field strengths

are calculated on a line in the E-W direction from the shower axis. There is no reason to expect that the field dependence on radial distance is different in any other direction as the radiation comes from vertical distances greater than the radial distance of observation.

Results from individual cascades.

Individual high energy cascades were run to investigate various aspects of radio emission from electron-photon cascades. The first problem was to decide on the energy of the cascades to be used for folding into model development curves. Various energies in the range 1 - 90 GeV were considered, taking into account that higher energy cascades take more computer time and that lower energy cascades have fewer particles and give wildly fluctuating results. Higher energy cascades are more suitable as they give a more realistic distribution of particles in the atmosphere than a number of lower energy cascades injected at different heights. The energy decided upon was 10 GeV. A test was carried out to investigate the difference between a 90 GeV cascade simulated as a 90 GeV cascade and a 90 GeV cascade formed by folding 10 GeV cascades into a 90 GeV development curve. The upper portion of fig. 8 shows the lateral distributions at 30, 60, 100 MHz for the 90 GeV cascade formed by folding, and the lower portion shows the same for a simulated 90 GeV cascade. The similarity of the shapes indicates that the curve from 10 GeV cascades plus folding gives a good representation and there is not much gained by using higher energy cascades.

Fig. 9 shows lateral distributions at 60 MHz for cascades injected vertically downwards at different heights. The figures on the curves indicate the distance from the top of the

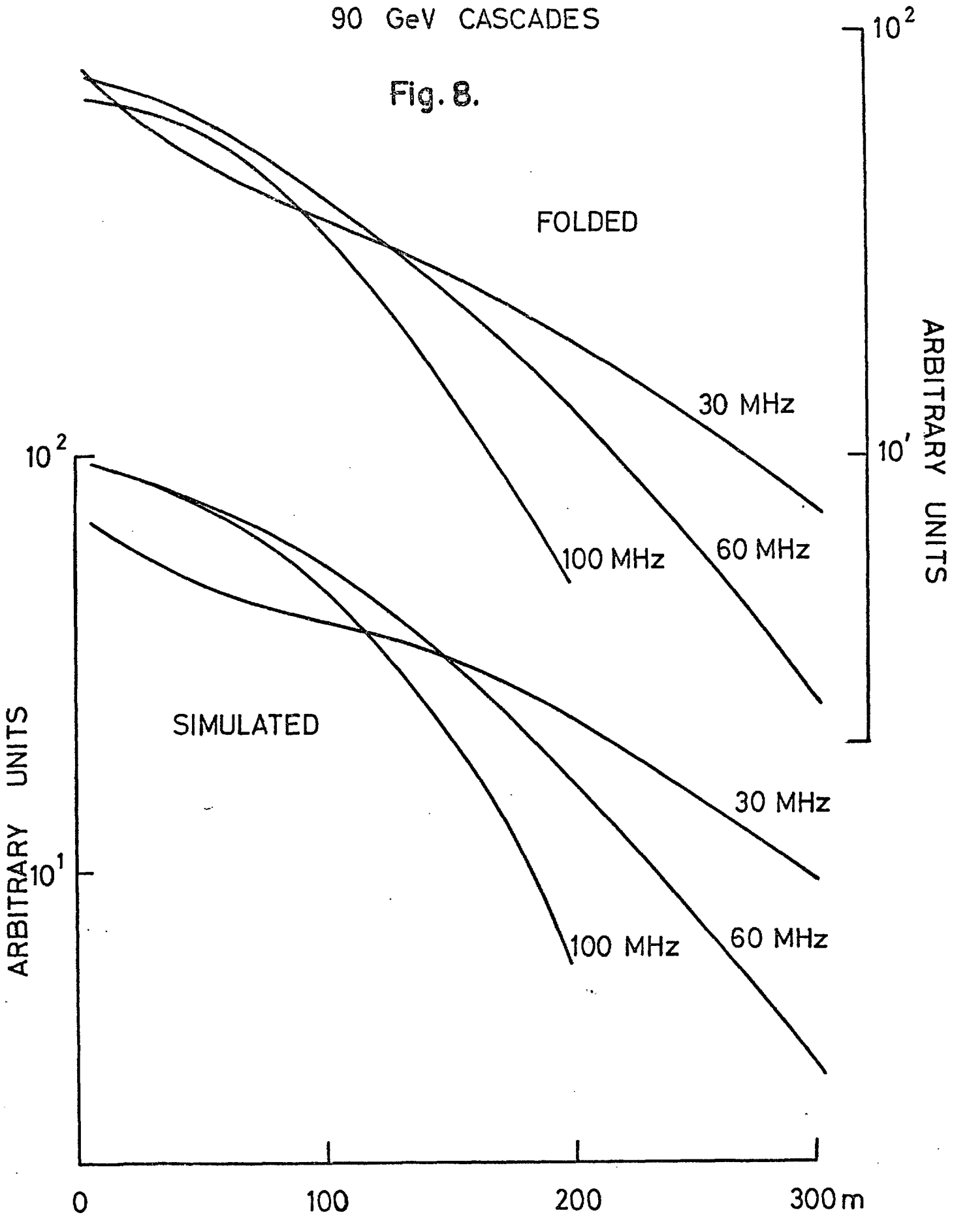
90 GeV CASCADES
Fig. 8.
FOLDED
30 MHz
100 MHz
60 MHz
SIMULATED
30 MHz
100 MHz
60 MHz
ARBITRARY UNITS
ARBITRARY UNITS
10^2
10^1
10^2
10^1
0
100
200
300 m

LATERAL DISTRIBUTIONS OF
CASCADES: DIFFERENT HEIGHTS.

Fig.9.

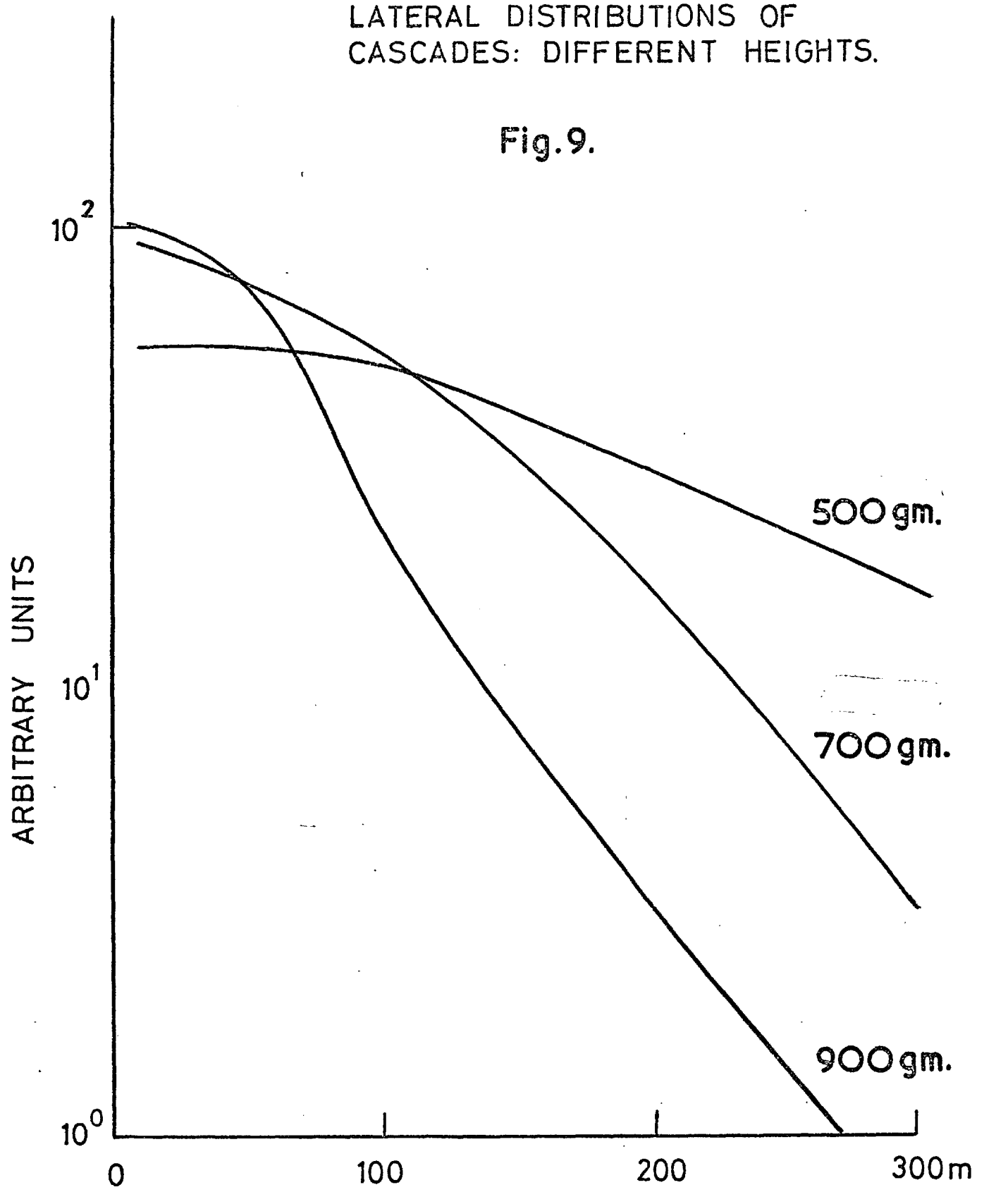

atmosphere at which maximum development occurs. The main features of the curves are that they are markedly different in shape and slope between 100 - 200m, and that there is a region of intersection. The change in slope can be attributed entirely to the height of maximum development as the cascades have identical longitudinal developments.

Fig. 10 shows the effect due to the variation in the zenith angle, θ, of the cascade axis. The azimuth angle is such that the variation in A, the angle between the cascade axis and the magnetic field, is equal to the variation in θ. The field strengths are normalised by dividing by sinA. The cascades were injected at the same depth in the earth's atmosphere. This means that the height of maximum development for a $\theta=30^{\circ}$ cascade is 160 gm further from the observer than for a $\theta=0^{\circ}$ cascade. The curves show similar differences to those displayed in fig. 9. The 700 gm curve in fig. 9 is the same curve that appears in fig. 10 as the $\theta=0^{\circ}$ curve. Comparing the $\theta=30^{\circ}$ curve to the 500 gm shows that they are very similar except that the former has a slightly steeper fall off exponent. This is in accordance with the general behaviour of the lateral distributions, that they depend chiefly on the distance of the maximum from the observer.

The above lateral distributions are normalised to energy and to sinA. This is the only type of normalisation that can be performed as the longitudinal developments are identical and almost the entire electron track length is above ground level. It must also be remembered that the longitudinal development extends through only a small thickness of atmosphere ($\sim$350 gm-cm^{-2}). This is the reason why for cascades at different heights in the earth's atmosphere the radiation patterns differ greatly.

LATERAL DISTRIBUTION OF CASCADES:
DIFFERENT ZENITH ANGLES

Fig. 10.

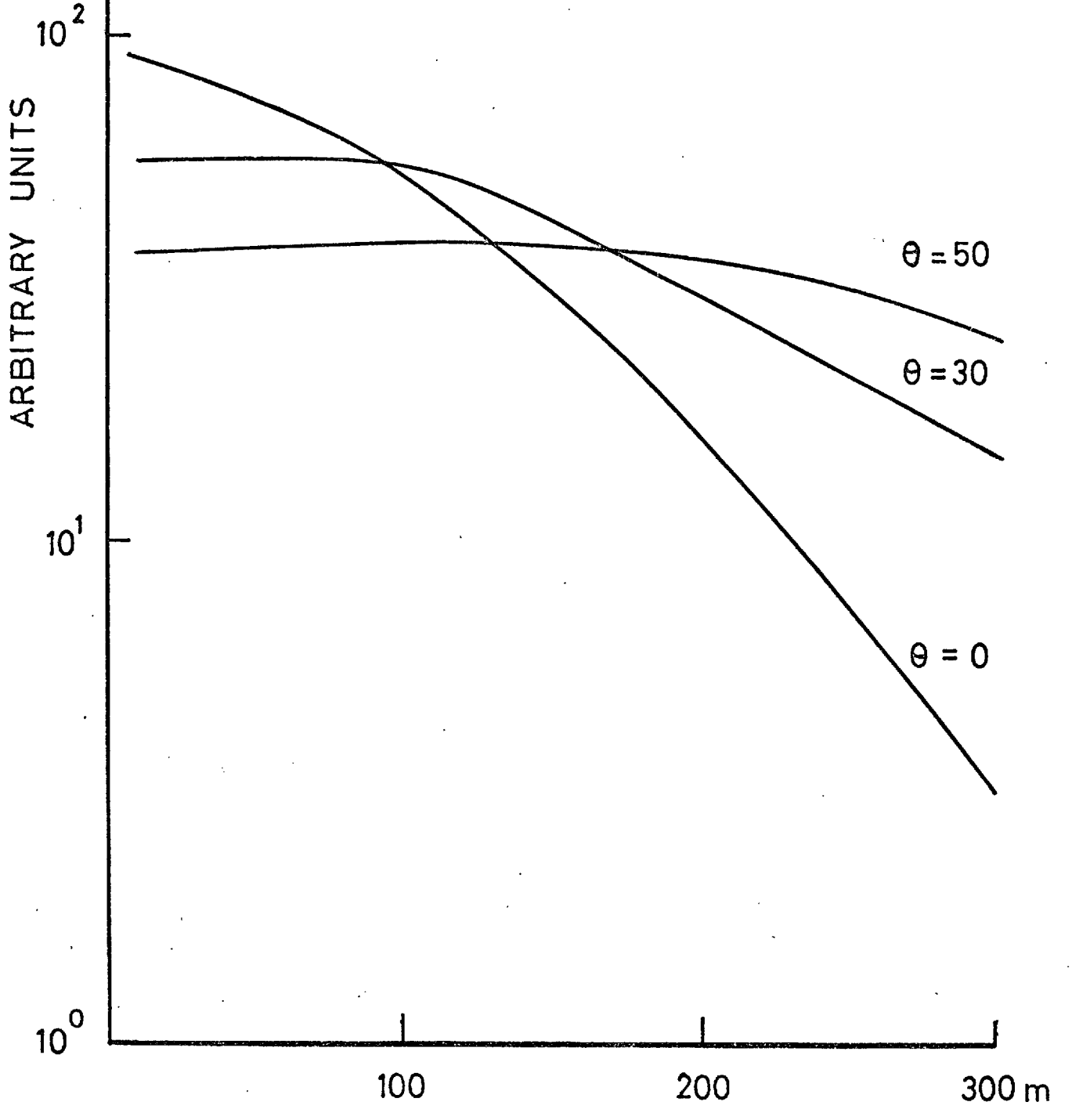

The charge excess mechanism.

A separate investigation into the radio emission from high energy cascades due to the charge excess mechanism was carried out as a separate exercise. The method of calculation of the emission is the same as that described for the geomagnetic mechanism using the Feynman formulation. The effect of the magnetic field is removed from the program and the elevations of the particles as a function of time, $\Theta(t)$, are formed. The production of a lateral distribution for this mechanism proved too time consuming on the computer as a large number of cascades would have been required to give a $\Theta(t)$ function which would be sufficiently free from random fluctuation.

To obtain an estimate of the field strength at 100m from the axis at 60 MHz the $\Theta(t)$ function at this distance was smoothed using exponential smoothing so that the growth of the curve was preserved and random effects reduced. The fourier transform of the second time derivative of the smoothed function was then formed to give the field strengths. For comparison the $\Theta(t)$ functions at 100m from the axis for the charge excess and geomagnetic mechanisms are reproduced in fig. 11 and their frequency spectra of their second time derivatives in fig. 12. The spectra are for vertical showers. From fig. 11 it is clear that the growth of $\Theta(t)$ for charge excess is slower than for the geomagnetic mechanism. This longer risetime is reflected in the frequency spectrum by a peak at a lower frequency as compared with the geomagnetic curve. For vertical showers the field at 60 MHz due to charge excess approaches 50% of the geomagnetically induced field. This fraction becomes less for inclined showers. At lower frequencies the charge excess field exceeds the geomagnetic for vertical cascades and is less at higher frequencies.

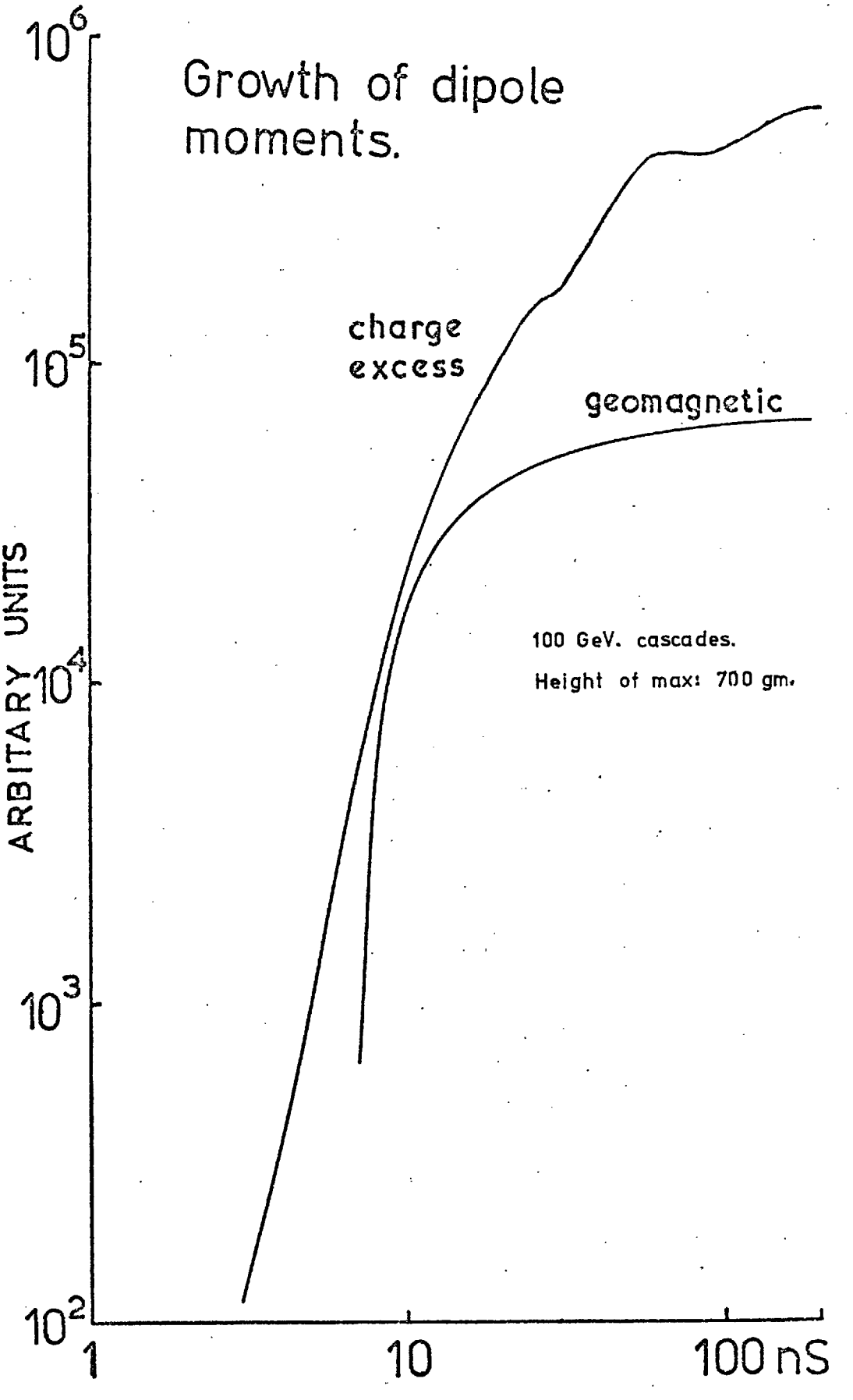
Growth of dipole moments.
charge excess
geomagnetic
100 GeV. cascades.
Height of max: 700 gm.
ARBITARY UNITS
10^6
10^5
10^4
10^3
10^2
1
10
100 nS

Fig. 11.

FIG.12: SPECTRA FOR HIGH ENERGY VERTICAL CASCADES.

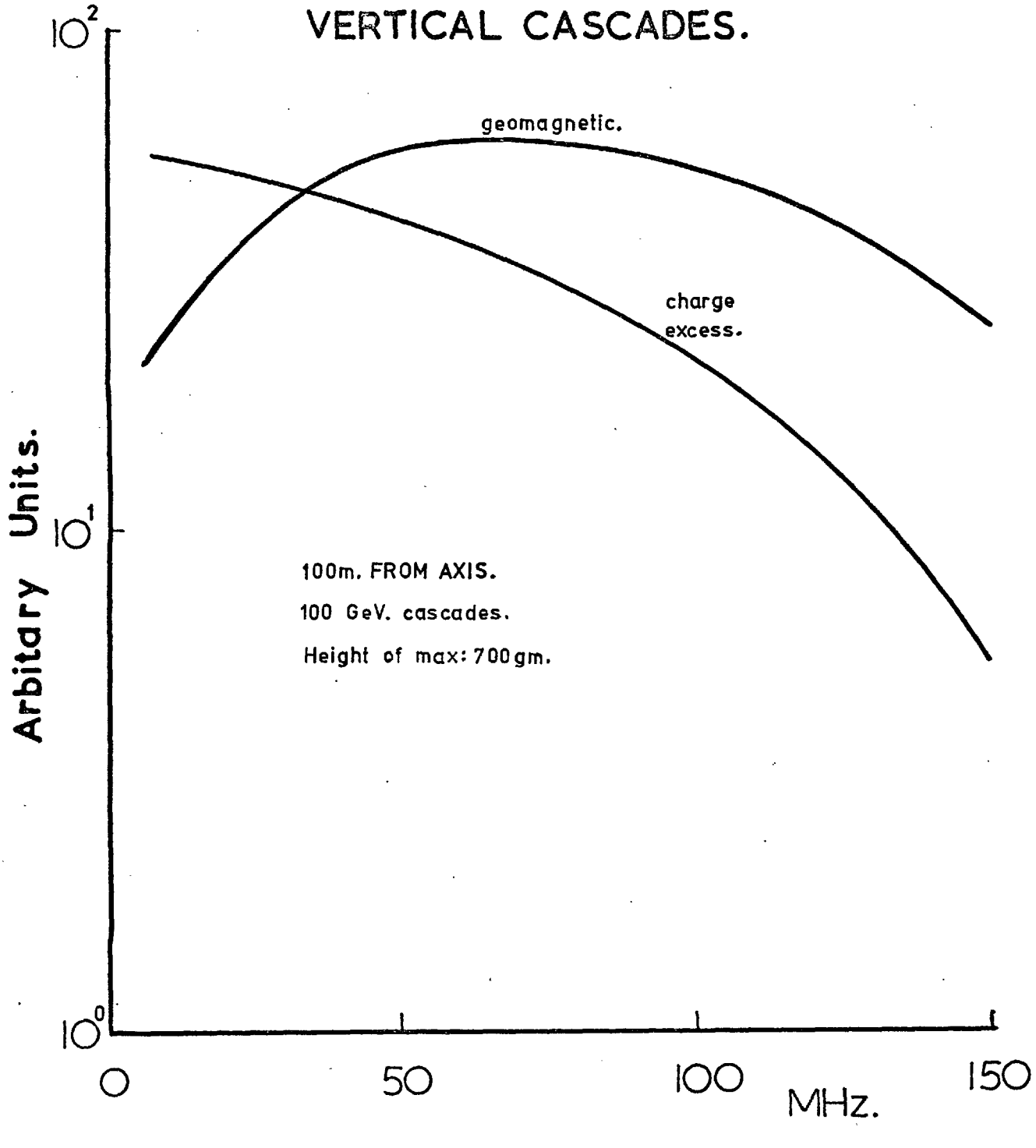

Folding to form a shower.

The $\Theta(t)$ functions were found and stored for 10 GeV cascades injected vertically downwards at each of forty height intervals of equal thickness. These functions were then folded with electron development curves representative of a shower at 10^{17} eV as produced from model calculations by a group working at Durham University. The folding curves were formed from the electron development curves by displacing the curves by 150 gm which is the thickness after injection at which a 10 GeV cascade reaches its maximum. Several development curves are used and are given in fig. 13.

Results of folding cascades into shower developments.

Fig. 14 shows the lateral distributions at 60 MHz obtained by folding the results for 10 GeV cascades with longitudinal development curves suggested by theory as reasonable representations of real air showers. The numbers on the curves in fig. 14 correspond to those on the longitudinal development curves given in fig. 13. The development curves, 1 - 4 , differ in their heights of shower maximum, but as regards build up to maximum and subsequent delay their shapes are very similar. The differences in their corresponding lateral distributions can therefore be attributed to changes in height of maximum.

It is assumed that the total energy in each shower is 10^{17} eV which means that the area under the development curve of each shower is the same, that is, the track length integral for each shower is the same. In the actual operation of an air shower array, it is possible for the total energy to be estimated incorrectly, by an amount that depends on changes in the longitudinal development. By way of illustration, we show in

FIG. 13 : ELECTRON DEVELOPMENTS AT 10^{17} eV.

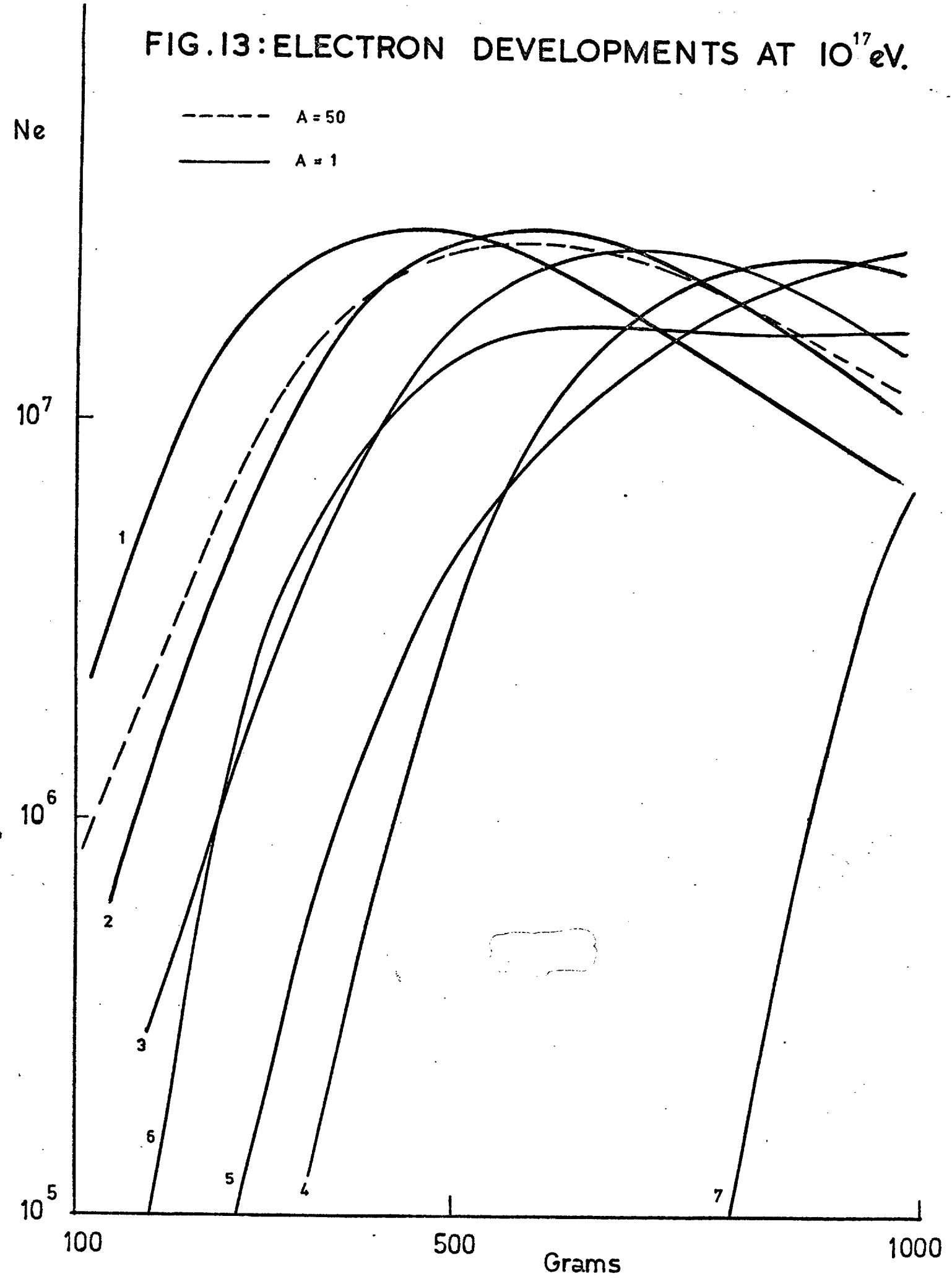

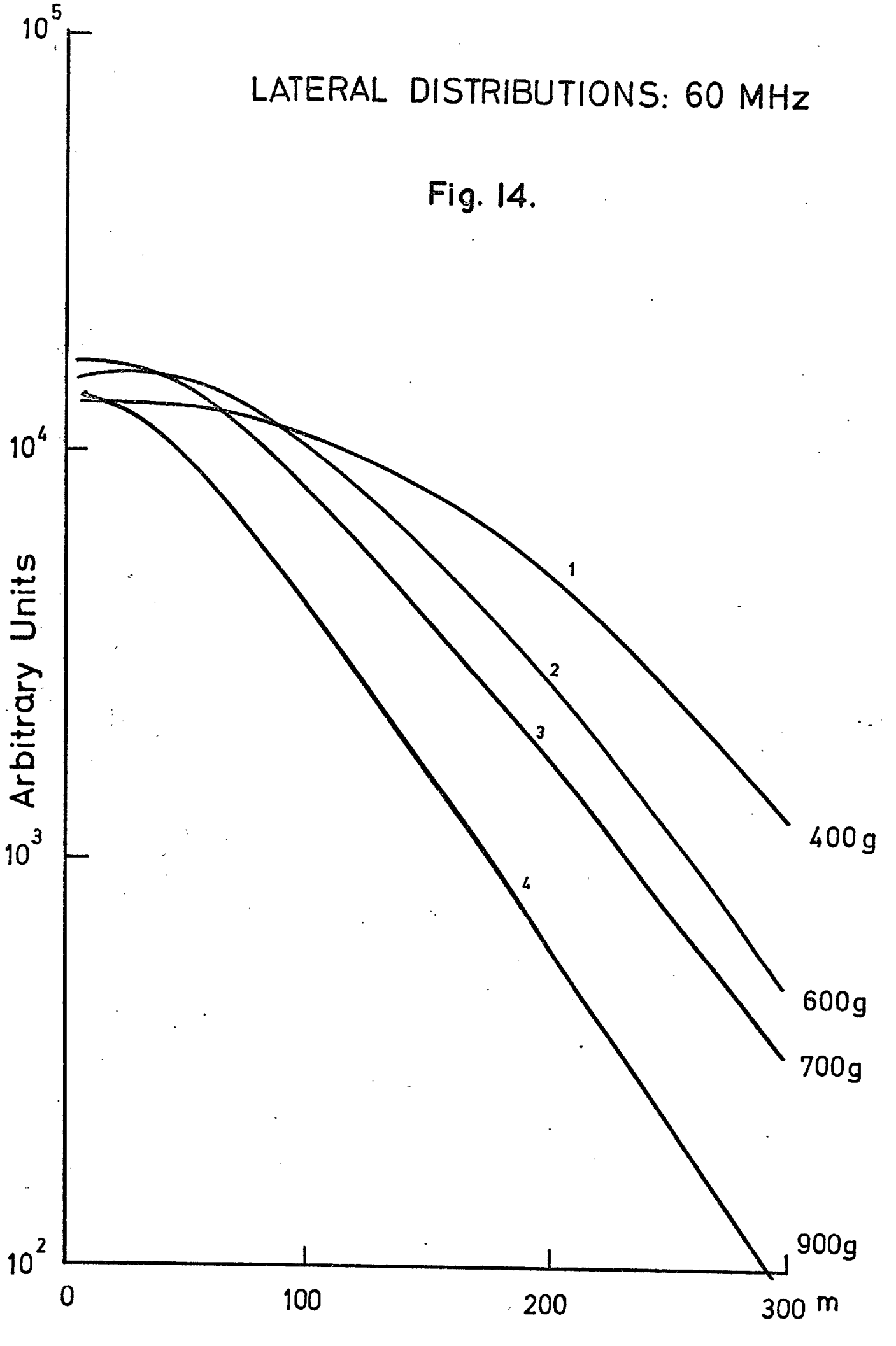
LATERAL DISTRIBUTIONS: 60 MHz
Fig. 14.
10^5
10^4
10^3
10^2
Arbitrary Units
0
100
200
300 m
1
2
3
4
400g
600g
700g
900g

fig. 15 the result of normalising to that length of the track length integral that occurs in the atmosphere, ignoring the contribution below ground level. This is what would happen if one normalised to shower size in an array that measured the size by the total amount of atmospheric Cerenkov light reaching ground level.

The assumption made above that the shower longitudinal development curves may differ in their height of maximum but not significantly in their rate of growth or decay cannot always be correct. Fig. 13 also shows some development curves with differing rates of growth and decay. The differences are of a kind not uniquely improbable according to current model simulations. The radio lateral distributions corresponding to the development curves 5 - 7 are shown in fig. 16, normalised to total shower energy, and in fig. 17 normalised to total Cerenkov light.

It is clear that changes in the shape of the development curve can have a marked effect on the radio lateral distribution. This applies particularly to the rate of build up to maximum. For example: curves 4 & 5 have different rates of growth and different heights of maximum which largely compensate one another and both give very similar lateral distributions. Curves 2 & 6 show the effect of changes in the rate of shower decay. Curve 7 represents an extreme fluctuation, which must nevertheless be considered possible.

From what has been said the following points emerge as regards the shape of the radio lateral distribution, shape of the shower development curve and the height of the shower maximum.

1) Beyond 150m from the shower axis the field falls off exponentially with distance and the fall off exponent is approximately the same for all showers.

LATERAL DISTRIBUTIONS: 60 MHz.

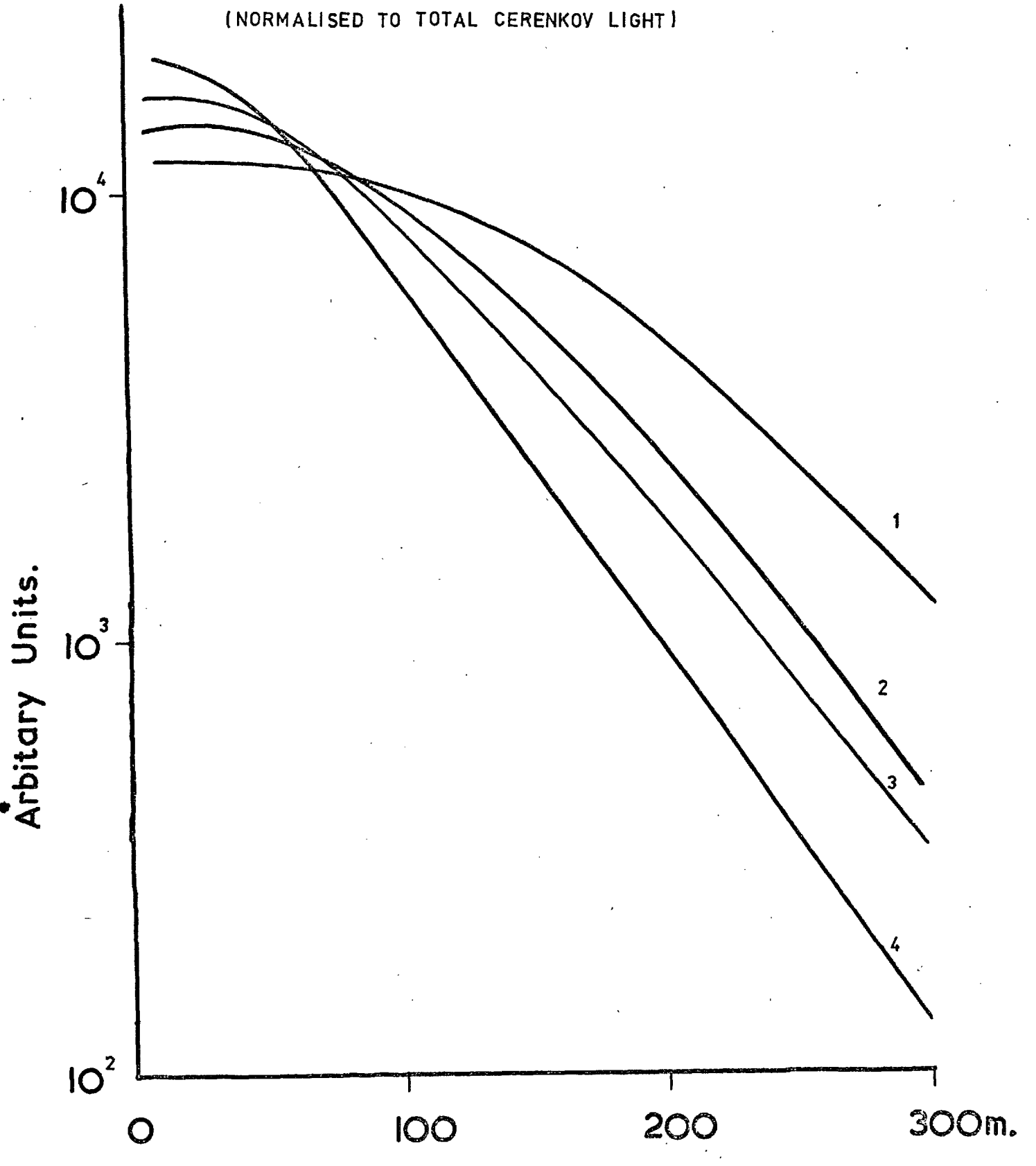

Fig. 15.

60 MHz DISTRIBUTIONS FOR DIFFERENT DEVELOPMENTS

Fig. 16.

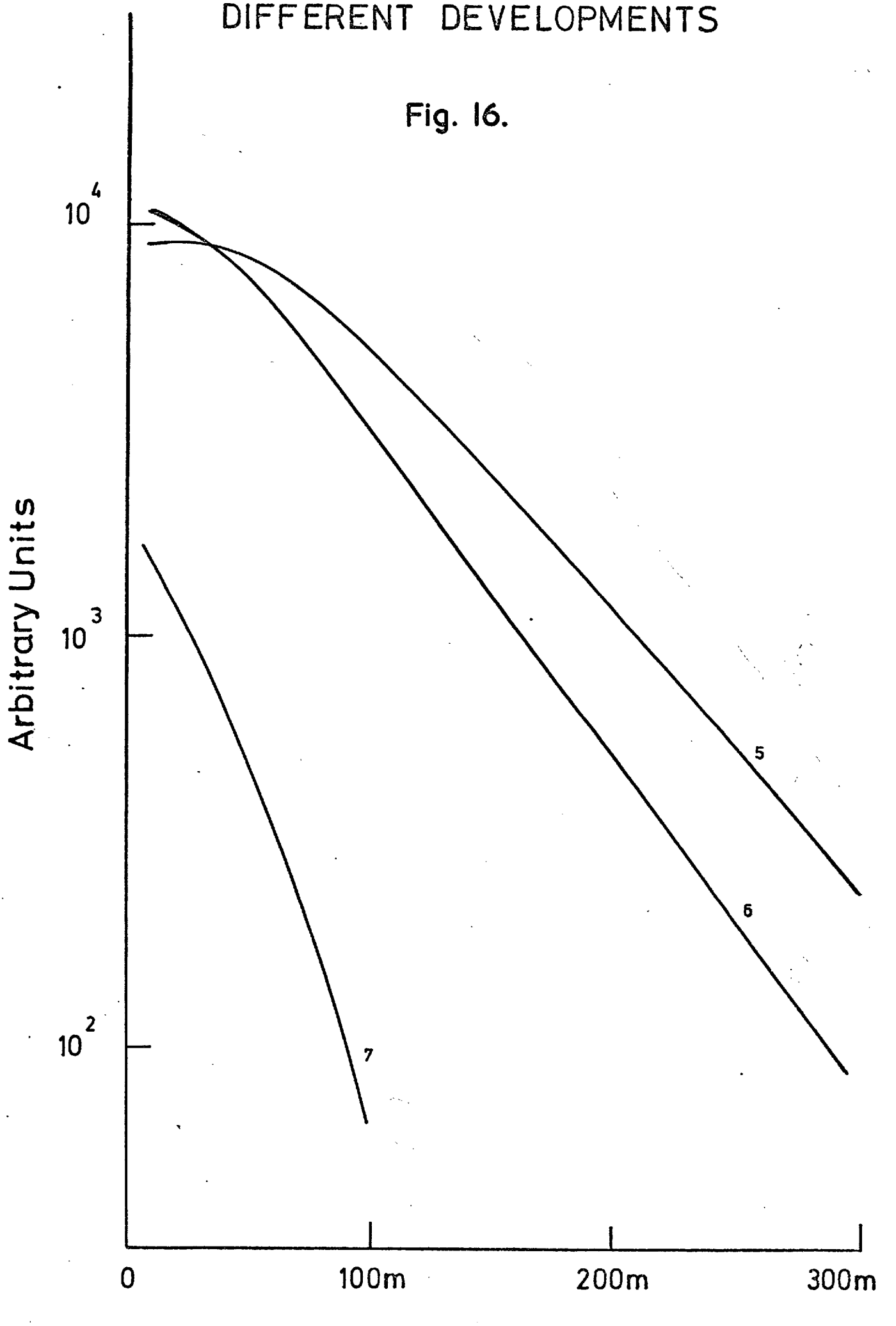

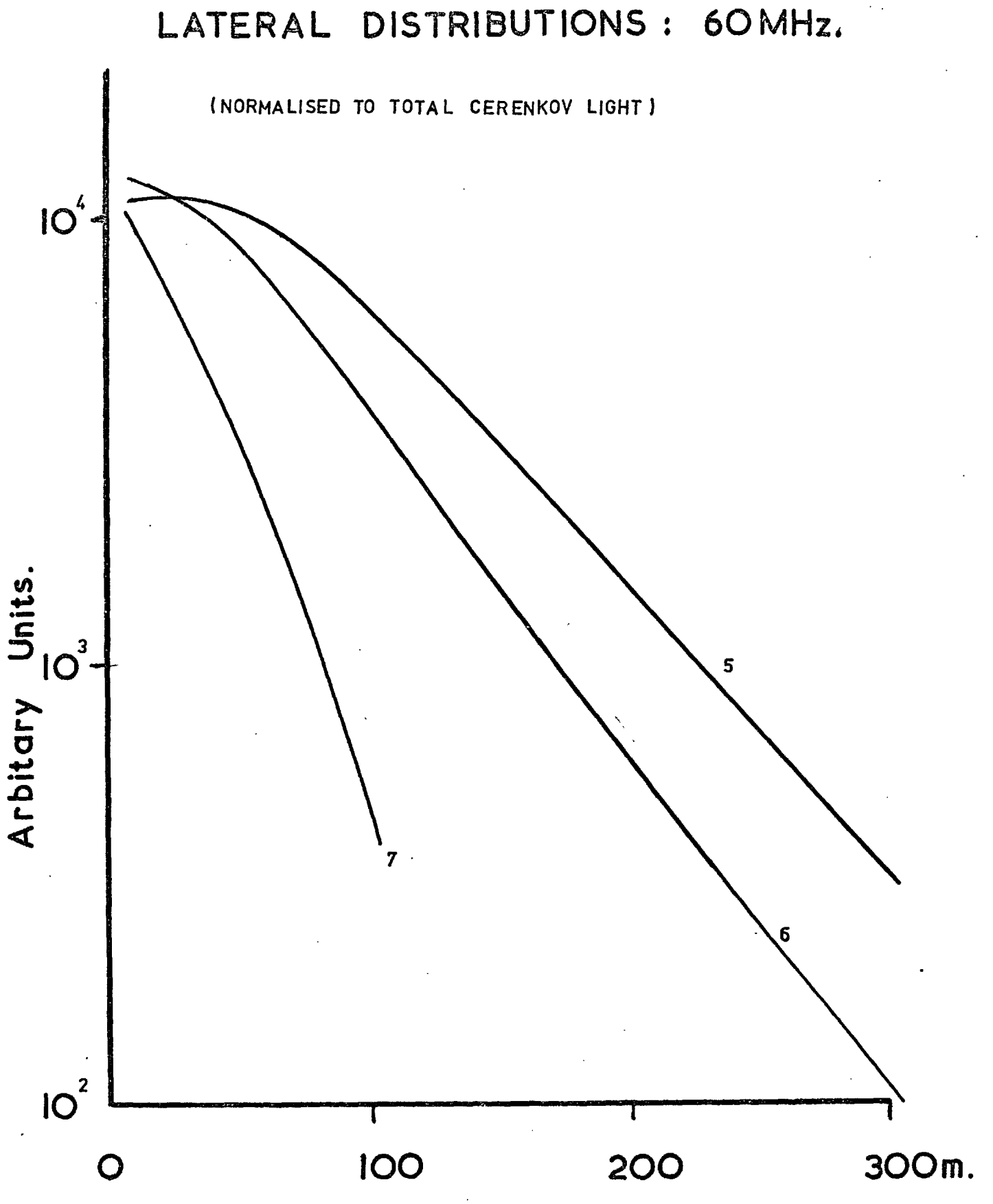
LATERAL DISTRIBUTIONS : 60MHz.
(NORMALISED TO TOTAL CERENKOV LIGHT)
Arbitary Units.
10^4
10^3
10^2
5
6
7
0
100
200
300m.

Fig. 17.

2) As the shower maximum comes lower in the atmosphere the lateral distribution is displaced downwards for distances >120m.

3) The region 0-120m is very sensitive to height of maximum and shape of development curve.

The asymptotic behaviour of the lateral distribution may be explained in the following way: at large distances from the axis the radio emission from early parts of the shower arrive first. Emission from lower in the shower arrives later and at a slower rate so that high frequency components are unaffected by later parts of the shower. Fig. 18 shows the delay in the arrival of signal from various parts of the shower for different radial distances.

Most of the radiation received comes from the region of maximum development. When this region is high in the atmosphere the density is less and the magnetic field is more effective in generating emission than in lower regions of the atmosphere. Also, at large heights the diffraction pattern is more widely spread at ground level. This results in fields spread over greater distances.

In the region near the axis the radio signal arrives in a different time sequence to that in which it was emitted (see fig. 18) because of delays due to refractive index. The effect of refractive index near the axis is to delay emission from earlier parts of the shower so that signals from higher parts of the shower are seen later than emission from lower regions. This is the exact opposite of the behaviour at large radial distances. Hence the region is more sensitive to changes lower in the shower.

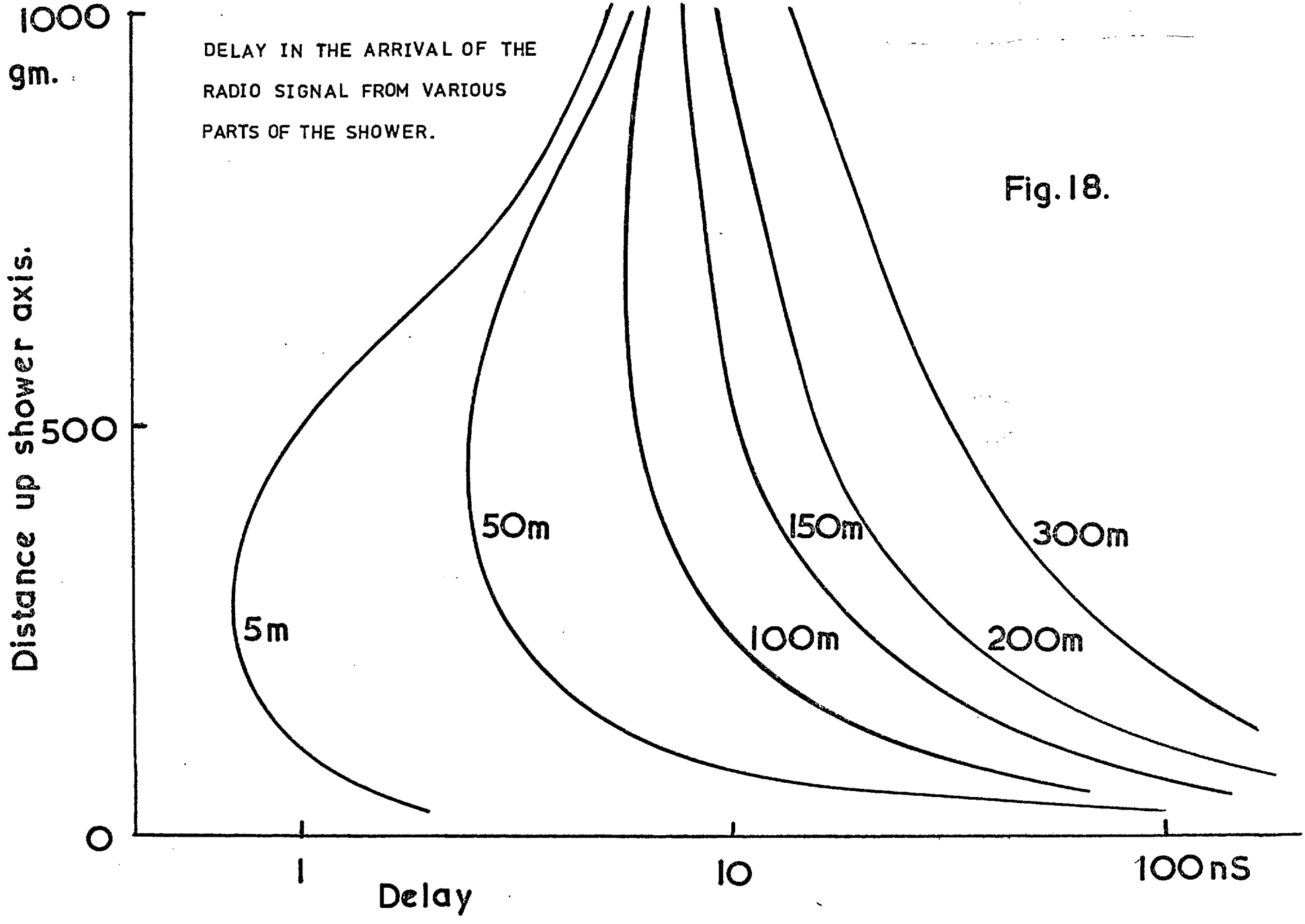
1000
gm.
500
0
Distance up shower axis.
DELAY IN THE ARRIVAL OF THE
RADIO SIGNAL FROM VARIOUS
PARTS OF THE SHOWER.
5m
50m
100m
150m
200m
300m
1
10
100nS
Delay

Fig. 18.

Behaviour at other frequencies.

Fig. 19 shows the frequency spectra at various radial distances for development curve 3 (fig. 13), which represents the average development of a 10^{17} eV proton. The form of the spectrum at each radial distance does not vary greatly for different shower developments, only the relative values between the spectra alter. It is therefore more useful to look at the lateral distributions at particular frequencies, especially at 20, 30, and 100 MHz for which experimental data exists. The lateral distributions for 100 MHz are shown in fig. 20. The most distinctive feature of these distributions is that for showers with very high maximum development there is a maximum value of field strength off axis and the higher the shower maximum the further from the axis this radio field maximum occurs. This is a consequence of atmospheric refractive index which shows up clearly at high frequencies because the delay caused by the refractive index on axis is sufficient to reduce the high frequency component. As the point of observation is moved away from the axis geometrical delays equal the refractive index delays resulting in emission from all parts of the shower to be seen at the same time and thus more high frequency component is present. The field strength falls away for the same reason as at 60 MHz. The fall off exponent for the 100 MHz distributions is larger than that at 60 MHz. This may be explained in terms of diffraction; as the frequency increases changes in the diffraction pattern occur more rapidly. The lateral distributions at large distances have the same correlation with height of maximum development as at 60 MHz.

The lateral distributions at 20 and 30 MHz are shown in figs. 21 and 22 respectively. The most significant difference

SPECTRA FOR AVERAGE 10^{17} eV PROTON

Fig. 19.

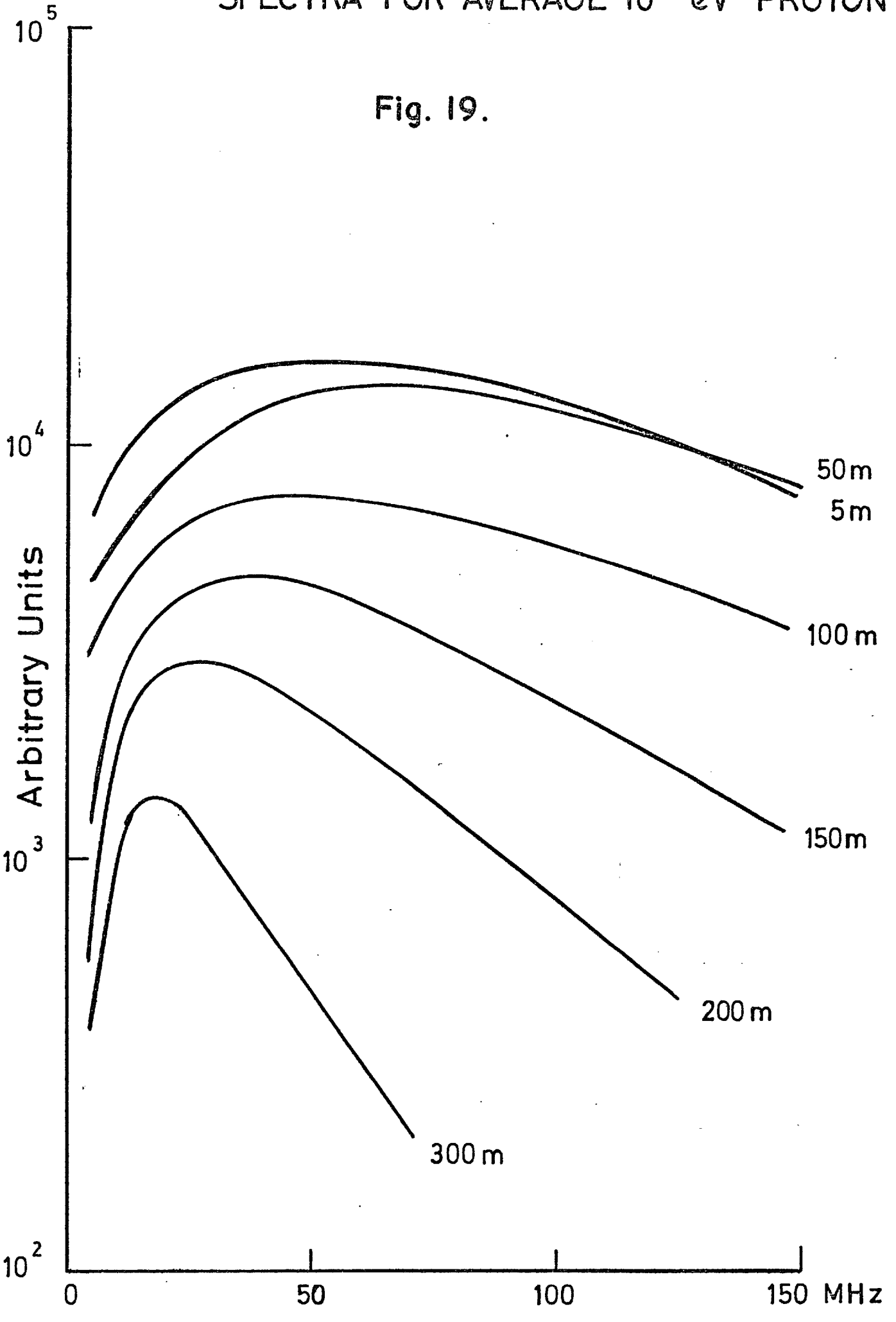

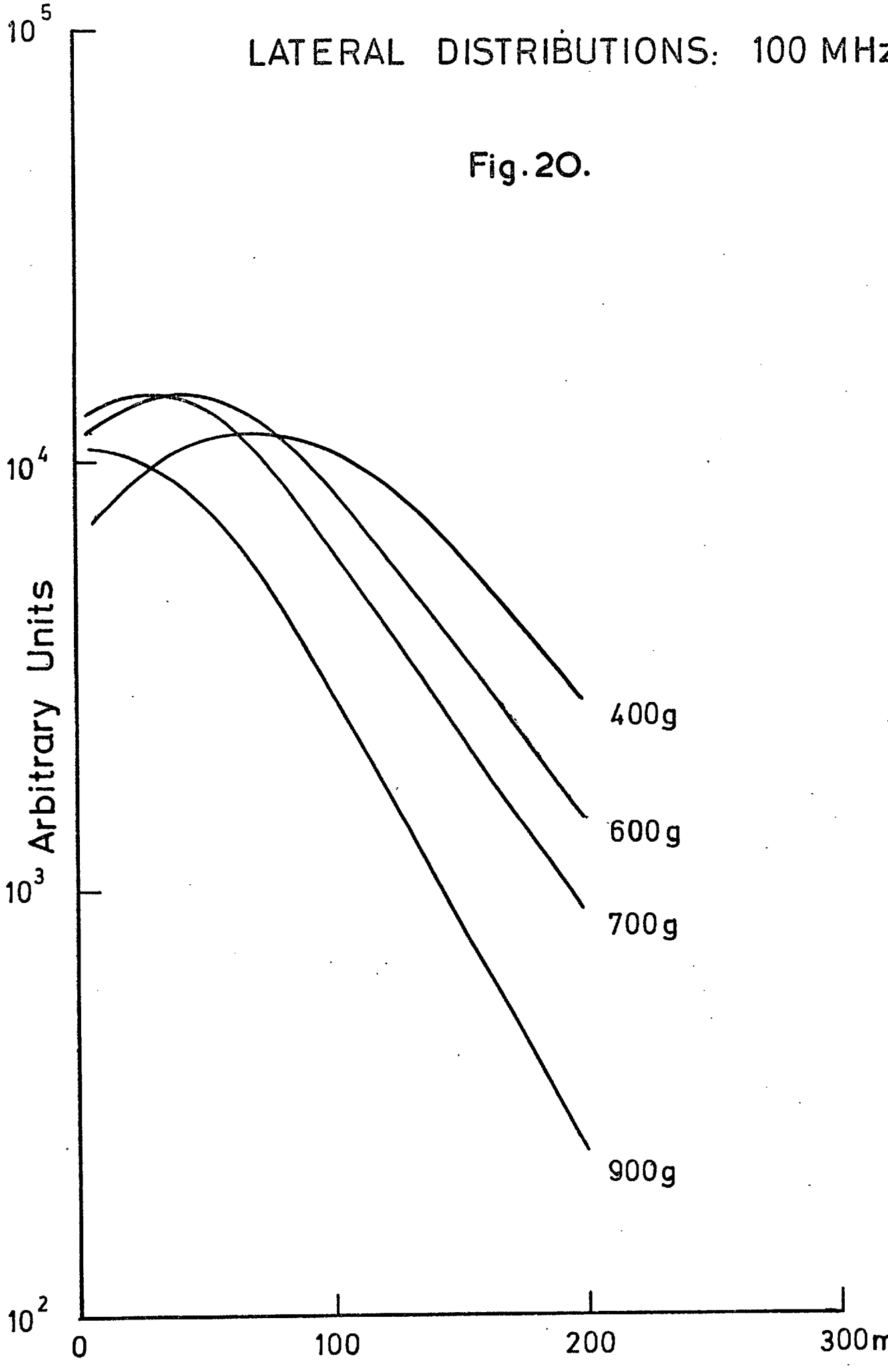
LATERAL DISTRIBUTIONS: 100 MHz
Fig. 20.
10^5
10^4
10^3
10^2
Arbitrary Units
400g
600g
700g
900g
0
100
200
300m

LATERAL DISTRIBUTIONS: 20 MHz

Fig. 21.

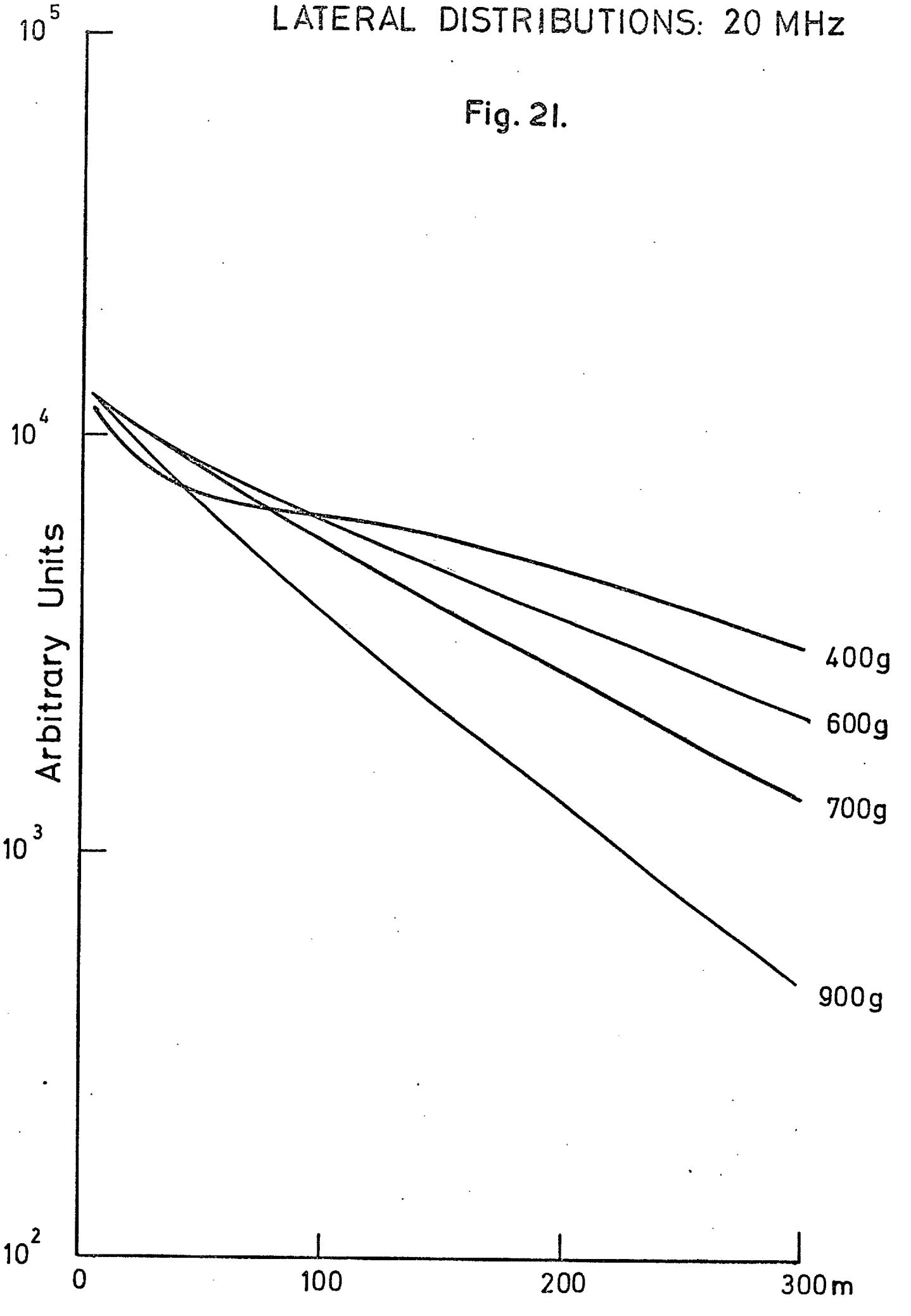

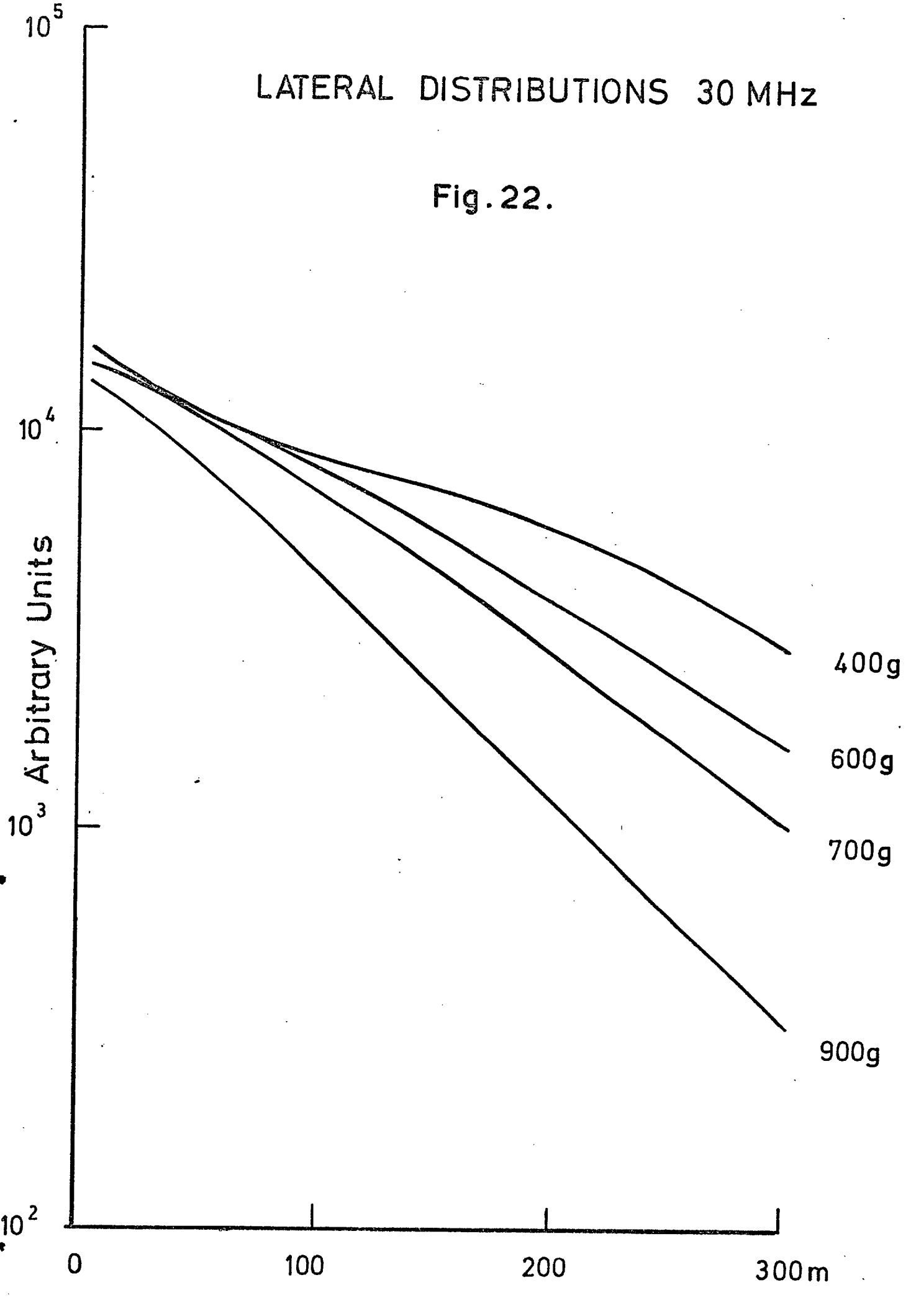
LATERAL DISTRIBUTIONS 30 MHz
Fig. 22.
10^5
10^4
10^3
10^2
Arbitrary Units
400g
600g
700g
900g
0
100
200
300m

in shape between these lower frequency distributions and those at higher frequencies is that the field rise to a maximum value on the axis for all showers. This also is a refractive index effect which delays the signals causing an increase in the low frequency component. The lateral distributions are flatter and fall off exponentially at large distances (>200m) from the axis and behave in the same manner as those at 60 MHz with respect to height of maximum development, but the relative displacements of the radio distributions are less at lower frequencies.

Field strength.

The normalised field strength at 100m from the axis at 60 MHz for the 'average' 10^{17} eV proton with its maximum development at 700 gm depth in the atmosphere was found to be 1.9 μV/m/MHz.

Comparison with past experimental results from other groups and Haverah Park.

The group at Moscow have a radio receiving array comparable to that at Haverah Park. This, too, produces radio lateral distributions for individual showers. The receiving system has operational frequencies at 32 and 58 MHz. Results from this group (Atrashkevitch 71, Khristiansen 72) consist of lateral distributions at these frequencies correlated with N_μ/N_e ratios. Fig. 23 compares the Moscow results with the calculated lateral distributions of high and average developing showers. It must be noted here that the theoretical curves are calculated for vertical showers and for a geomagnetic mechanism. A comparison shows that the Moscow results indicate a flattening of the lateral distribution in the region 0 - 100m, the flattening being more marked at the lower frequency. Flattening of the calculated

Comparison of the Moscow results with present theory.

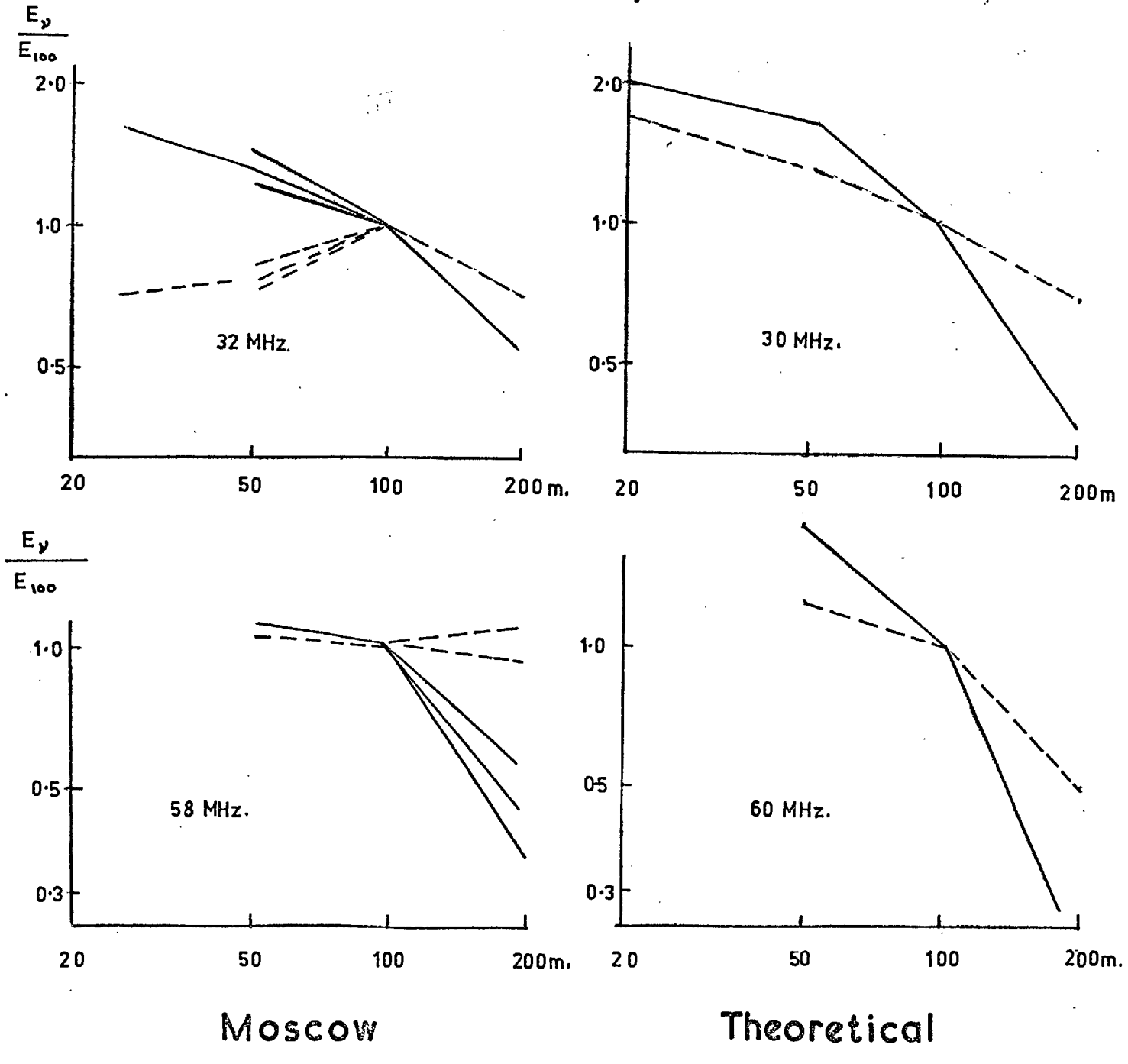

Moscow

Theoretical

Fig. 23.

distributions occur when the height of maximum development is raised in the atmosphere; however the shape of the 32 MHz Moscow lateral distribution cannot be reproduced even by raising the maximum development to a depth of 400 gm. There appears to be better agreement between theory and experiment at 58 MHz. The shower energy at Moscow is 10^{17} eV, the value for which the theoretical curves are calculated.

The 22 MHz results from Calgary (Clay et al. 71) are in sharp contrast to the Moscow results at 32 MHz. The interesting feature in the Calgary distribution is that the field increases sharply, by a factor ~5 from 100m to 10m from the axis. The calculations indicate an increase of 2-3 (fig. 21).

The results from the previous experiment at Haverah Park (Allan et al. 71) gave information on the lateral distributions at 32,60, and 105 MHz. They were composed of measurements of several showers and hence cannot give any detailed structure, but only give the general trend of fall off of field strength with increasing radial distance. There is good agreement between the results and the calculated lateral distributions at the three frequencies, especially at 105 MHz.

From what has been said there appears to be some disagreement between different experimental groups, and between experiment and theory, particularly in the frequency range 22 - 32 MHz. This suggests that while the geomagnetic mechanism is dominant at higher frequencies some other radiation mechanism becomes more important at lower frequencies. A likely candidate is the charge excess mechanism for which we have seen has a maximum in its spectrum at the lower frequencies.

Chapter Three

Experimental Radio.

Introduction.

In the period 1970-71, just before the present work began, the radio experiment at Haverah Park consisted of the simultaneous operation of six radio channels: two each at 32, 60, and 105 MHz. The antennas were situated adjacent to each other on the present site A shown in fig. 24. The polarisations of the antennas were North-South and East-West. Further details of this experiment are given by Prah (71). Data from this experiment was used in planning the present experiment.

The new array.

The new array consists of five sites (fig. 24), each site having two receiving systems with different polarisations. The sites are located in the sector closest to Huts 1,3 and 4. The polarisation directions of the antennas at three sites are North-South and East-West. The other two have polarisations North-West-South-East and North-East-South-West. It was decided to have polarisations of NW-SE and NE-SW because it was found from the previous experiment that the East-West channel often had large off-screen pulses while the North-South channel had a zero signal. This is expected as the geomagnetic mechanism is thought to be the dominant mechanism for radio emission. If the antennas are rotated through 45° then a large East-West pulse can be accommodated between the two thus increasing the dynamic range. Each site yields the amplitudes of two orthogonal horizontal components. This leads to an ambiguity in the direction

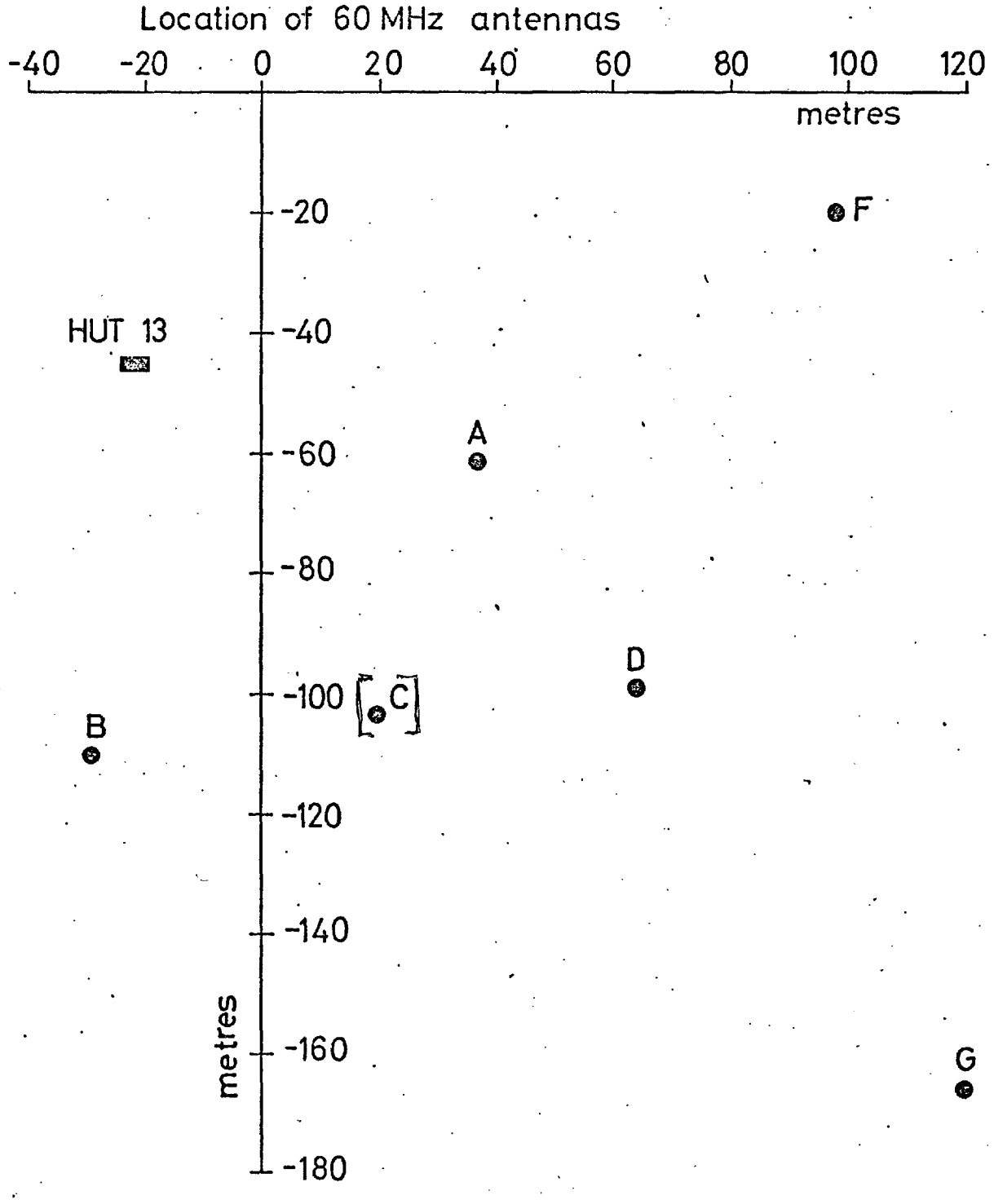
Location of 60 MHz antennas
-40
-20
0
20
40
60
80
100
120
metres
-20
-40
-60
-80
-100
-120
-140
-160
-180
metres
HUT 13
A
B
C
D
F
G

Fig. 24.

of the horizontal electric field. This ambiguity is reduced if two orthogonal horizontal components are known in different directions. Having N-S & E-W and NW-SE & NE-SW polarisations has this advantage in determining the direction of the electric field. This is important for mechanism determination.

The choice of frequency for the array was 60 MHz, as it was found previously that the signal to noise at this frequency was sufficient to permit operation at all seasons of the year. At lower frequencies large changes occur in the level of background noise. The 60 MHz frequency band is not without problems as it is amongst the V.H.F. television frequencies and suffers from pick up in the tail of the bandpass characteristics.

Antennas and sites.

The antennas used are of the folded dipole type. They are constructed out of ½" copper pipe for rigidity and have dimensions as shown in fig. 25. Commercial baluns act as impedance transformers with an impedance ratio of 6:1. A single polarised antenna system consists of two horizontal folded dipoles mounted parallel to each other $\lambda/2$ apart and at a height of $\lambda/4$ above an earth screen. The antennas are coupled together, in phase, via a 75Ω cable $\lambda/2$ in length to a T-junction which is connected to the preamplifier through a relay. The relay is used in calibration procedures carried out from the radio recording centre, located in Hut J3. A complete antenna site consists of two such systems mounted orthogonally with respect to each other in a boxing ring configuration. This type of antenna system is used as it has a suitable bandwidth and polar gain. The impedance figures and polar diagram are given in figs. 26 and 27. A subsidiary experiment was carried out to test the polar gain of

FIG. 25: THE 60 MHz ANTENNA SYSTEM.

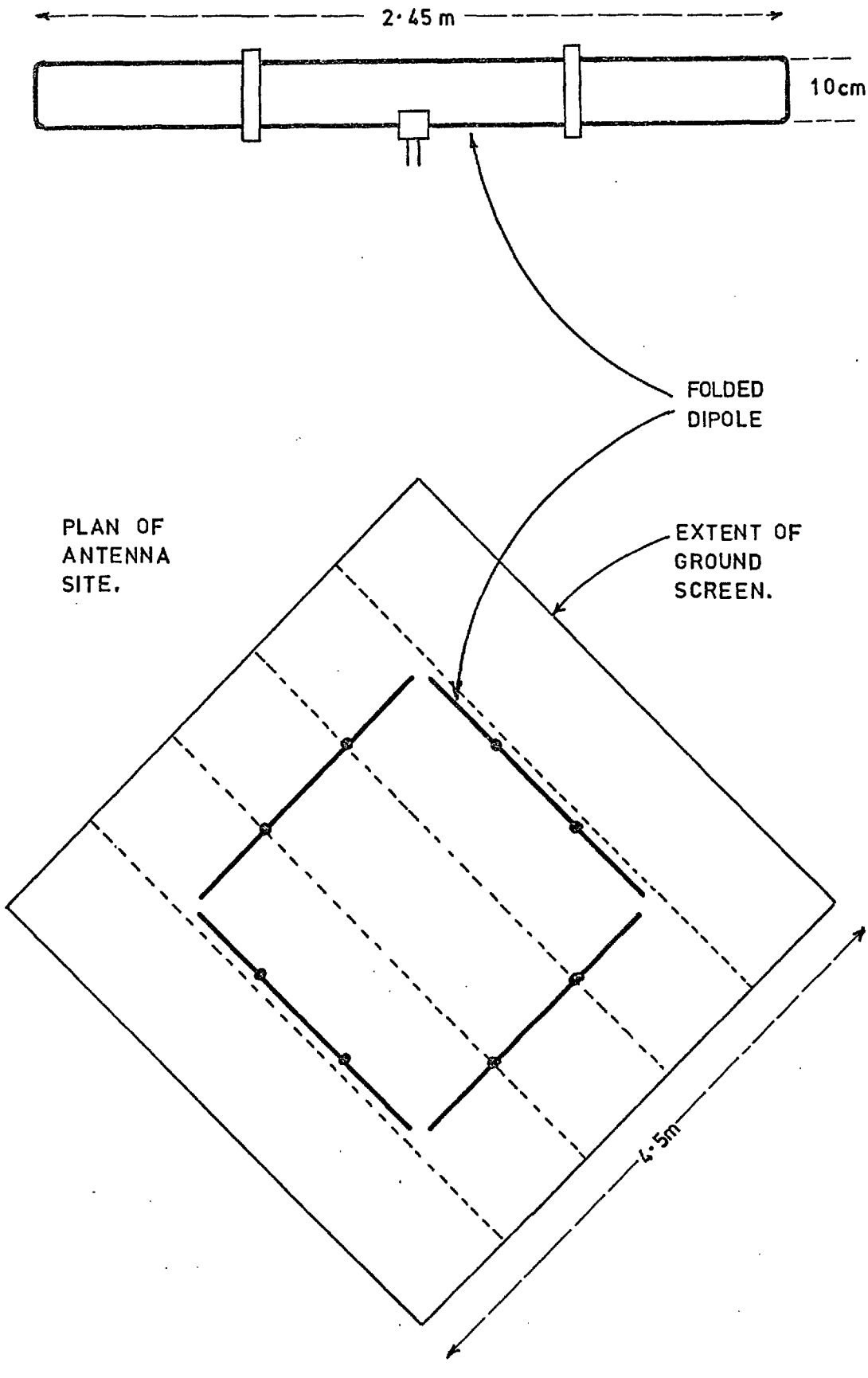

FIG. 26: IMPEDANCE FIGURES FOR A SINGLE ANTENNA SYSTEM.

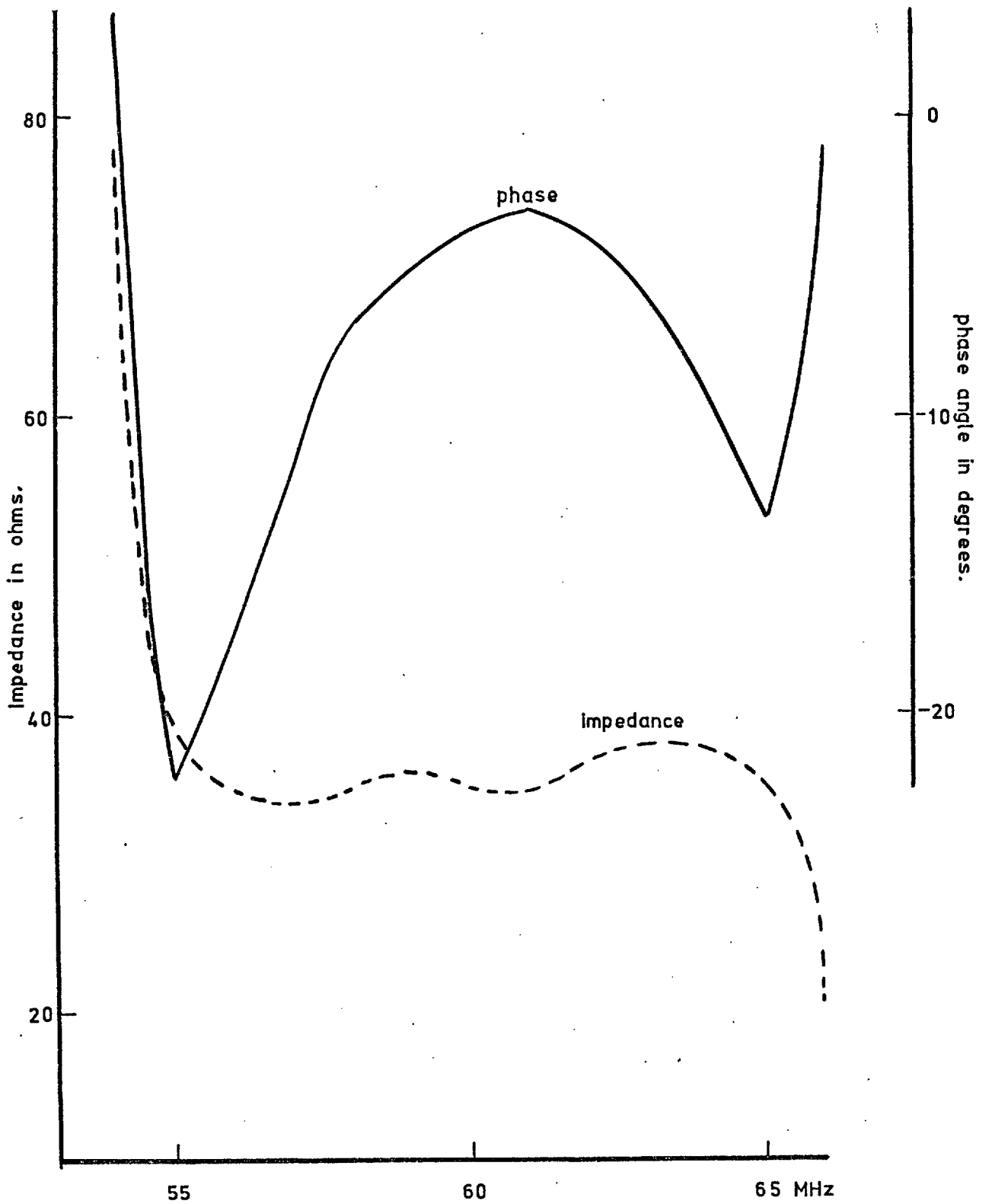

FIG.27: NORMALISED POLAR DIAGRAMS FOR E-W ANTENNAS.

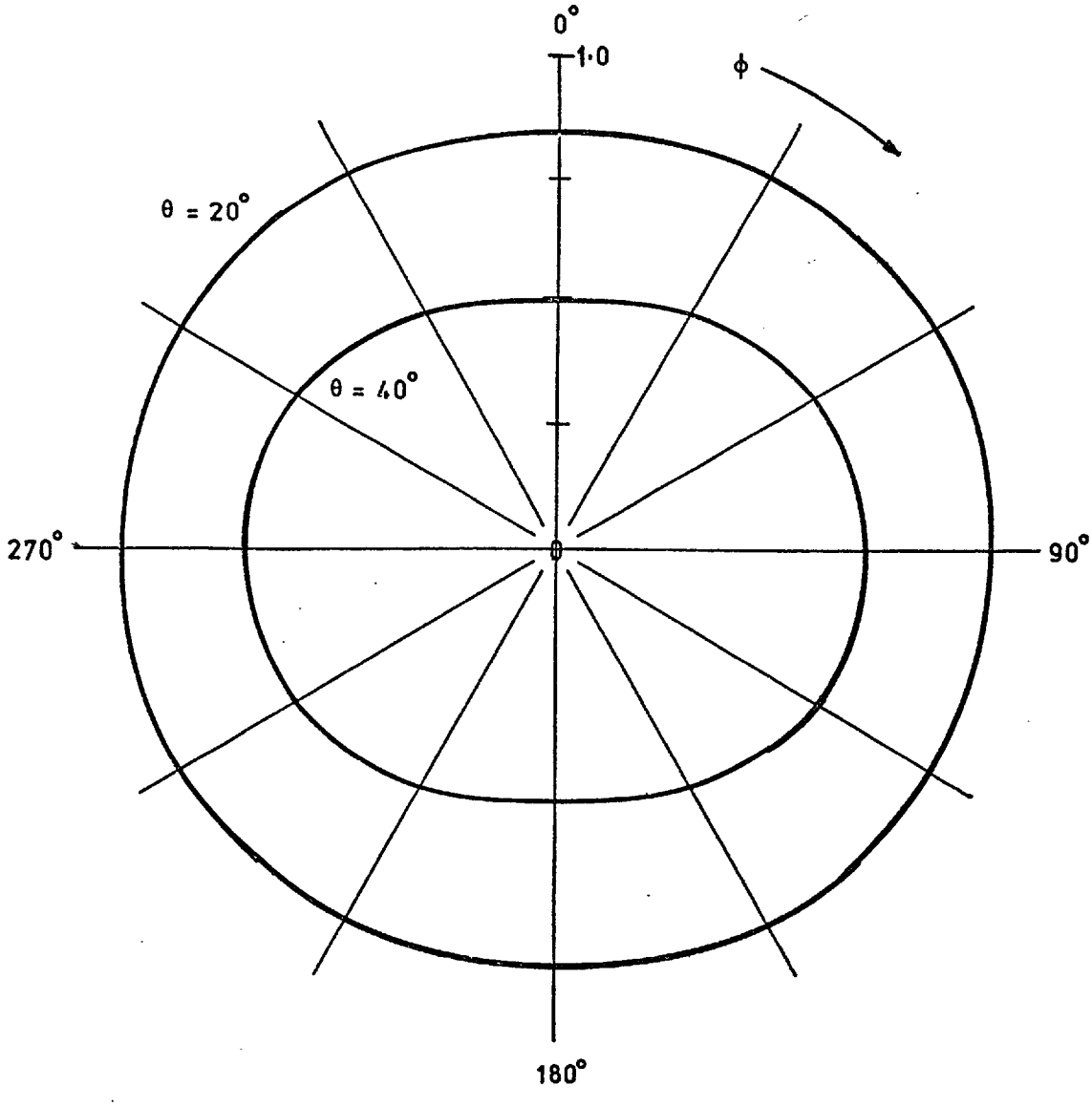

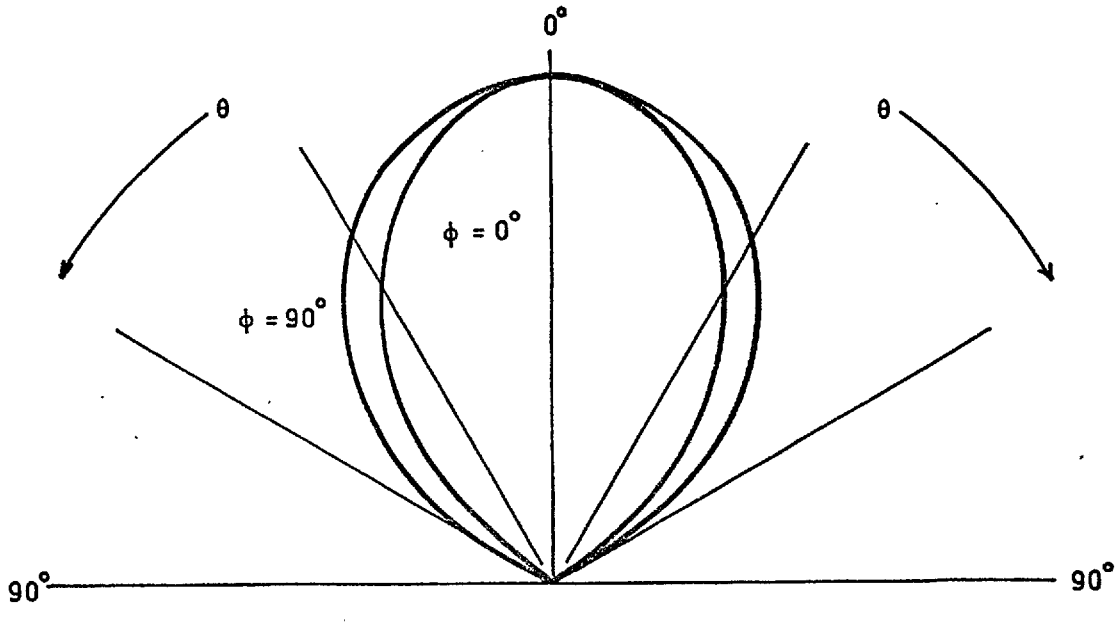

system. Two single dipoles were set up with the same polarisation as the system at site A at a distance $\sim 3\lambda$ from the boxing ring. The technique used was to make simultaneous observations through two different antenna systems at the same point in the shower plane for each observable shower. The experiment was left in operation for a month and results were analysed in the following way. It was assumed that the polarisation of the electric field falling on both systems was the same. This means that the ratio of the two horizontal components are the same for both systems. If experimentally these ratios are found to be the same then the polar gain of the boxing ring system can be trusted since polar gains of single dipoles are well known. The systems were found to agree for showers with zenith angles $\theta \leq 40^\circ$. In the range $40^\circ < \theta < 60^\circ$ two of the nine observed showers showed a slight disagreement. From this it was concluded that the polar giagram of the folded dipole in the boxing ring configuration can be trusted out to 40°.

The gain of an antenna can be expressed through the power it absorbs from a given radiation field, E volts/metre. The nett power flux at the antenna is $E^2/120\pi$ watts/m^2 and the power absorbed by the antenna:

$$W = \frac{E^2}{120\pi} G(\theta,\phi)$$

where $G(\theta,\phi)$ is the effective area presented to the field in the direction (θ,ϕ). A natural unit of area for radiation of wavelength λ is $\pi\lambda\!\!\!^{-2}$ where $\lambda\!\!\!^{-} = \lambda/2\pi$. One therefore writes:

$$G(\theta,\phi) = g\,\pi\lambda\!\!\!^{-2}\,a(\theta,\phi)$$

where g is the maximum power gain, $a(\theta,\phi)$ is the normalised polar diagram and equals one for $\theta = 0^\circ$. For the boxing ring

antennas g = 9.8 calculated from the mutual impedances (Kraus, 65). If the input of the receiver has an impedance of R ohms, then the voltage appearing across the input is:

$$V_R = (RW)^{\frac{1}{2}}$$

For $\theta = 0°$

$$E = 0.52V_R \text{ V/m.} \quad \text{for the system.}$$

The r.f. system.

A complete channel consists of a preamplifier under a weatherproof cover at the antenna site connected via a 50Ω cable to a booster amplifier at the main radio hut (Hut 13). Depending on the time at which the signal is to be displayed it is passed through appropiate delay cables. The inevitable attenuation makes booster amplifiers essential. Further amplification takes place in the main amplifier where there is also a linear detector stage. The output from the main amplifier is fed into a multiplexer unit where the video signal receives further amplification and is channelled to its appropiate time window for display on the scope (see fig. 28). The system impedance in 50Ω throughout from the input of the preamplifier to the input of the multiplexing unit. Subsequently the impedance level is 1500Ω . The inputs of all devices were matched to within 5% of 50Ω . The output impedances varied by up to 30% of 50Ω at 60 MHz. Careful matching of inputs or outputs is important as this removes ghost pulses. In this case it was much easier to match inputs than outputs. Matching was easy to attain as all devices had surplus gain. Except at the preamplifiers, matching was achieved using matching attenuators connected to the inputs. A loss of gain is unimportant. For the preamplifiers which had reactive inputs, matching to 50Ω at 60 MHz

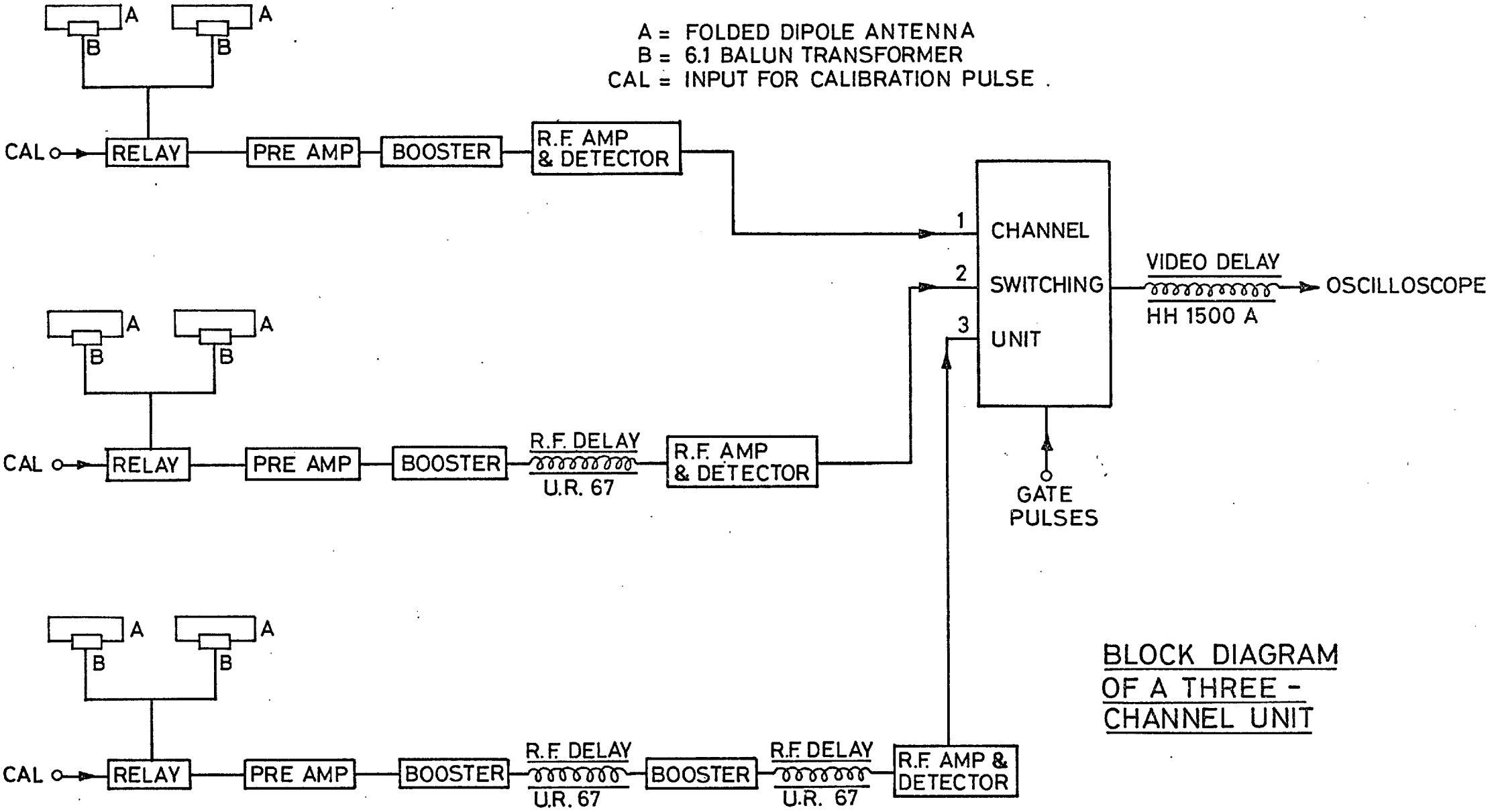

BLOCK DIAGRAM OF A THREE - CHANNEL UNIT

Fig. 28.

was done with the aid of a Polyskop and a Hewlett Packard impedance meter. The electrical gain was adjusted throughout the system to prevent saturation at an early stage. Table 1 shows typical values of characteristics for a single channel. The bandwidths of the channels are essentially determined by the preamplifiers, as their bandwidths are smaller than those of following amplifiers. This was done in order to prevent saturation of sucessive stages.

The display system.

By using a multiplexing system and suitable delays it is possible to display three radio channels on a single scope trace. The trace was divided into three portions by two blanking markers during which time switching by the multiplexers occurred. The drive pulses for the multiplexers are generated by a chain of flip-flops which are triggered off by the Local Trigger (see fig. 29). The flip-flops also provide the blanking markers for timing measurements. The blanking of the scope is done in such a way that the portions displaying the radio channels are brightened up instead of suppressing the trace when switching occurs. In this way spurious pulses triggering the scope do not expose the film when there is no Local Trigger. A 10 μS trace is divided into three bright portions of ~3 μS separated by two blanking markers of ~0.3 μS. There is no additional delay on the signal displayed first, but the second and third have delays of 2.5 μS and 5 μS. Between the multiplexers and the scope there is an additional delay of 4.5 μS which stores the signal for the time it takes the 500m array to detect a coincidence.

When there is a Local Trigger the timing sequence of the flip-flops is initiated and a gate is opened to receive a Main Array

TABLE 1: CHARACTERISTICS OF A SINGLE CHANNEL.

Bandwidth	6.4 MHz.
Gain	82 db.
Gain of multiplex unit	6 db.
Noise figure of preamplifier	4 db.

TABLE 2: R.F. DELAYS IN THE SYSTEMS INCLUDING THE ADDITIONAL DELAY DRUMS.

SITE	CHAN. No.1.	CHAN. No.2.
A	3.25	3.21
B	0.68	0.69
D	6.02	5.91
F	3.26	0.93
G	5.99	6.88

The delay times are in microseconds and are due only to the passage of the signal through cable (Uniradio UR67).

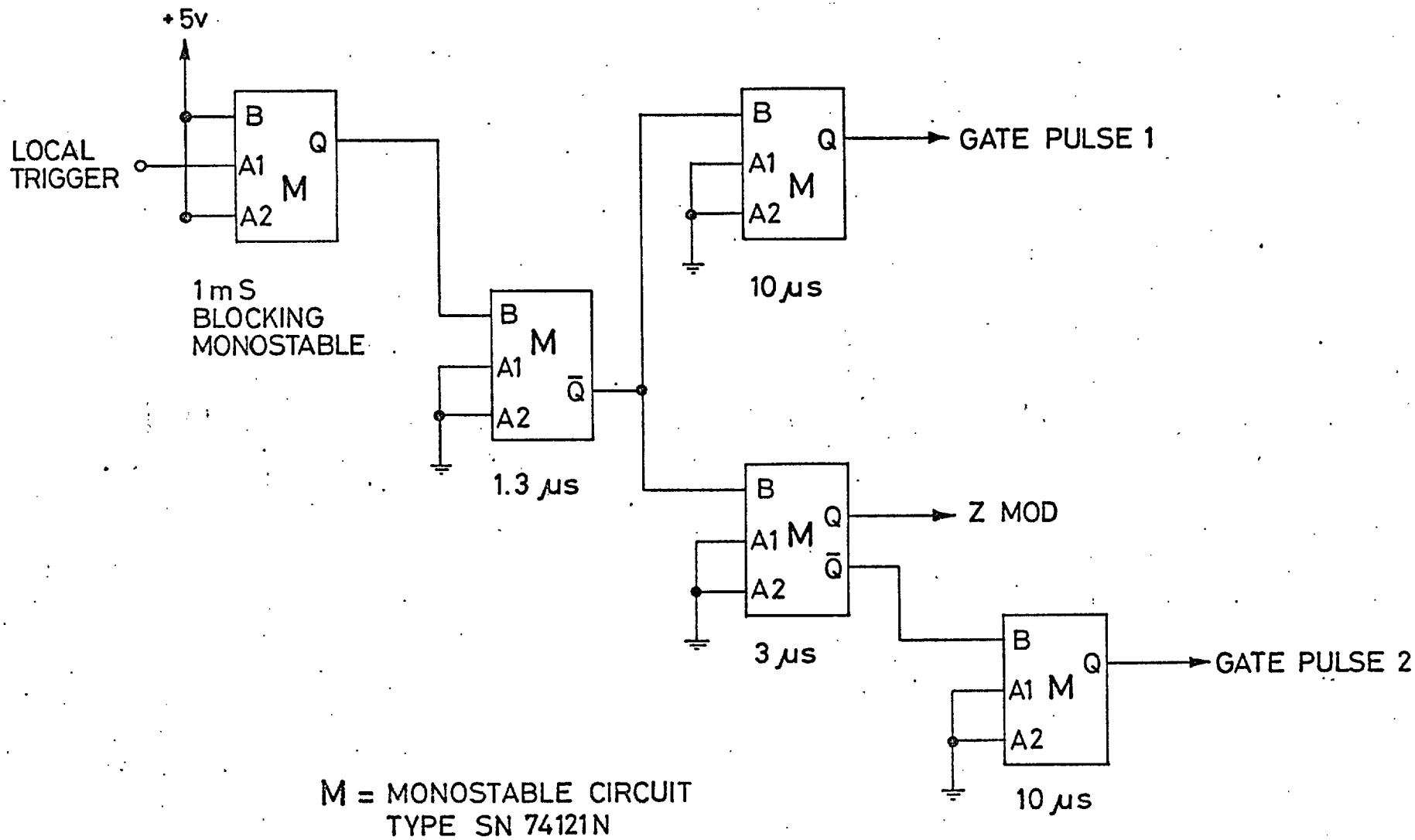

Fig. 29. THE FLIP-FLOP CHAIN

Trigger. The Main Array Trigger arrives later: it triggers the scope and causes the film to move on in the camera after exposure. The scope trace is recorded on 35 mm film together with a register number which is related to the time of day. The display system has a dead time of 1 mS.

System calibrations.

1) Absolute calibration.

The experimental setup is shown in fig. 30. The output from a C.W. radio frequency oscillator Marconi, type 901A, is modulated with a 10 μS pulse at a rate of 2 kHz and fed via an attenuator matching pad to the input of the preamplifier. The output is observed and measured on a scope coupled directly to the output of the main amplifier. The C.W. oscillator is set at 60 MHz and the amplitude is varied using the calibrations on the control dial. The voltages appearing on the output of the attenuator pad are related by a constant factor to the voltages on the control dial; thus a curve of output versus input voltage is obtained. The linear portion of this curve gives the gain of the system up to the output of the detector stage. The gain of the whole system is obtained by multiplying the slope of this response curve by the gain of the multiplex units which are linear devices and saturate well after the r.f. stages saturate.

2) Bandwidth measurement.

To measure the bandwidth, the same experimental setup is used as for (1). An input level in the linear region of the response curve found above is selected. The frequency of the oscillator is varied in 1 MHz steps and the output versus frequency curve is plotted until the output falls to noise level. The bandpasses are also viewed on the Polyskop to check if there are any rapid

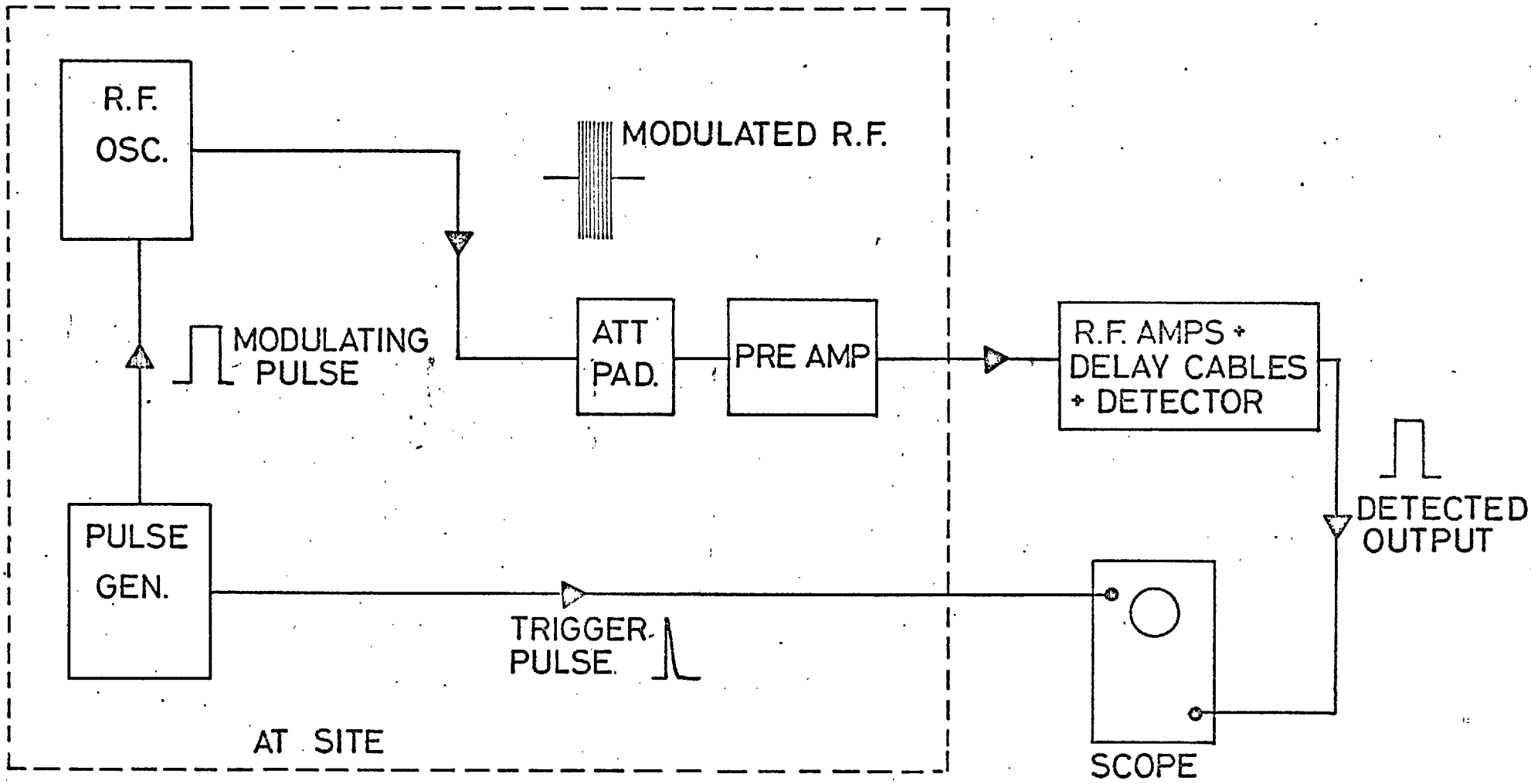

PULSED C.W. CALIBRATION OF SYSTEM

Fig. 30.

variations which might be overlooked because of the 1 MHz steps used in the calibration. In all cases no rapid variation was seen.

Two approaches were used in the evaluation of bandwidths. The first was to calculate a bandwidth defined by:

$$\delta\nu = \int \frac{G(\nu)d\nu}{G(\nu_o)}$$

The contribution to the bandwidth from the tails of the bandpass curve was estimated by extrapolation. On average the tails were found to contribute ~3% of the total bandwidth. The second approach was to normalise the bandpass curves calculated for several tuned circuits in cascade at the 3 db points. The bandpass curve of n tuned circuits in cascade is given by:

$$B_n = \frac{1}{Q^n}\left[y^2 + \frac{1}{Q^2}\right]^{\frac{n}{2}}$$

where Q is the Q value of the circuit and

$$y = \frac{\nu}{\nu_o}\left(1 - \frac{\nu_o^2}{\nu^2}\right)$$

It was found that the bandpass determined by both approaches were within ~10% of each other. In successive recalibrations of the system the first method of estimation was adopted.

3) Pulse calibrations.

The experimental setup for the pulse calibration is given in fig. 31. It uses a 10 nS input pulse. The purpose of calibrating this way is that it tests the whole system in a manner very similar to which the system is used. The results obtained in the absolute C.W. calibration are in fact trustworthy only for small signals, since non-linearities appear at smaller input voltages with C.W. than they do with pulses. To calibrate with pulses the 10 nS pulse is fed into the preamplifier via a variable attenuator.

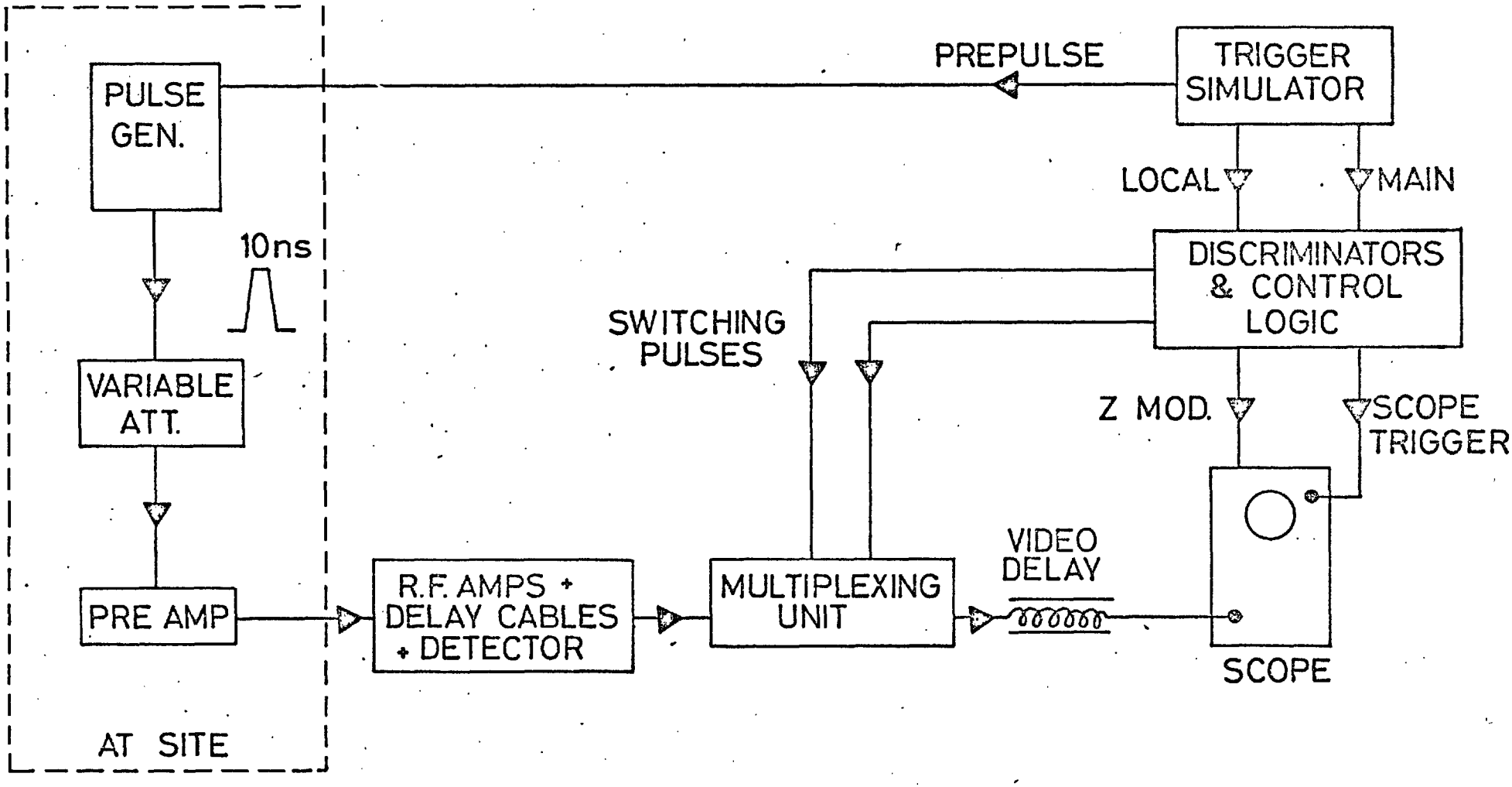

PULSE CALIBRATION OF SYSTEM

Fig.31.

The output is observed on the recording scope. The curve of output versus attenuation factor is obtained. As it is difficult to measure the amplitudes of short pulses the linear portion of this curve is given the same gradient as that of the linear portion of the absolute C.W. calibration curve. This makes the measurement of the amplitudes of short pulses unnecessary.

Calibrations of the kind described above are carried out at intervals of two months. In addition to this, the gains are checked for variation every 3-4 days internally from Hut 13. A 10 μS pulse of 60 MHz C.W. is fed into the preamplifiers at each site for three fixed levels of input. The variation in the output is recorded and is used in computing the field strength.

4) Automatic calibration.

It was found that the gains fluctuated on average ~15% and at most 30%. Temperature changes appear to be the principal cause. The daily range of temperature variation during winter months is slow and can be tracked with sufficient accuracy with the internal calibrations at 3-4 day intervals. However, the daily fluctuation of temperature during summer months is much greater. It was therefore decided to install a system which provided a calibration pulse after every event. The calibrator consisted of a 60 MHz crystal-controlled oscillator and a fast gate to provide pulses of 60 MHz. A single pulse of C.W. was fanned out through attenuators and then distributed to the preamplifiers at each site. After each air shower event, relays on the preamplifiers were switched from the antennas to receive a calibration pulse. The output from this calibration is recorded on the film after each event and incorporated in the calculation of the field strength.

5) Timing.

A calibration to evaluate delays in the system was carried out with the purpose of locating the expected position of the radio pulse on the film trace as this greatly aids subsequent film reading. The electronic delays were measured to the sites by timing the arrival of the reflection of a pulse sent down the cable. The scope used in this measurement was a Tektronix 556. This has a facility which enables timing to be done with an accuracy of 20 nS. Delays from the sites are given in table 2. The r.f. delay in the drums of delay cables are also measured in this way.

Accuracy of calibrations.

All of the preceding calibrations with the exception of (5) depend on voltage amplitudes read off a scope. The accuracy to which a scope can be read is 0.5 mm which is 1% of the largest deflection read. The accuracy of the calibrations are about 2-3% at full scale deflection. This could be inferred by feeding a signal into the scope and then doubling it using high quality attenuators. The noise in the system is a major contributor to the sources of error. For large voltages the error is that of the scope. For smaller voltages the noise level remains the same but the signal drops, also reading becomes more subjective as "the middle of the noise" has to be determined. In the evaluation of bandwidths the error is probably less than 10%. It is found that successive calibrations of the same bandwidths gave values varying by 7%. About the same accuracy can be claimed for the other calibrations as a reading of a scope is involved and a single parameter is evaluated from several readings, e.g. bandwidth, slope. Before each calibration is carried out, the scope itself

is calibrated.

Noise.

The main source of noise at Haverah Park, when television is off, is cosmic noise. The level of the noise observed is comparable to the values given by David and Voge (69) at 60 MHz. Television interference was more severe on certain sites than others. Fig. 32 shows the level of television signal picked up in decibels above the background at 60 MHz as it appears on the antennas. Fig. 33 shows its appearance through the system. To reduce the amount of the television signal picked up a bandpass filter of the type described as a coil saving bandpass filter (Zverev, 67) was included in the system. The result of the inclusion of the filter is shown in fig. 34. The filters have an added advantage in that the bandwidths are well defined in that there are virtually no tails at high and low frequencies.

The presence of noise in any system causes errors in the measurement of a signal. The noise can either add or subtract from the signal. The quantity which is measured is signal plus noise added taking account of phase. For a continous signal the problem can be overcome by using a square law detector which has a transfer characteristic:

$$V_{out} = AV_{in}^2$$

The input voltage is signal plus noise, hence:

$$V_{out} = A(V_s + V_n)^2$$

$$= A(V_s^2 + V_n^2)$$

since $V_s.V_n$ averages to zero. The noise can be measured in the absence of signal and then be subtracted out and the input signal

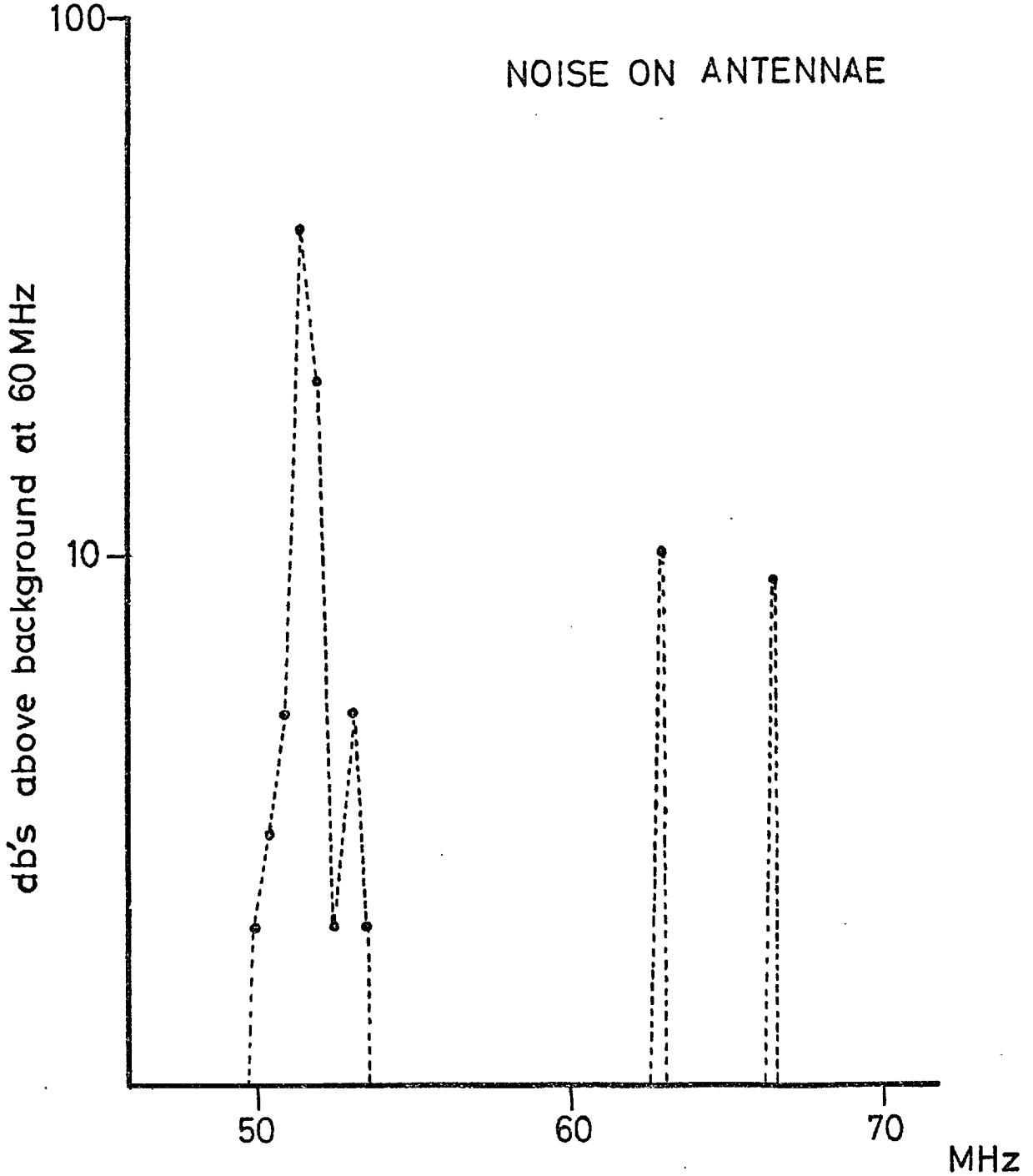
NOISE ON ANTENNAE
100
10
db's above background at 60 MHz
50
60
70
MHz

Fig. 32.

FIG. 33: APPEARANCE OF NOISE THROUGH SYSTEM.

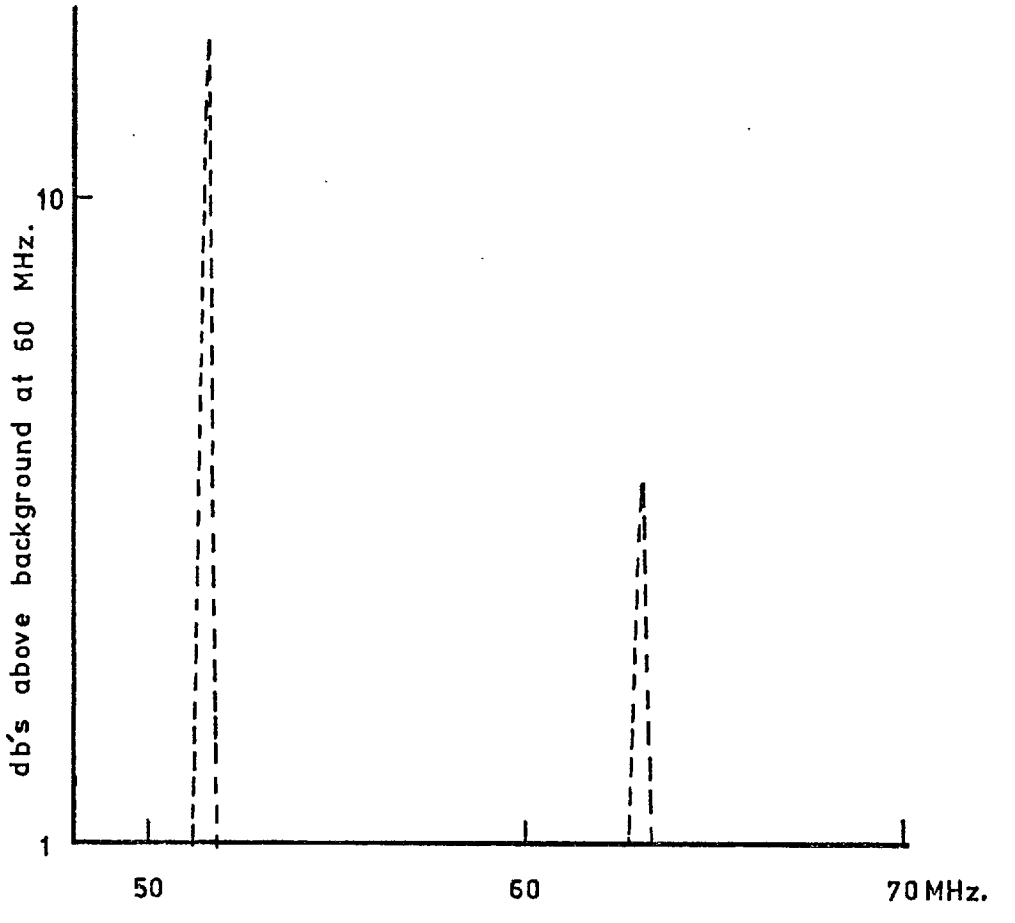

FIG. 34: NOISE SEEN THROUGH SYSTEM WITH FILTERS.

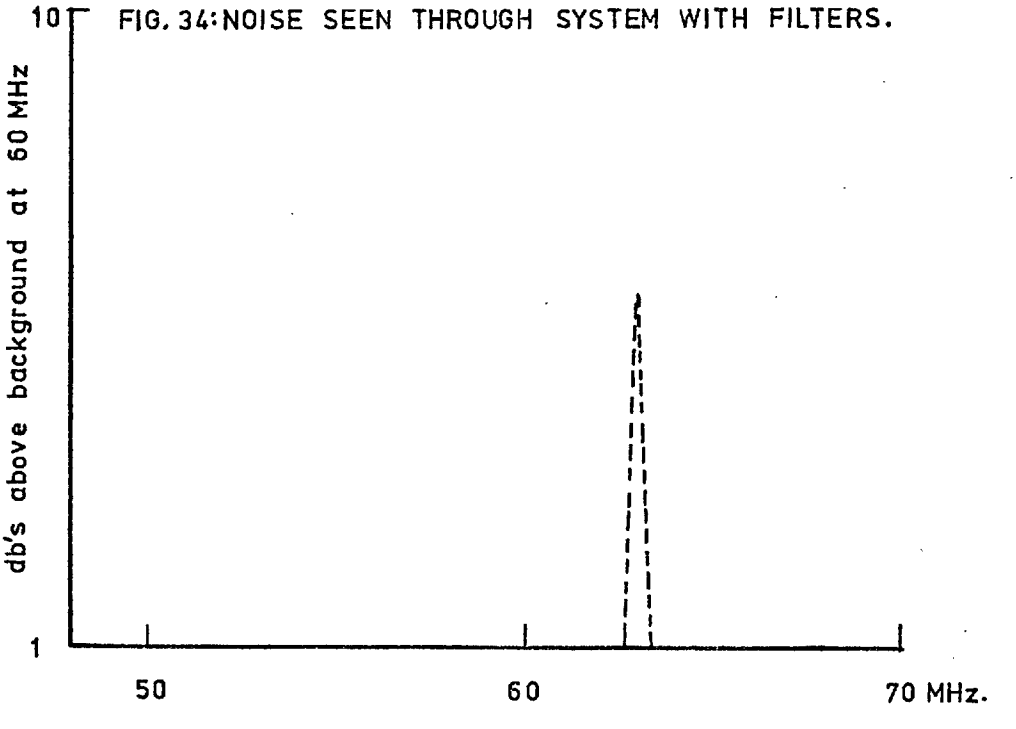

obtained. The radio signals with which we are concerned are impulses which last for a short time ($\sim 1/\delta\nu$) during which phase relations change only little. So $V_s.V_n$ does not average to zero and remains unknown. In the present experiment, linear detectors are used and a pulse amplitude consisting of signal plus noise is read together with the surrounding noise level. For our purposes linear detectors are more suitable. If there is C.W. present on the antenna this causes a change in the level of D.C. at the output. For a linear detector the output signal and noise adds or subtracts from the D.C. level. For square law detectors, the output signal and noise is also a function of the D.C. level. Linear detectors also have an advantage over the square law detector in that they allow a greater dynamic range.

Analysis of data.

A record of a shower consists of two frames of 35 mm film, each frame on a separate film. A record is read if there is one or more channels with a signal of height twice the largest peak noise pulse (~4 times r.m.s. noise level). The signal must also arrive at the expected time to be accepted as a genuine radio pulse. In reading a pulse height a zero line has to be fitted to the lowest excursions made by the trace. A trace is rejected if there is a large amount of C.W. contamination on the channel. Severe C.W. contamination manifests itself by causing the trace to drift in the time of observation. Together with data provided by the 500m array, field strengths and perpendicular distances are computed to give the lateral distributions of those showers which have a $\chi^2 \leq 2$ for the particle data. The data is also examined to determine the radiation mechanism. The results are presented in the next chapter.

Chapter Four

Experimental Results.

Present results.

The radio array has been in operation since June '72 and since then 109 showers of zenith angle $\leq 40^{\circ}$ which satisfy conditions described in the previous chapter have been recorded. The results are analysed with two aims in mind: firstly for a mechanism check on the emission and secondly to study the variation in the height of the shower maximum from the shape of the radio lateral distribution. A mechanism check was carried out by studying the arrival directions of showers producing radio pulses and by comparing the polarisation of the horizontal electric field to that of the theoretical polarisations predicted by different mechanisms. The study of the arrival directions shows that there is a North-South asymmetry and that radio showers tend to have large zenith angles. The angle of dip at Haverah Park is 68° and comparing this to the arrival directions shown in figs. 35 and 36 give a strong indication that the radio production mechanism is one of geomagnetic charge separation. No disagreement was found for the predicted polarisation for the geomagnetic mechanism of the horizontal electric field within the limits of error due to noise. Until the construction of the new array the polarisation could only be checked by comparing the ratio of the horizontal components to the modulus of the theoretical ratio. When there are pulses at sites A or B and D or F or G a sign can also be attributed to the ratio because of the different antenna orientations of A, B and D, F, G. This makes the polarisation test more exacting than previously. For suitable showers the experimental ratios agreed

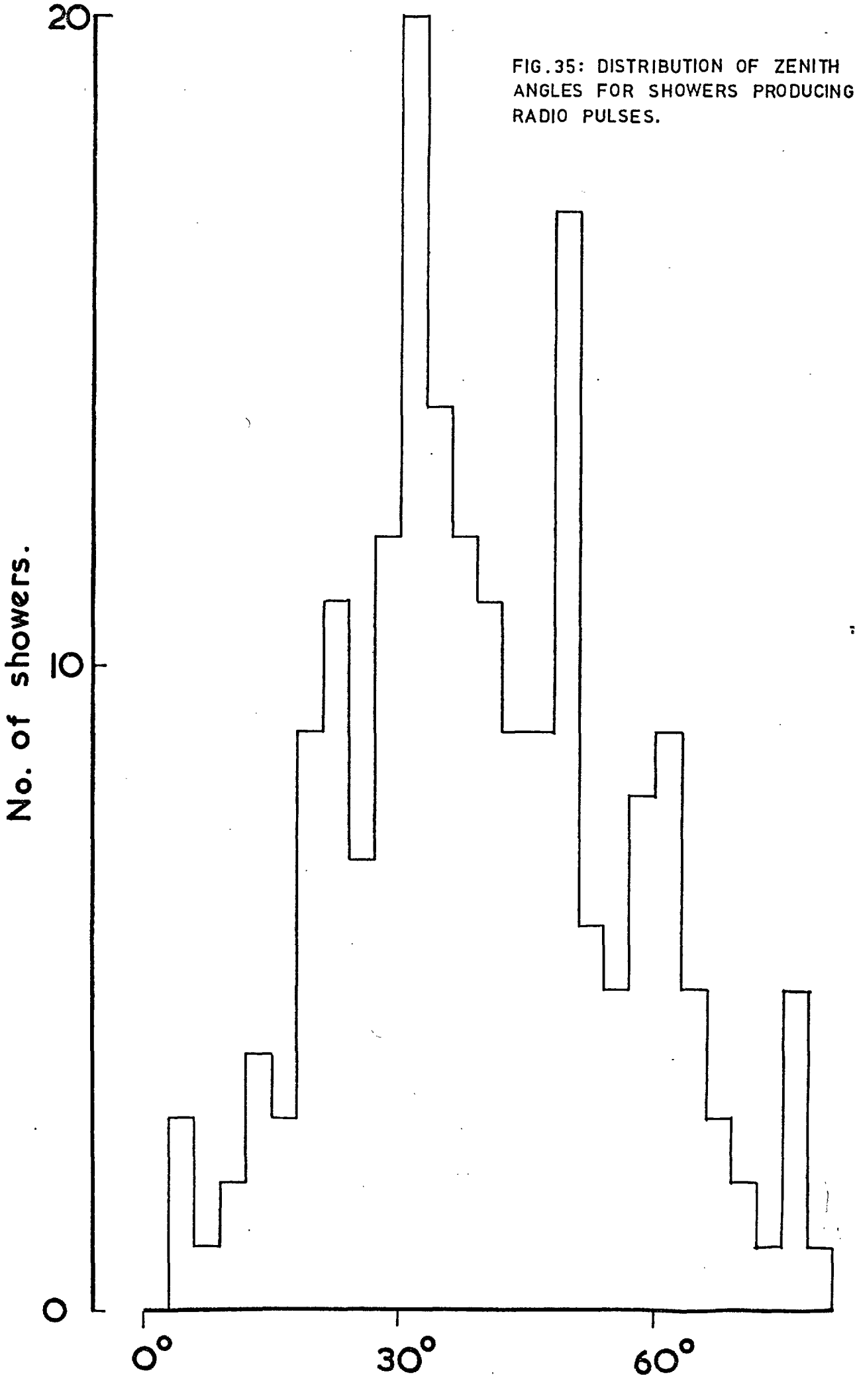

FIG. 35: DISTRIBUTION OF ZENITH ANGLES FOR SHOWERS PRODUCING RADIO PULSES.

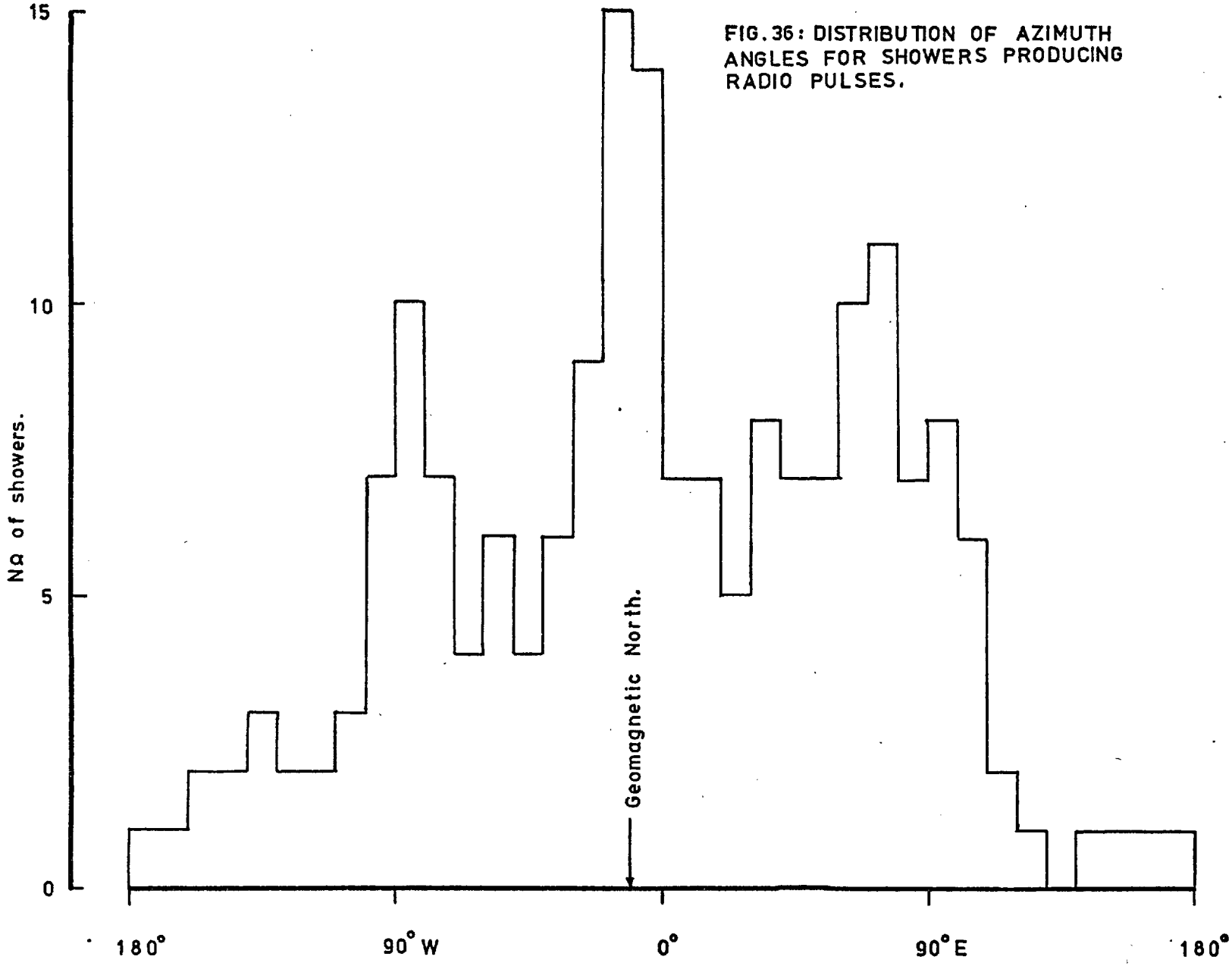

FIG. 36: DISTRIBUTION OF AZIMUTH ANGLES FOR SHOWERS PRODUCING RADIO PULSES.

in value and sign with the predicted ratios.

The experimental lateral distributions are shown in figs. 37, 38 and 39 for different zenith angle ranges chosen so that the height of maximum development of the shower moves away from the antennas in steps of 100 gm. The energies in the first group vary by a factor ~9, while in the remaining groups the factor is ~5. Within any one group there is a mixing of the positions of the radio lateral distributions with respect to energy, although there seems to be a trend for higher energy showers to have their radio lateral distributions displaced downwards, but the number of showers is too small to give a definite indication. Inspection of the lateral distributions shows that with increase in zenith angle the rate of fall of the electric field decreases.

The question requiring an answer in cosmic ray studies is the question of the mass of the primary particle initiating an extensive air shower. Theoretical models for different masses of primary particle indicate that for light particles there is a large fluctuation in the depth in the atmosphere at which the first interaction occurs. For protons the figure quoted is ~100 gm (Turver et al, 73) at a mean depth of 700gm for an energy of 10^{17} eV. The depth of penetration is believed to increase by ~60 gm for a factor of 10 increase in the primary energy. Heavier particles have a smaller fluctuation, somewhat as if they consisted of a superposition of several low energy proton cascades. For a particle with A=50 the depth of penetration is 600 gm for an energy of 10^{17} eV.

As demonstrated by the radio calculations in chapter two fluctuations in the height of maximum cause fluctuations in the radio lateral distributions. It remains therefore to determine if there are fluctuations present in the lateral distributions.

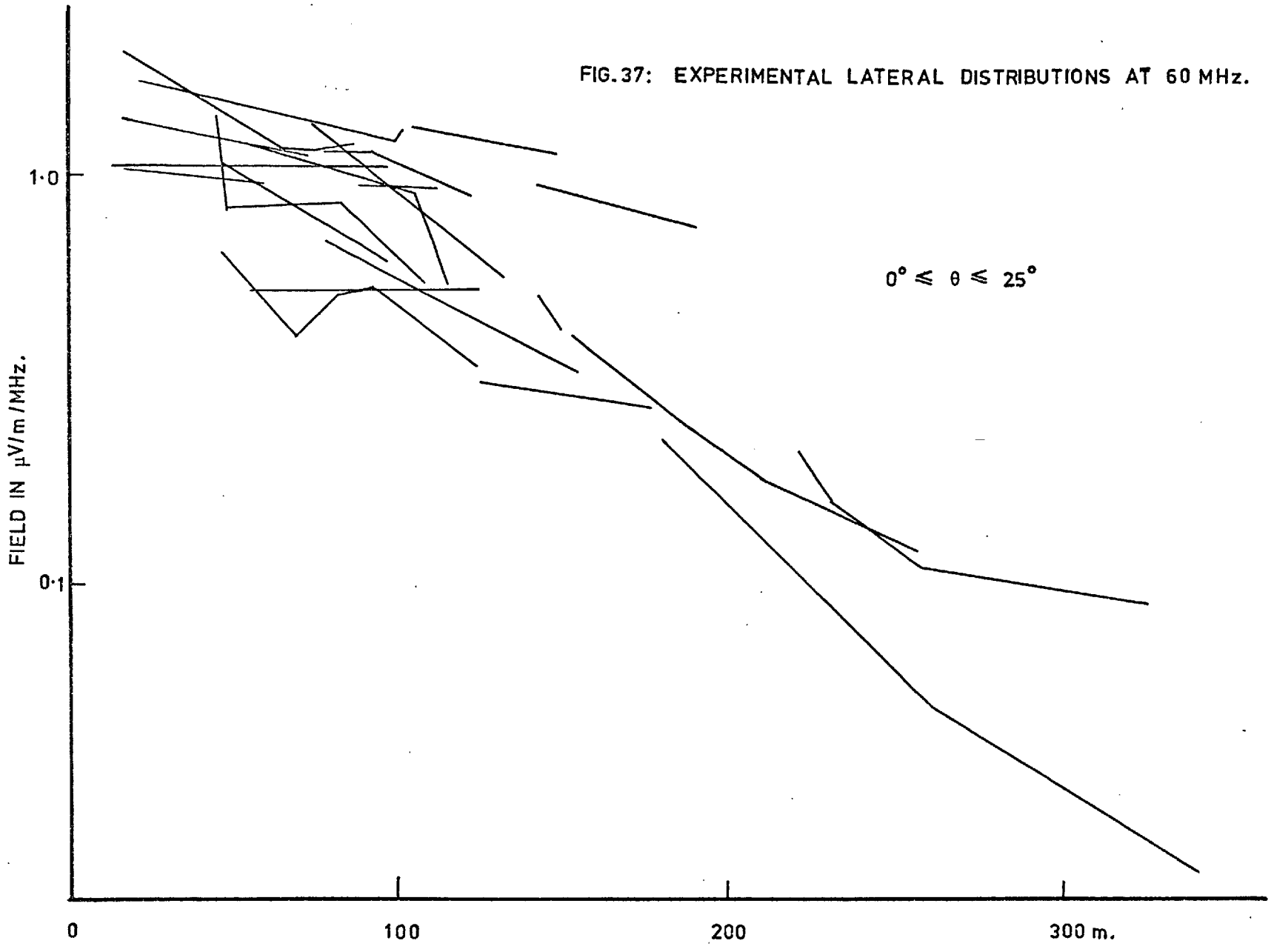
FIG. 37: EXPERIMENTAL LATERAL DISTRIBUTIONS AT 60 MHz.
$0° \leq \theta \leq 25°$
FIELD IN μV/m/MHz.
1·0
0·1
0
100
200
300 m.

FIG. 38: EXPERIMENTAL LATERAL DISTRIBUTIONS AT 60 MHz.

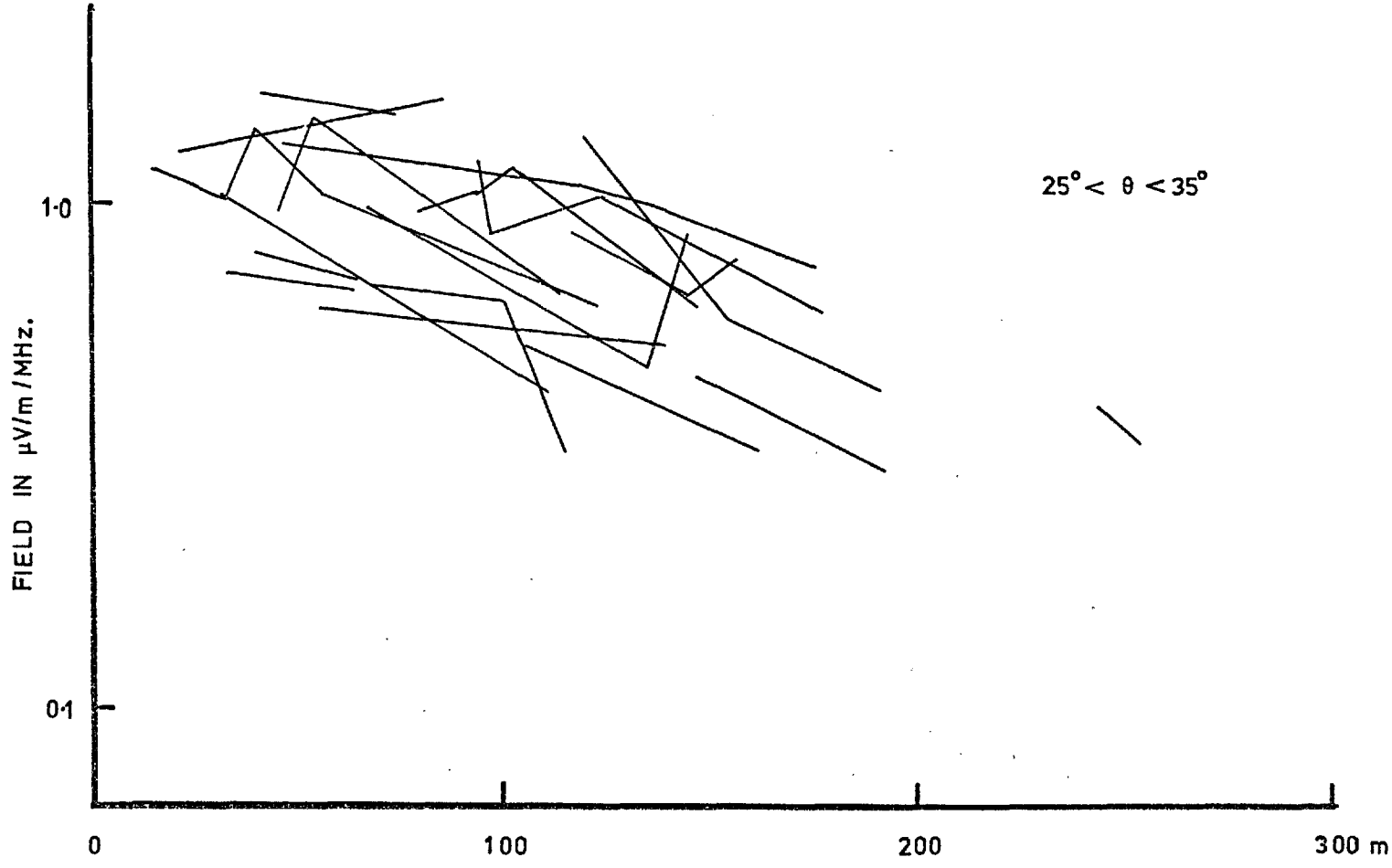

FIG. 39: EXPERIMENTAL LATERAL DISTRIBUTIONS AT 60 MHz.

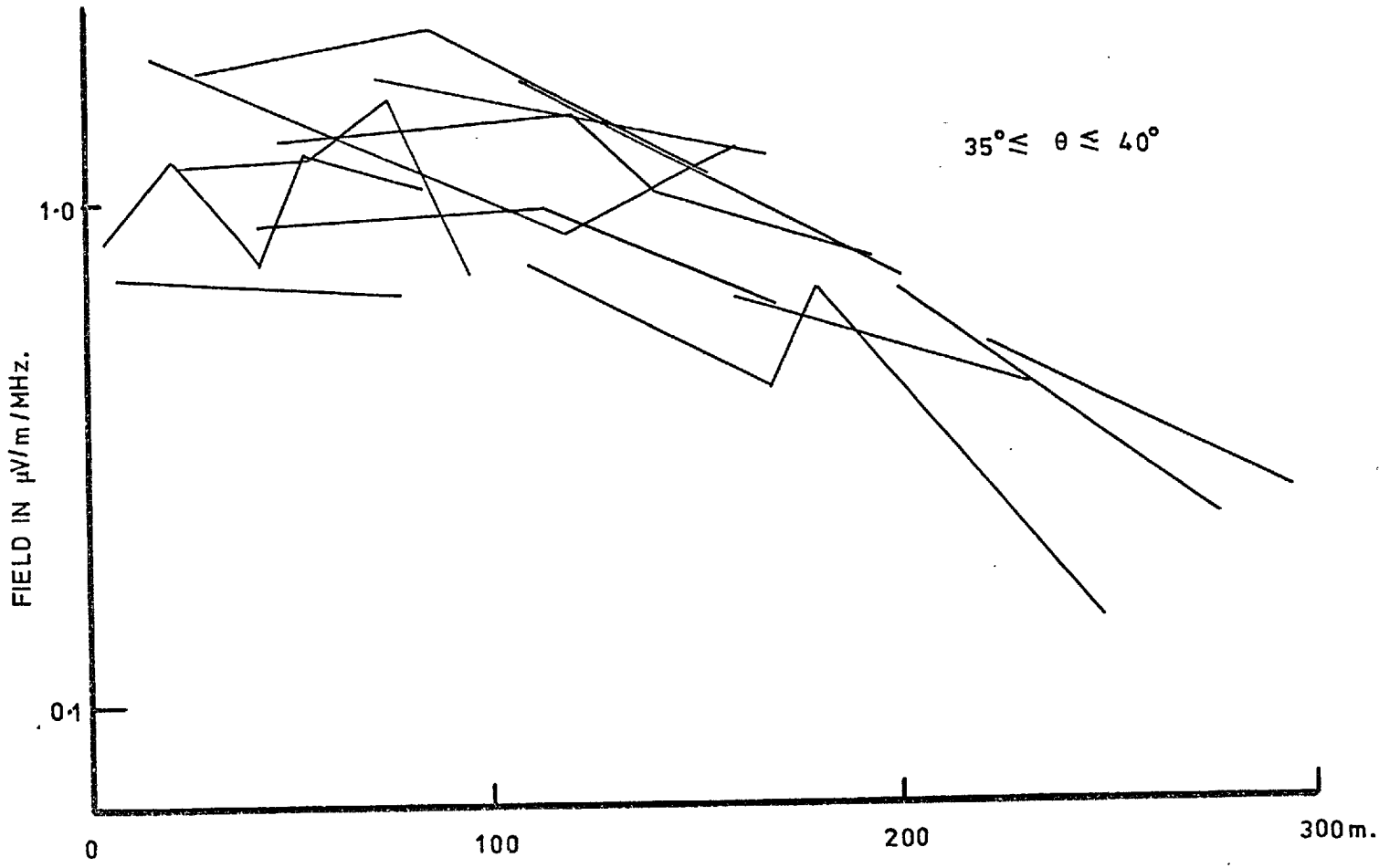

As can be seen from figs. 37, 38 and 39 it is difficult to attribute a parameter to each lateral distribution and relate this to fluctuations in the height of maximum development because the lateral distributions extend over different radial distances. In order to attribute a parameter the centre of gravity was found for the two or more points for each lateral distribution in plot of logarithmic field strength against distance. The centres of gravity and single data points from showers producing only one point with radial distances ≥ 50m are plotted in figs. 40, 41 and 42 for the three zenith angle ranges. A parameter associated with the height of maximum development was attributed to these points by superposing the theoretical lateral distributions on figs. 40, 41 and 42. The theoretical curves act as contours at 100 gm depth intervals. The number of points falling between two contours were binned and a histogram was formed for each of the zenith angle categories. The positioning of the contours on the groups is the same. The resulting histograms are plotted in figs. 43, 44 and 45. Table 3 shows the statistics of the three histograms.

Each bin is of 100 gm width. The three categories are separated by 100 gm due to the zenith angle categorisation and one would expect a difference of 100 gm in the mean values of the distributions. The differences in the mean values of are: 50 ± 45 gm and 110 ± 45 gm. These values are consistent with the expected value. The widths of the histograms do not change systematically with variation in θ and have similar values. From this one may assume that the fit of the contours to the experimental lateral distributions remains the same for the different zenith angle ranges.

A bin width is representative of the possible fluctuations that might occur within a category due to change in energy and

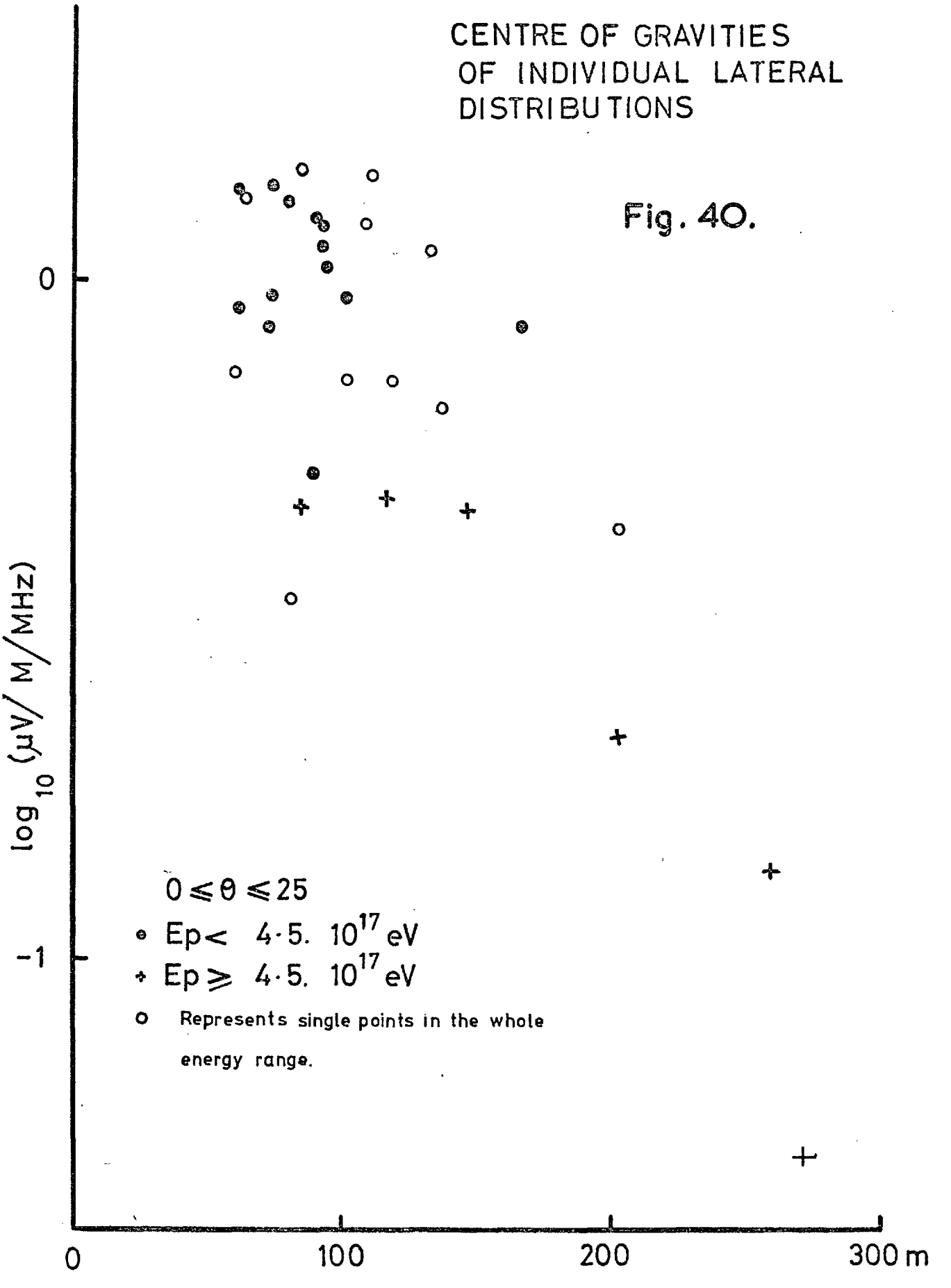
CENTRE OF GRAVITIES
OF INDIVIDUAL LATERAL
DISTRIBUTIONS
Fig. 40.
0
-1
log10 (μV/ M/MHz)
0 ≤ θ ≤ 25
Ep < 4·5. 10^17 eV
Ep ≥ 4·5. 10^17 eV
Represents single points in the whole energy range.
0
100
200
300 m

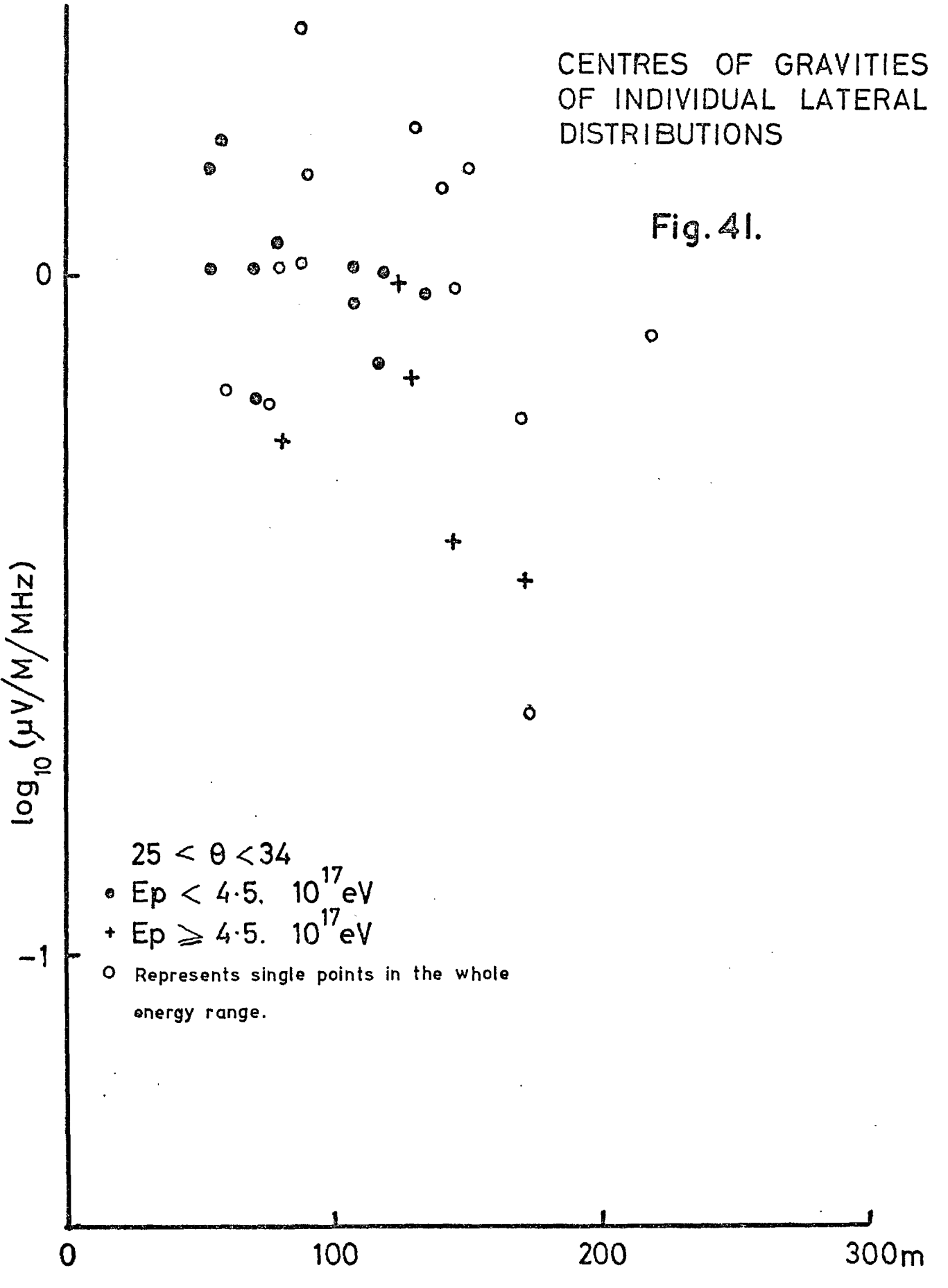
CENTRES OF GRAVITIES
OF INDIVIDUAL LATERAL
DISTRIBUTIONS
Fig. 41.
0
-1
log10 (μV/M/MHz)
25 < θ < 34
• Ep < 4·5. 10^17 eV
+ Ep ≥ 4·5. 10^17 eV
o Represents single points in the whole energy range.
0
100
200
300m

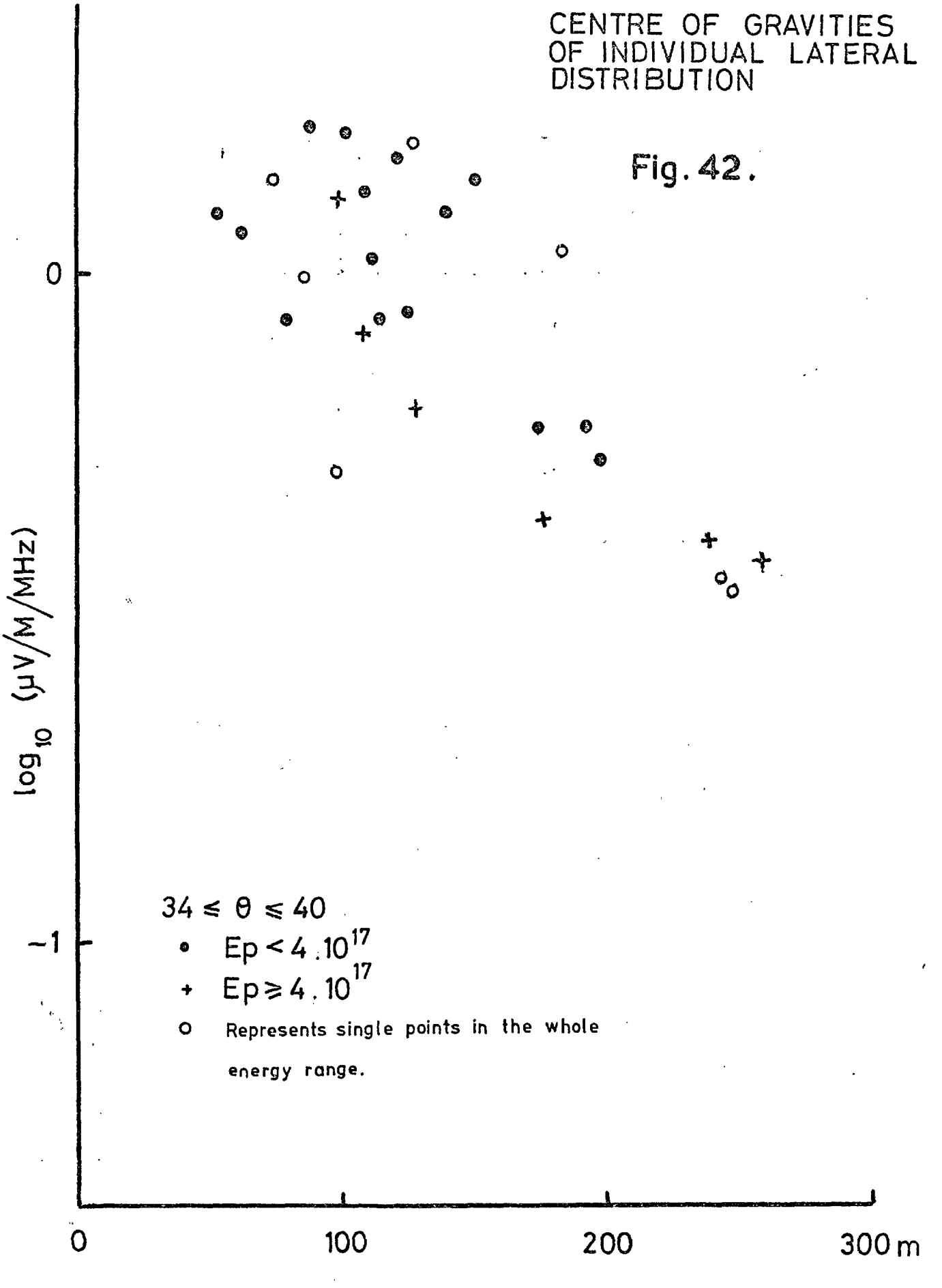
CENTRE OF GRAVITIES
OF INDIVIDUAL LATERAL
DISTRIBUTION
Fig. 42.
0
−1
log10 (μV/M/MHz)
34 ≤ θ ≤ 40
• Ep < 4 . 10^17
+ Ep ≥ 4 . 10^17
o Represents single points in the whole energy range.
0
100
200
300 m

FIG. 43: HISTOGRAMS FORMED FROM EXPERIMENTAL RESULTS AND THEORETICAL CONTOURS FOR : $0^{\circ} \leq \theta \leq 25^{\circ}$

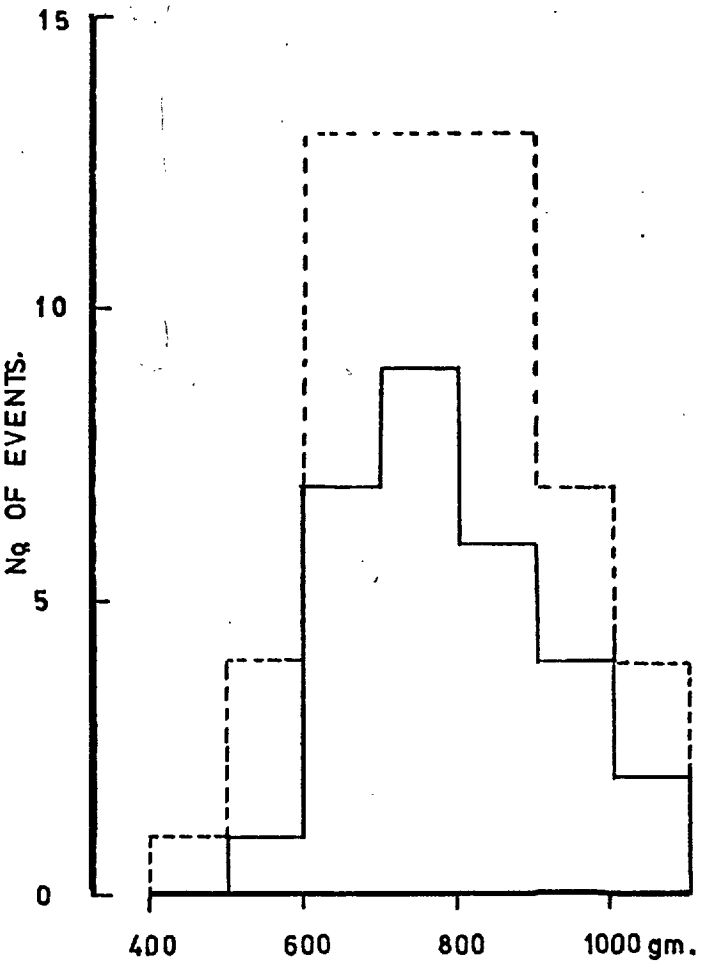

The solid histogram is formed from centres of gravity. The dashed histogram is formed from the individual points for the same showers. Both histograms give the same results.(see table 3)

HISTOGRAM RESULTS

FIG.44: ZENITH ANGLE RANGE : $25^{\circ} < \theta < 35^{\circ}$

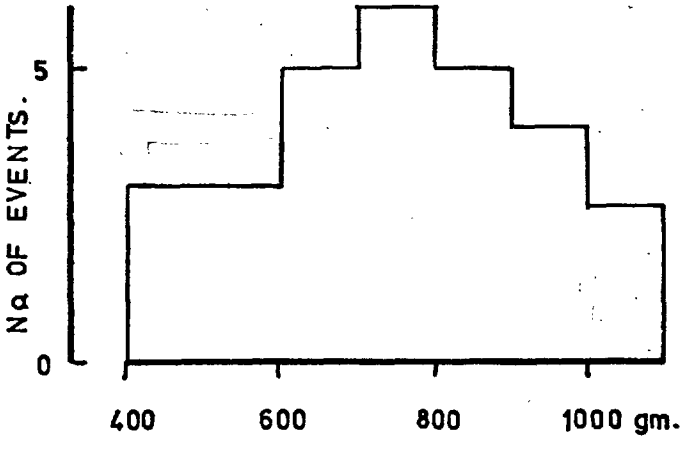

FIG.45: ZENITH ANGLE RANGE : $35^{\circ} \leq \theta \leq 40^{\circ}$

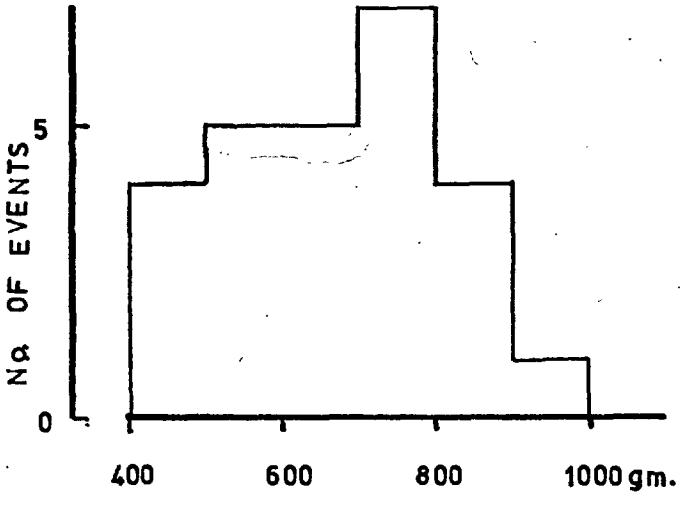

TABLE 3: STATISTICS OF HISTOGRAMS IN FIGS. 43, 44 & 45.

	FIG. 43		FIG. 44	FIG. 45
	SOLID	DASHED		
MEAN:	790 $gm.cm^{-2}$	780 $gm.cm^{-2}$	740 $gm.cm^{-2}$	630 $gm.cm^{-2}$
R.M.S. DEVIATION:	145 $gm.cm^{-2}$	149 $gm.cm^{-2}$	170 $gm.cm^{-2}$	140 $gm.cm^{-2}$
STANDARD ERROR:	27 $gm.cm^{-2}$	20 $gm.cm^{-2}$	32 $gm.cm^{-2}$	26 $gm.cm^{-2}$

variation in zenith angle, thus the width of the distribution may be attributed to real fluctuations in shower development or instrumental fluctuations. Before determining the source of the fluctuations the field strength in the range 80 - 120m is examined. The field strengths are binned to form a histogram which is shown in fig. 46. The mean value is 1.1 μV with a r.m.s. deviation of 0.3 μV. The estimate of the accuracy of the 0.3 μV is ~13%. Theoretical calculations show that for fluctuations in shower development the field strength at 100m from the shower axis also varies. The maximum variation in this field strength due to measurement error is less than 30%.

Returning to the histogram (fig. 43) for showers with $0^\circ \leq \theta \leq 25^\circ$, a 30% fluctuation in the field strength at 130m from the axis together with a variation of ±20m in axis location would lead to a width of 100 gm in the histogram. The width of the histogram is 150 gm (accuracy of 20%). This means that the observed fluctuation is not entirely instrumental but contains a component which comes from shower development. The relative accuracies of the measurements do not permit an estimate of the component due to the fluctuation in shower development apart from that it exists.

A further analysis was carried out using the same data in the range $0^\circ \leq \theta \leq 25^\circ$. Individual shower points at distances greater than 50m from the shower axis together with the theoretical contours were used to form a histogram in the same way as before. The resulting histogram is also shown in fig. 43 (dashed). The results from the second histogram are almost the same as that of the first (see table 3). This gives confidence in the result because it means that it is not a feature of the analysis.

The theoretical contours used in the analysis are those formed from longitudinal developments of the types 1-4 shown in fig. 13.

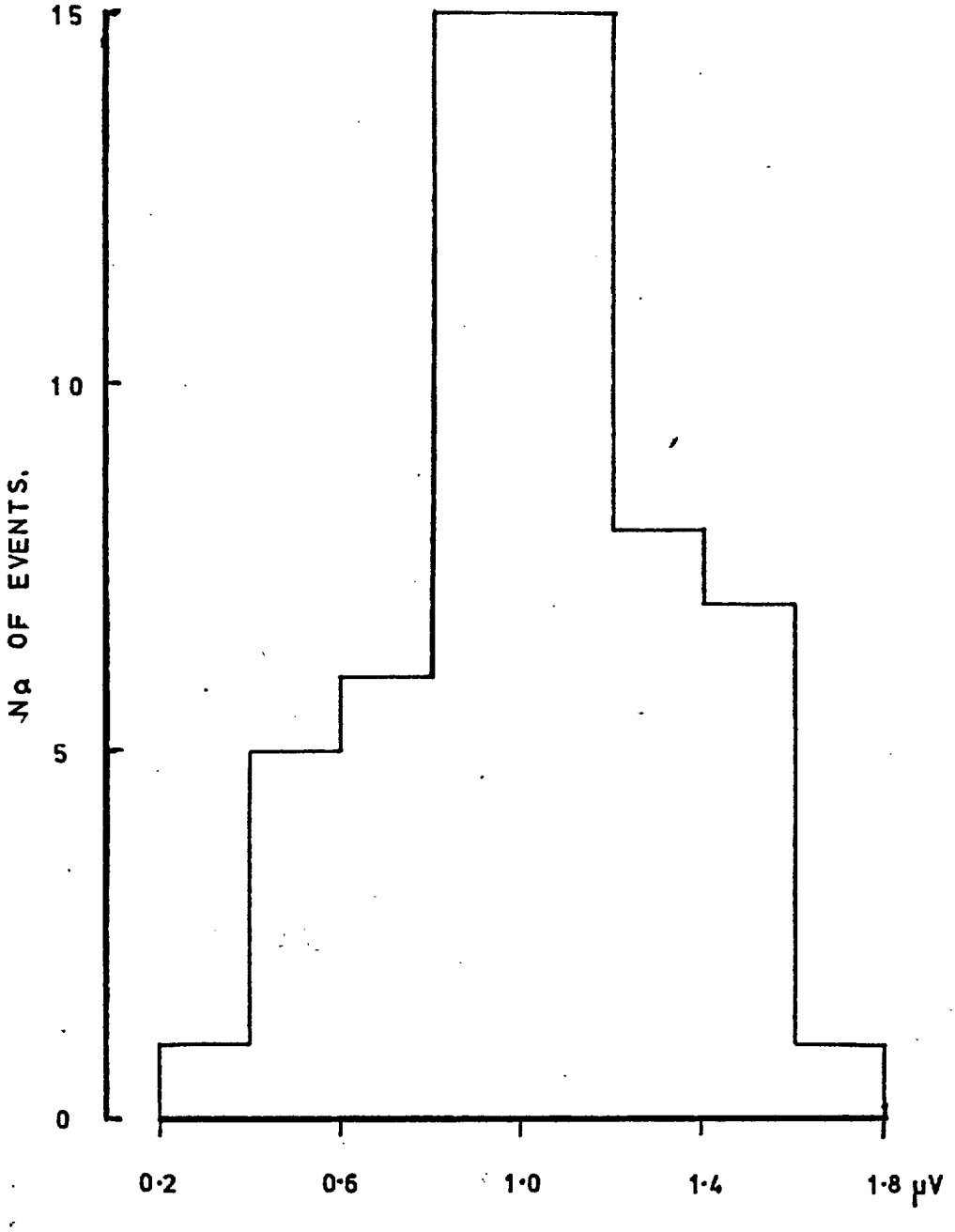

FIG. 46: HISTOGRAM OF THE FIELD STRENGTHS IN THE RANGE 80–120m.

The mean value is 1·1 μV and the r.m.s. deviation is ~0·3 μV. This means that the radio measurement error is < 30%.

These curves which have clearly defined heights of maximum development occur most frequently in the computer simulation of extensive air showers. As can be seen from fig. 13 there are curves which do not have a clearly defined height of maximum. Although such longitudinal developments may exist it is impossible to attribute a height of maximum correctly. The real presence of such showers would cause a scatter in the histograms because of the wrongfully attributed heights of maximum. The conclusion that scatter due to fluctuations in longitudinal developments exists, is still true but the extent of the scatter due to variation in the height of maximum is uncertain.

Chapter Five

Future Developments.

Problems with the present experiment.

There are essentially three problems with the present radio experiment.

1) Noise. - The presence of noise, viz. television is probably the greatest problem. The inclusion of filters has virtually removed the television but has meant a loss in bandwidth of 30% which results in a 30% reduction of radio signal but only a 15% reduction of random noise. The overall effect has been to leave the signal to noise ratio the same as before the inclusion of the filters. The inclusion of filters is an improvement because bandwidths are more clearly defined and the television is removed which leads to an increase in recording time. A solution which was considered before the inclusion of the present filters and may be reconsidered was to widen bandwidths and to use bandstop notch filters to cut out the television. The idea was dismissed at first for three reasons: first the building of good notch filters at 60 MHz presents several constructional problems, and secondly the estimation of the resulting bandwidths presents difficulties, and matching over wide frequency ranges is not easily achieved.
2) Dynamic range. - To deal with the range in energy of the showers observed, ~10, and the variation in the sine of the angle made with the shower axis, ~2.5, one requires a dynamic range of at least 25. The present arrangement has a range of ~15 at most and is set up to accommodate the lower energy, more frequent showers. High energy inclined showers saturate

channels up to 200m from the axis. The dynamic range could be increased in several ways, each having advantages and disadvantages. One simple solution would be to erect more sites with the same gain over a larger area. When there is a large shower saturating certain channels there will be some sites far enough away from the shower axis which will not be saturated. This arrangement has the inherent disadvantage that large showers can only be studied at large distances, but it does increase the collection rate for smaller showers. A better solution would be to increase the size of the array and intersperse lower gain sites among the others. Then high energy showers could be studied over a wide range of radial distances. This solution is less efficient in terms of shower collection because, although there has been an increase in the number of sites, the collecting area has not increased.

The actual cause of the lack of dynamic range is the method by which the data is recorded, photography from an oscilloscope. An oscilloscope has a limited deflection and the gain has to be high enough so that an estimate of the noise level may be made. The obvious solution here is to change the recording method and use digitising techniques with the output recorded on paper or magnetic tape. The solution is an expensive one but will have to be seriously considered if any large expansion in the radio is made. The tedium of reading a large number of channels from film presents a dangerous source of error.

3) Main Array data. - Even after the precision of the radio experiment has been improved there is still the Main Array data to consider and which has its own errors. The most serious errors are those in the estimates of the primary energy and in the shower axis location. The degree of accuracy of the

density at 500m is claimed to be ~20% from which the energy is obtained. Recent calculations show that this figure may be higher. Fluctuations in the radio data indicate that the primary energy is measured to better than 50% if there is no systematic variation in primary energy measurement due to shower development. The error in core location is ±20m. This is serious because it means that the radio field near the axis, where it is large, cannot be utilised for lateral distribution studies. For points near the axis an uncertainty in the core location leads to apparently large fluctuations in the radio field. At large distances the radio lateral distribution shows a smooth trend but the whole distribution may be systematically displaced. This is evident from the experimental lateral distributions.

There are plans to set up a number of additional particle detectors at Haverah Park which will lead to an improvement in data.

Future plans.

It is proposed to increase the number of sites to six and relocate the existing site A. This will give an array with a spacing of ~80m (see fig. 47). The receiver gains will be reduced by a factor of two to raise the upper limit of the measureable field strength. This expansion takes to the limit the number of channels that can be handled within reason for film reading on two scopes. There exists facilities for recording a further three channels but these will be used for auxiliary experiments. The solution of the noise problem has been deferred for the present time as the filters were only included in Feb. 73. The question will be reopened after this latest expansion has taken place and has been in operation for some time.

The existing antenna system has a large beamwidth and is capable of gathering a large amount of noise and interference

DETECTOR SITES AT HAVERAH PARK (EXPANDED RADIO ARRAY)

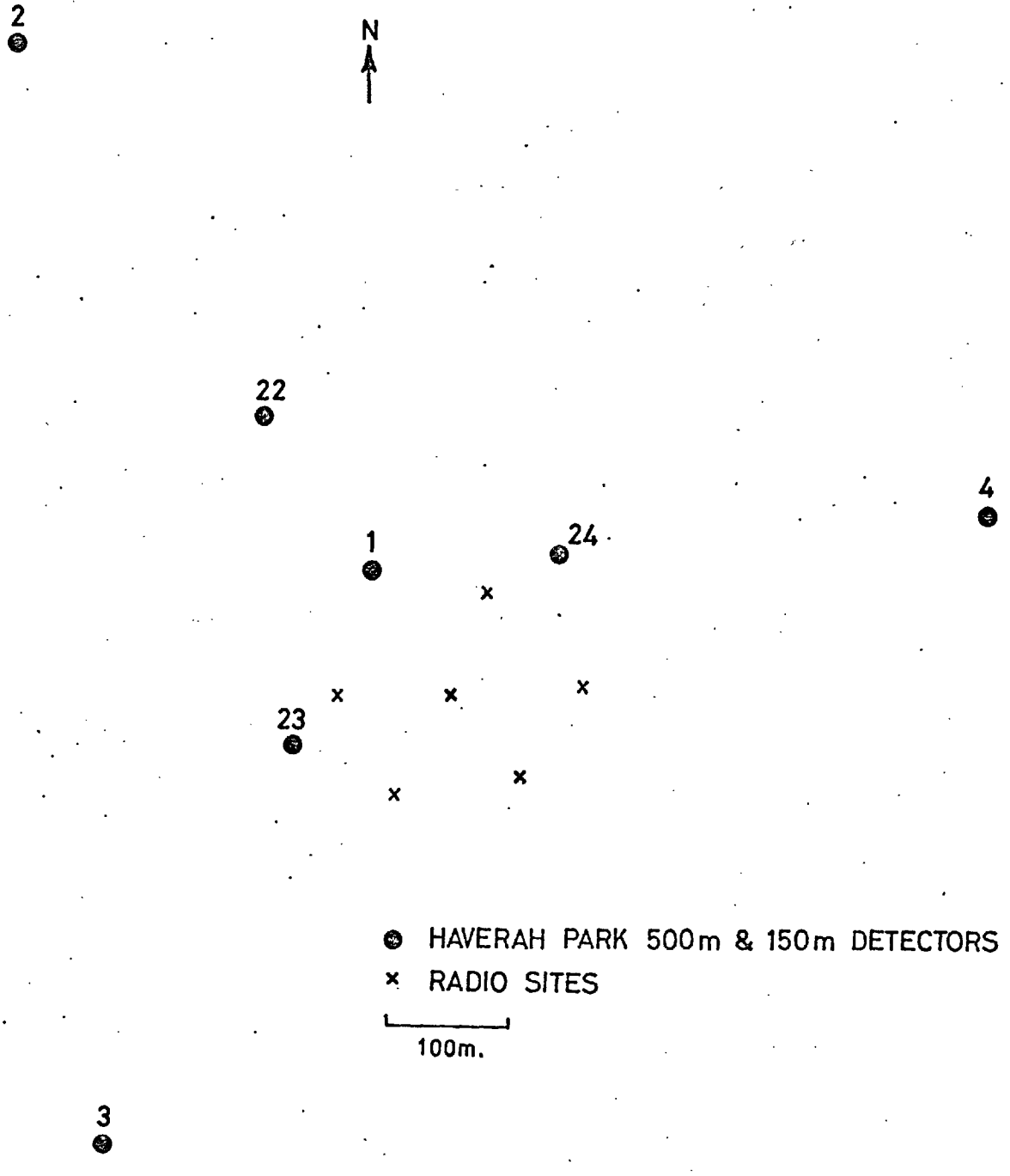

Fig. 47

arriving at zenith angles $>40^{\circ}$. A narrow beamwidth, higher gain antenna would be more suitable. As there is spare recording capacity for two additional channels, antenna designs could be tested without disturbing the existing experiment.

An auxiliary experiment planned for this summer at Haverah Park is aimed at resolving the conflicting results obtained at low frequencies (<3 MHz) from air showers. Theoretical predictions by Allan (72) indicate that the emission should be orders of magnitude below that seen by many workers: Allan et al. (70), Stubbs (71), Hough et al. (71), Khristiansen (72), and Stubbs et al. (72).

As mentioned earlier in chapter two there seems to be some disagreement in the results obtained in the region 22-32 MHz. Theoretical calculations show that the charge excess mechanism should be more dominant at these frequencies. A further experiment could be set up to resolve the differences in these experimental results and to determine the fraction of charge excess emission that is present in the total.

The role of radio.

The present array has been in operation for approximately nine months and has produced over one hundred lateral distributions with $0^{\circ} \leq \theta \leq 40^{\circ}$ suitable for analysis. The next nine months should produce another hundred lateral distributions of better quality because of the new auto-calibration system in operation which has improved precision. At the present time the precision of the radio measurements are greater than those of core location. With the present arrangement the study of fluctuations are just within the experimental limits. Fluctuation studies will have to be confined to showers with $\theta \leq 25^{\circ}$ as the radio lateral distribution

becomes less sensitive to fluctuations as the zenith angle increases. The collection rate for showers in this range is approximately forty per year. To double the statistical accuracy of the present measurements would require a period of about three years of operation. With this kind of time scale of operation the radio experiment would also be capable of providing information about the variation in height of maximum development with change in energy.

Previous calculations of the radio lateral distributions Allan (71), Hough (72) led to unduly optimistic estimates of the sensitivity of the radio lateral distribution to the height of maximum and of the increase in this sensitivity with increasing radial distance. The work presented in chapter two and calculations by Allan (73) indicate there is only a slight increase in sensitivity with increase in radial distance and that the lateral distribution is less sensitive to the height of maximum than was previously expected. At this frequency, 60 MHz, the present theory appears to fit in with the observed experimental lateral distributions. If present core location is improved then radio measurements near the shower axis would be more trustworthy and useful as they have a higher signal to noise ratio. This would help in categorising showers.

The fluctuation in the height of maximum development is also being investigated by the particle group at Leeds. At present they are concerned with studying the thickness of the shower disc at a certain distance from the shower axis and correlating this to the height of the region where mu-mesons are produced. The results and details of this work are given by Watson et al. (73).

An atmospheric cerenkov light detector has also been set up at

Haverah Park by the Durham group to investigate the feasibility of using such a detector in determining fluctuations in shower development.

The two methods mentioned above, together with radio, provide three different ways of looking at the same shower. The three methods will provide three answers. If all the answers are the same the confidence in the result will be greater. It therefore seems that radio will play a complementary role to the existing facilities at Haverah Park.

Appendix

Calculation of the field strengths.

i) Calculation of the horizontal components.

Consider a horizontal dipole polarised in the East-West direction as shown in fig. 48. Suppose a shower of direction with zenith and azimuth angles θ and ϕ falls near the antenna. If the electric field lies in the shower plane then the East-West dipole, OA, will be sensitive to the component of the field lying in the direction AB in the shower plane and is obtained from the polar diagram for the direction (θ,ϕ). The horizontal component is given by multiplying the field in AB by $\cos\psi$ where:

$$\cos\psi = (1 - \sin^2\theta\sin^2\phi)^{\frac{1}{2}}$$

For a North-South polarised antenna $\cos\psi$ is given by:

$$\cos\psi = (1 - \sin^2\theta\cos^2\phi)^{\frac{1}{2}}$$

ii) Calculation of the field strength in the shower plane.

If $\underline{E}$ is the electric field strength and lies in the shower plane and $\underline{S}$ is the direction of the shower then

$$\underline{E}.\underline{S} = 0$$

now $$\underline{S} = \underline{i}(\sin\theta\sin\phi) + \underline{j}(\sin\theta\cos\phi) + \underline{k}(\cos\theta)$$

where $\underline{i},\underline{j},\underline{k}$ are the unit vectors in the x,y,z directions.

Evaluating the dot product and solving for the z component yields:

$$E_z = -(E_x\tan\theta\sin\phi + E_y\tan\theta\cos\phi)$$

FIG.48: CALCULATION OF A HORIZONTAL COMPONENT OF THE ELECTRIC FIELD IN THE E-W DIRECTION.

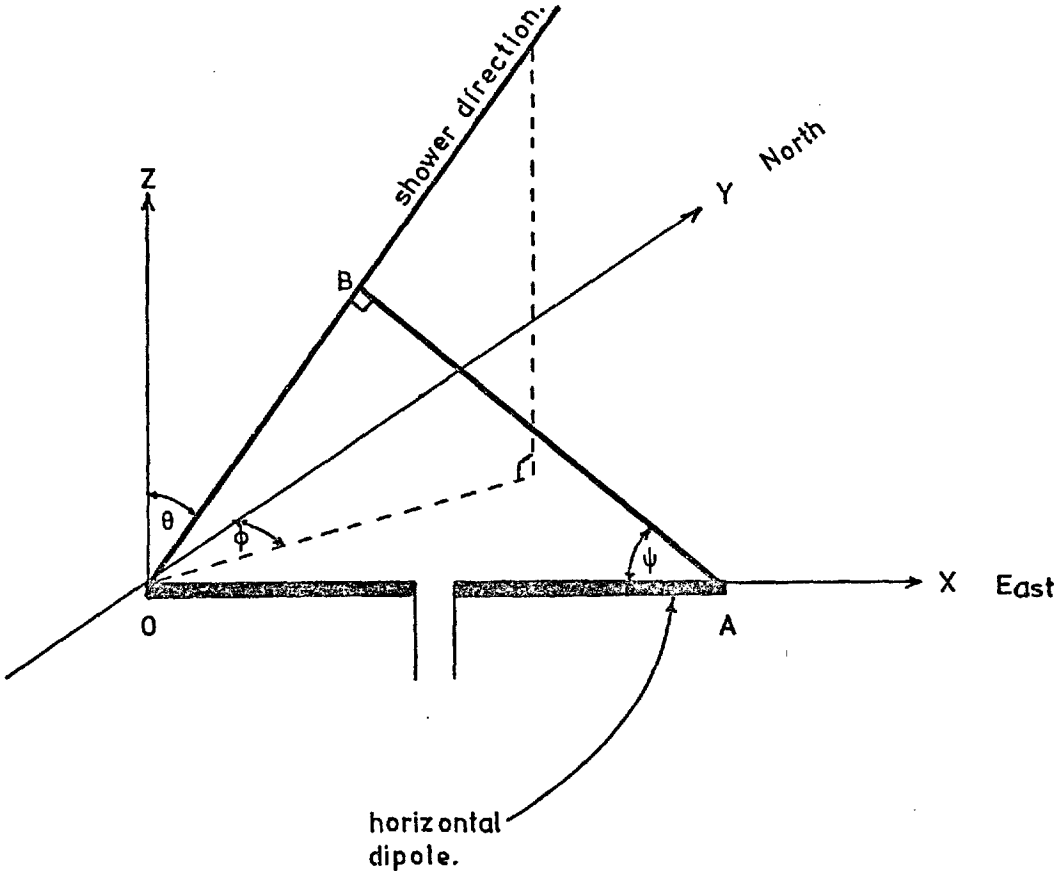

E_x and E_y are found from i) and are magnitudes of the components in these directions. A sign has to be attributed to E_x and E_y. As the geomagnetic mechanism is the dominant mechanism producing radio emission the signs given are those predicted by this mechanism and are obtained from the following expressions:

$$x \longrightarrow \sin\theta\cos\phi\sin D + \cos\theta\cos D$$

$$y \longrightarrow -\sin\theta\sin\phi\sin D$$

where D is the angle of dip of the magnetic field. Once signs have been attributed to E_x and E_y, E_z can be found. The total field is determined from

$$E_T = (E_x^2 + E_y^2 + E_z^2)^{\frac{1}{2}}.$$

iii) Normalisation of the field strength.

The field strength is given in $\mu V/m/MHz$ for a 10^{17} eV shower. The field is also normalised with respect to $\sin\alpha$ where α is the angle that the shower axis makes with the geomagnetic field.

REFERENCES.

The initials PICCR represent the Proceedings of the International Conference on Cosmic Rays.

Chapter 1

Colgate. S.A. 1968, Can. J. of Phys., 46, S476.

Colgate. S.A. 1969, PICCR (Budapest), 1, 353.

Fermi. E. 1949, Phys. Rev., 75, 1169.

Fowler. P.H., Perkins. D.H. 1964, Proc. Roy. Soc. A, 1374, 401.

Gold. T. 1969, Nature, 221, 25.

Greisen. K. 1965, PICCR (London), 2, 609.

Hillas. A.M. 1969, PICCR (Budapest), EAS3.

Hillas. A.M., Hollows. J.D., Hunter. H.W., Marsdem. D.J. 1971, PICCR (Hobart), 3, 1001.

Hollows. J.D. 1968, PhD thesis, Univ. of Leeds.

Jelley. J.V. 1967, in: Prog. in Elem. Part. & C.R. Phys., Vol IX, North-Holland.

Miesowicz. M. 1971, in: Prog. in Elem. Part. & C.R. Phys., Vol X, North-Holland.

Ostriker. J.P., Gunn. J.E. 1969, Astrophys. J. 157, 1395.

Tennant. R.M. 1967, Proc. Phys. Soc., 92, 622.

Chapter 2

Allan. H.R. 1971, PICCR (Hobart), 3, 1108, 1113

Allan. H.R., Jones. J.K., Mandolesi. N., Prah. J.H., Shutie. P. 1971, PICCR (Hobart), 3, 1097, 1102.

Atrashkevitch. V.B., Khristiansen. G.B., Vedeneev. O.V., Prosin. V.V. 1971, PICCR (Hobart), 3, 1124.

Baxter. A. J. 1967, PhD thesis, Univ. of Leeds.

Baxter. A.J. 1969, J. Phys. A, 2, 50.

Bethe. H.A. 1953, Phys. Rev., 89, 1256.

Castagnoli. C., Silvestro. G., Picchi. P., Verri. G. 1969, Nuovo Cimento, 63B, 373.

Clay. R.W.,Hough. J.H., Prescott. J.R. 1971, PICCR (Horbart)

Colgate. S.A. 1967, J. Geophysical Research, 72, 4869.

Crawford. D.F., Messel. H. 1970, The Electron Photon Distribution Function., Pergamon Press.

Feynman. R.P., Leighton. R.B., Sands. M. 1963, "The Feynman Lectures on Physics", Vol. 1, Addison- Wesley.

Fujii. M., Nishimura. J. 1969, PICCR (Budapest), EAS 69.

Jelley. J.V., Fruin. J.H., Porter. N.A., Weekes. T.C., Smith. F.G., Porter. R.A. 1965, Nature, 205, 327.

Jelley. J.V., Charman. W.N., Fruin. J.H., Smith. F.G., Porter. R.A. Porter. N.A., Weekes. T.C., McBreen.B. 1966, Nuovo Cimento, X46, 649.

Kahn. F.D., Lerch. I. 1966, Proc. Roy. Soc. A, 289, 206.

Kristiansen. G.B. 1972, Paper given at the European Symposium on Cosmic Rays (Paris), unpublished.

Lerch. I. 1967, Nature, 215, 268.

Marsden .D.J. 1971, PhD thesis, Univ. of Leeds.

Rossi. B. 1965, High Energy Particles, Prentice Hall.

Spencer. R.E. 1971, PhD thesis, Univ. of Manchester.

Chapter 3

David. P., Voge. J. 1969, Propagation of Waves, Pergamon Press.

Kraus. J.D. 1965, Antennas, McGraw-Hill.

Prah. J.H. 1971, MPhil thesis, Univ. of London.

Zverev. A. 1967, Handbook of Filter Synthesis, Wiley.

Chapter 4

Turver. K.E., Dixon. H, Hough. J.H., Smith. G. 1973, Haverah Park Internal Report.

Chapter 5

Allan. H.R., Clay.R.W., Jones. J.K. 1970, Nature, 225, 253.

Allan. H.R. 1971, Prog. in Elem. Part. & C.R. Phys., Vol. X, North-Holland.

Allan. H.R. 1972, Nature, 237, 384.

Allan. H.R., Jones. J.K., Shutie. P.F., Sun. M.P. 1973, PICCR (Denver), To be published.

Hough. J.H., Prescott. J.R., Clay. R.W. 1971, Nature. P.S., 232, 14.

Hough. J.H. 1973, H.P. int. report, Turver et al.,see ref.Chap 4.

Kristiansen. G.B. 1972, see ref. Chap. 2.

Stubbs. T.J. 1971, Nature. P.S., 230, 172.

Stubbs. T.J., Felgate. D.G., 1972, Nature, 239, 151

Watson. A.W., Wilson. J.G. 1973, [redacted], to be published.

ACKNOWLEDGEMENTS.

The author wishes to express his gratitude to the following:

Professor H. Elliot.

Dr. H. R. Allan.

Dr. J. K. Jones.

Mr. D. Pearce.

Dr. J. H. Hough.

The members of the Haverah Park Group
at the University of Leeds.

The Science Research Council.